 

*REVIEWS OF TOPICAL PROBLEMS*

PACS numbers: **95.35.+d**, 98.62.Dm, 98.62.Gq

# Dark matter in galaxies

A V Zasov, A S Saburova, A V Khoperskov, S A Khoperskov

DOI: https://doi.org/10.3367/UFNe.2016.03.037751

## Contents



**Abstract. Dark matter in galaxies, its abundance, and its distribution remain a subject of long-standing discussion, especially in view of the fact that neither dark matter particles nor dark matter bodies have yet been found. Experts' opinions range from 'a very large number of completely dark galaxies exist' to 'nonbaryonic dark matter does not exist at all in any significant amounts'. We discuss astronomical evidence for the existence of dark matter and its connection with visible matter and examine attempts to estimate its mass and distribution in galaxies from photometry, dynamics, gravitational lensing, and other observations (the cosmological aspects of the existence of dark matter are not considered in this review). In our view, the presence of dark matter in and around galaxies is a well-established fact. We conclude with an overview of mechanisms by which a dark halo can influence intragalactic processes.**

**Keywords:** structure of galaxies, dark matter

**A V Zasov** Lomonosov Moscow State University,
Sternberg Astronomical Institute,
Universitetskii prosp. 13, 119992 Moscow, Russian Federation
E-mail: zasov@sai.msu.ru
Lomonosov Moscow State University, Faculty of Physics,
Leninskie gory 1, str. 2, 119991Moscow, Russian Federation
**A S Saburova** Lomonosov Moscow State University,
Sternberg Astronomical Institute,
Universitetskii prosp. 13, 119992 Moscow, Russian Federation
E-mail: saburovaann@gmail.com
**A V Khoperskov** Volgograd State University,
Universitetskii prosp. 100, 400062 Volgograd, Russian Federation
E-mail: khoperskov@volsu.ru
**S A Khoperskov** Ural Federal University named after the First President of Russia B N Yeltsin,
ul. Mira 19, 620002 Ekaterinburg, Russian Federation;
Institute of Astronomy, Russian Academy of Sciences,
ul. Pyatnitskaya 48, 119017 Moscow, Russian Federation
E-mail: sergeykhoperskov@gmail.com

Received 15 January 2016, revised 28 February 2016
*Uspekhi Fizicheskikh Nauk* **187** (1) 3 – 44 (2017)
DOI: https://doi.org/10.3367/UFNr.2016.03.037751
Translated by K A Postnov; edited by A M Semikhatov

## 1. Introduction

Dark matter (DM) is one of the fundamental problems of modern astrophysics. It remains unsolved because the nature of DM is unknown and there is no clear understanding of its relation to observed astronomical objects. Nevertheless, to date, a large amount of information has been obtained that allows estimating the DM amount and distribution and the role it plays in the evolution of cosmic objects. The number of scientific papers directly or indirectly discussing DM continually increases (Fig. 1), which reflects the great interest in this field and the steadily growing amount of observational data. Clearly, no review is able to pretend to grasp the whole problem.

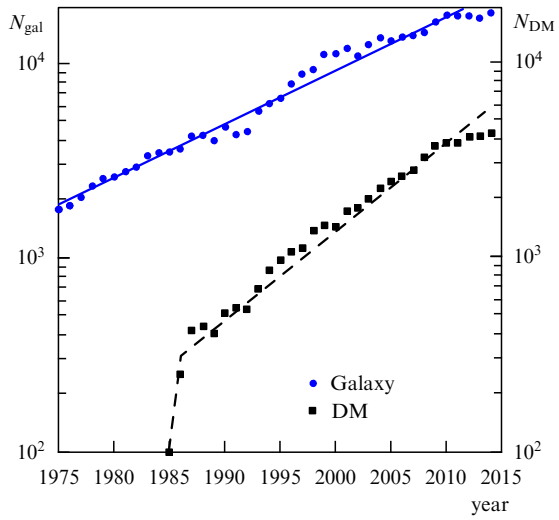


**Figure 1.** Dynamics of the number of papers per year devoted to galactic studies, $N_{gal}$ (key word 'galaxy'), and to dark matter (key words 'dark matter' or 'dark halo') according to NASA's Astrophysical Data System (ADS). A nearly exponential growth is seen: $N_{gal} \propto \exp(t\,[\text{year}]/15.8)$, $N_{DM} \propto \exp(t\,[\text{year}]/9.4)$.

First of all, we must properly understand the term 'dark mass' or 'dark matter'.

All cosmic bodies and media are sources of radiation in some spectral range, although they can appear 'dark' in the optical range (for example, dark nebulae identified with molecular clouds). Dark matter or dark mass traditionally referred to a medium that manifests itself only through gravitational interaction with 'visible' objects, although it is not possible to rule out its dim glowing, for example, in gamma rays due to DM particle annihilation, which is being sought in observations (see, e.g., [1]). The notion of dark matter does not reduce to some forms of matter that are exotic or in low abundance in nature, because the total DM mass in galaxies and their systems must significantly exceed that of all visible, 'bright' matter.

Here and below, the term 'bright' refers to observable matter consisting of atoms (baryonic matter), which includes all types of stars and rarefied interstellar and intergalactic gas, as well as small bodies, including small dust particles, i.e., all matter consisting of baryons (protons and neutrons). There are various estimates of the DM density and different opinions on its role in the evolution of observed galaxies and their systems. There are all grounds to believe that the DM density in many galaxies greatly exceeds the baryonic matter density, even within the optical range, although opinions can be found in the literature that DM is unnecessary or at least its role is significantly exaggerated. In any case, the existence of large DM masses can be considered a well-developed hypothesis, which will persist until DM particles (or bodies) are reliably detected.

The notion of dark (hidden) mass and its historical development have been discussed in recent years by many authors. Different aspects of this problem can be found in Refs [2–5].

Zwicky was apparently the first to justify the existence of hidden mass in galaxy clusters [6], and more than 60 years ago the term 'dark matter' was first used in the modern sense in the title of a paper [7]. However, Zwicky considered the velocity of galaxies in clusters and not internal motions in individual galaxies. At nearly the same time, J Oort found a mass deficit in explaining the attraction force to the Galaxy disk, although his estimates were not very reliable from the modern standpoint. In addition, Oort could not take the mass of gas in the Galactic disk into account. Later, it became clear that the observed mass deficit is the general property of all galactic systems, and the larger the scale of the system, the larger should be the mass of DM required for its virialization.

The modern stage of the DM concept started in the 1970s due to the necessity to explain gas kinematics in massive galaxies — the extended rotation curves of galactic gas components that do not decrease even beyond the stellar disk boundary [11–14]. The need to introduce an additional mass also arose from modeling the mass distribution in elliptical and dwarf spheroidal galaxies that have no disks (see Sections 2.3 and 3.3).

The discovery of the hierarchical structure of the Universe in the 1980s [15], including superclusters and giant voids, and numerical modeling of the structure formation in the expanding Universe gave fresh impetus to the development of DM ideas (see, e.g., [16, 17]). The bulk of cosmological data in the commonly adopted model of the expanding Universe suggest the dominance of dark mass over baryonic matter: the DM mass fraction is about a quarter of the total mass, including dark energy, and the baryonic fraction is merely around 4–5%, which in turn is an order of magnitude higher than the total mass of luminous matter concentrated in galaxies. Thus, both DM and most of the baryonic matter remain undiscovered by direct observations; apparently, the latter is due to hot gas in dark halos and in the intergalactic gas (there is simply no place to hide).

Numerical models of galaxies and their system formation assume that galaxies arose from a DM-dominated medium. A galaxy itself — more precisely, its baryonic part — forms at the 'bottom' of the potential well created by collisionless DM inside a three-dimensional dark halo. Therefore, what we are used to calling a galaxy is located deep inside an extended DM halo. The theoretical size of this halo (the so-called virial radius $R_{vir}$) is about one order of magnitude larger than the observed optical diameter. Therefore, modern galaxy models also include an extended massive halo in addition to baryonic components, although part of DM must be present within the optical boundaries of galaxies, including inside star–gas disks.

In this review, we mainly focus on astronomical evidence of DM related to the gravitational action of DM on baryonic matter, and on DM mass estimates, setting aside the issue of the nature of nonbaryonic DM and experimental searches for DM particles and their possible annihilation radiation; the interested reader is referred, for example, to reviews [18–22].

We note the so-called alternative hypotheses aimed at explaining the observations without invoking the DM hypothesis. First of all, these are theories based on a modified Newtonian gravity, in which the gravitational acceleration $a_g$ deviates from the classical Newtonian expression $a_N = GM/r^2$, and at large $r$ significantly exceeds $a_N$, asymptotically approaching the value $(a_N a_0)^{1/2}$ with the constant $a_0 \approx 10^{-8}$ cm s$^{-2}$. This is the so-called modified Newtonian dynamics (MoND) (see [23–26] and the references therein). The attractiveness of this approach is based on a natural explanation of the dependence of the luminous (i.e., baryonic) mass of galaxies on the radial velocity corresponding to the rotation curve plateau (the so-called Tully–Fisher baryonic relation), which is indeed close to $M_{bar} \propto V^4$. Other

forms of the gravitational potential differing from the classical expression have also been proposed [27]: $\Phi(r) = -Gm/r + \Phi_{\rm NN}(r;m)$ or $\Phi(r) = -Gm/[r(1+\delta(r))]$.

From the theoretical standpoint, the main problem of these models is the use of additional hidden parameters that are absent in the classical theory. The MoND uses the parameter $a_0$, and the Hořava–Lifshitz theory [27] uses four parameters for the function $\Phi_{\rm NN}(r;m)$; a similar situation occurs in conformal gravity [26] and in other theories exploiting diverse gravitational potentials. However, only observations of galaxies and their systems can play a decisive role in testing different approaches; in some cases, such observations reveal serious discrepancies with the MoND predictions.

The discussion and critical analysis of the modified models from both the theoretical and observational standpoints can be found in [25, 28, 29]. In particular, the MoND approach has met with serious problems in interpreting gravitational fields deduced from weak lensing observations of galaxy clusters filled with an X-ray emitting gas, in which accelerations are very small. The triaxiality or, generally, lack of spherical symmetry in the gravitational potential distribution at large distances from galaxies is also difficult to bring into agreement with a simple modification of the gravity law. We note that the apparently increasing inconsistency between the Newtonian and real motion of bodies with decreasing velocities can be reproduced in numerical simulations of galaxy formation in the standard ΛCDM (Lambda–Cold Dark Matter) model without using additional universal constants [30].

Among nonstandard DM theories, the mirror DM theory should be mentioned. In this theory, DM particles are identical to those of ordinary matter but have 'mirror quantum properties' without being antiparticles. The 'mirror partners' cannot interact directly with the ordinary matter, except by the gravitational channel; but the mirror particles interact among themselves exactly as the ordinary particles do (see the discussion in [20, 31]). We also note a theoretical possibility considered by Blinnikov and coauthors that DM exists in the form of a large number of collapsed bodies made of antimatter (collapsed low-mass antimatter stars), which could be produced in the very early Universe under certain assumptions [32]. In some papers, DM models of primordial black holes are considered (see the discussion of this model and its applications in [33]). Other exotic DM models are also considered in the literature; however, their observational tests are difficult.

Different papers examine the possibility that a significant fraction (if not all) of DM inside galaxies could consist of unobservable and thus unaccounted for baryonic mass related to very cold molecular hydrogen [34] or another medium distributed like the interstellar gas (see, e.g., [35]). This conclusion about the relation of DM to the observable gas in galaxies was, however, criticized in [36]. The unaccounted for and hence not directly registered interstellar gas indeed exists in our and other galaxies (the so-called dark molecular and atomic gas), as suggested by indirect observations, but the amount of this gas is far too insufficient to explain the required mass of DM.

We stress, first, that the analysis of observations in this review is carried out exclusively using the classical Newtonian potential. Second, the nature of the unseen component in our discussion of observational manifestations of DM is not very important. The additional gravity from DM can be partially due to the unseen baryonic components, but cosmological data suggest that the bulk of DM must have a nonbaryonic origin.

Vast observational data obtained by ground-based and space telescopes in the last decade suggest that in the framework of fundamental physical models, the conclusion about the existence of DM in galaxies and beyond seems to be inevitable. However, the existing estimates of DM properties and its mass and density distribution in galaxies have been quite contradictory so far, and the DM effects on internal processes in galaxies, although extensively discussed, remain poorly understood. Observations of galaxies that reveal the existence of DM are complemented by another approach based on the construction of numerical dynamical models of stellar, gas, and star–gas gravitating systems with constantly increasing reliability and credibility. In the so-called $N$-body models, the number of particles already approaches the number of stars in galaxies and is far above the number of stars in large globular clusters and dwarf galaxies ($N \sim 10^7 - 10^9$ or more). We show in this review that the use of numerical simulations enables us to better understand the mass distribution in galaxies and to follow their dynamical evolution, where DM should play a large, if not decisive, role.

We here consider the main arguments in favor of the existence of nonbaryonic, nonrelativistic DM and different methods to find it in galaxies, as well as its relation to characteristics of galaxies, without delving into cosmological aspects of the problem, which are widely discussed in the literature.

## 2. Mismatch between kinematic and photometric mass estimates

The problem of the existence of dark or hidden mass in nature became relevant when large-scale measurements of galactic velocities made it possible to apply the virial theorem (the modulus of the gravitational energy of a system is equal to twice the total kinetic energy of its components) for pairs, groups, and clusters of galaxies. However, the fact that we measure only one velocity component of each system's member (except for several nearest galaxies in which proper motions of stars are measured) makes the mass estimate model-dependent. Nevertheless, the difference between the dynamical mass of the entire system and the photometrically determined mass of stars is too large to be accounted for by estimate errors.

Measurements of the velocity of galactic satellites and the galaxies forming pairs confirmed that the dark halo can extend far beyond the optical boundary and fully dominate in the regions almost free of stars and gas. The integral mass of galaxies with account for DM in these remote regions can be an order of magnitude larger than the total visible mass. For example, the mean ratio of the mass to the total visible luminosity in the K infrared band (2.2 μm) in galactic pairs, determined for more than 500 pairs, turns out to be very high for a stellar population: only 11 solar units [37]; for galaxy groups, it is more than two times as high, $M/L_{\rm K} = 26$ solar units [38]. For comparison, models of a purely stellar old population give $M/L_{\rm K} \lesssim 1$.

The mass of the Local Group of galaxies could apparently be determined more precisely. This mass is mainly contained in two galaxies: the Andromeda nebula and the Milky Way; however, the motion of the Sun relative to the Local Group barycenter is not known precisely. By assuming that the total

momentum of galaxies in the Local Group is close to zero, Diaz et al [39] obtained the total mass of the Milky Way $(0.8 \pm 0.5) \times 10^{12} M_\odot$ and that of M31 $(1.7 \pm 0.3) \times 10^{12} M_\odot$, which significantly exceed the total mass of stars and gas in these galaxies. This conclusion for nearby galaxies is confirmed by diverse estimates of the DM-to-baryonic-matter mass ratio [40]. Various estimates of the mass of the Local Group are given in [41]. From an analysis of the velocity field, the authors of [41] obtained the integral mass $(1.9 \pm 0.2) \times 10^{12} M_\odot$. This is apparently the most accurate mass estimate at present. It exceeds the total mass of observed stars and gas in the Local Group of galaxies by many times.

Estimates of the DM-to-stellar-mass ratio within the optical boundaries of an individual galaxy are less uncertain than the integral mass estimates; however, we do not a priori know either the dark halo shape or its radial density profile.

In this section, we primarily consider galaxies with comparatively thin rotating star–gas disks. These galaxies include lenticular, spiral, and irregular ones (S0, S, and Irr), excluding dwarf irregular galaxies (dIrr), in which the disk thickness can be comparable to their radius and the stellar and gas velocity dispersion is comparable to the rotation velocity.

The disk density distribution in the considered galaxies is the sum of the surface density of stars, gas, and DM inside the disk: $\Sigma(r) = \Sigma_*(r) + \Sigma_g(r) + \Sigma_{DM}(r)$. The last term is taken into account only if the disk is assumed to contain a sizable fraction of DM.

The DM mass estimate in a galaxy reduces to the problem of separating the luminous (i.e., baryonic) components (stars and gas) from the total mass of the galaxy. The density of cold gas $\Sigma_g(r)$ can be estimated most reliably because it is derived directly from the gas radio emission. Here, the problem of accounting for the 'dark' gas remains, whose radiation is not detected due to its low temperature or a large optical depth of clouds in radio lines, and for molecular gas, also due to photodissociation of molecules that are used to estimate its amount. However, in most cases, it is stars, not gas, that mainly contribute to the disk density. Photometry enables determining the brightness and color distribution in a galaxy: from the center, near which the bulge mostly contributes to the brightness and stellar mass, to the far disk periphery, where the surface brightness is several hundredths or thousandths that in the center.

The radial brightness distribution in the stellar disk, $I(r)$, is typically described by the exponential law $I(r) = I(0) \exp(-r/r_d)$, where $r_d$ is the radial disk scale. The disk size, as well as the size of the entire galaxy, is a conventional quantity, because there are no sharp boundaries. For certainty, the galaxy radius is usually assumed to be the effective radius $R_e$ comprising half the integral luminosity, or the so-called photometric (optical) radius $R_{opt}$ corresponding to a certain isophote, which is usually related to the 25th stellar magnitude per square second in the B-band (this is close to the galaxy size visible in a good image), although stellar disks extend far beyond.

In normal-brightness galaxies, $R_{opt}$ is $(3-4)r_d$; however, there is a whole class of low-surface-brightness disk galaxies (LSB galaxies) with a much smaller $R_{opt}/r_d$ ratio. Frequently, the stellar density decreases with $r$ beyond the optical radius much more steeply than at smaller $r$; nevertheless, there are objects for which the exponential brightness law holds up to 10 radial scales $r_d$ (for example, for NGC 300 [28]), or galaxies in which, in contrast, the brightness decrease becomes even flatter at large $r$ [42]. The rotation curves obtained from optical observations rarely reach $R_{opt}$, but in gas-rich galaxies it is possible to follow the disk rotation by the neutral hydrogen line (HI) up to several $R_{opt}$.

In the 1980s, when after a period of not very precise radio measurements, progress in optical observations enabled estimating rotation velocities of several galaxies at different distances from the centers, it became evident that the rotation velocities remain high even at the far disk periphery. This led to the conclusion that there is a missing mass, apparently forming a dark halo, whose gravitational field is responsible for the high circular velocities. We note that observations carried out on the 6 m BTA telescope of the Special Astrophysical Observatory of the Russian Academy of Sciences (SAO RAS) significantly contributed to studies of the disk kinematics of S galaxies [43].

The widespread opinion is that the extended flat parts of the rotation curves $V(r)$ found in many disk galaxies directly suggest the presence of dark halos. In fact, this is not exactly the case, and these flat parts can be explained without invoking the DM hypothesis. A smooth rotation curve without sharp local velocity gradients of any form can always be explained either by assuming that almost all the mass is contained in a spherical halo or by assuming that the halo is absent and there is only one axially symmetric disk with a certain radial density law (any intermediate variants are also allowed).

The first case is trivial: for a spherically symmetric mass distribution, the total mass $M(r)$ within a radius $r$ reflects the change in the radial velocity $V_c(r)$ along the radius: $M(r) = rV_c^2/G$, and for any radial velocity distribution, unless it drops faster than $r^{-1/2}$, the corresponding mass distribution can be found.

The second case is not so obvious: the relation between $M$ and $r$ for the disk is more complicated because the gravitational potential estimate at a given radius requires the knowledge of the density distribution at all $r$, and then the disk parameters can be chosen such that the resulting rotation curve is close to the observed one. The classical example is the so-called Mestel disk. This is a thin disk in which the local surface brightness decreases inversely proportionally to the distance to the center: $\Sigma(r) = \Sigma(r_d) r_d/r$, where $r_d$ is the radial disk scale. For the Mestel disk, the calculated circular velocity does not change with the radius $r$, i.e., the rotation curve is a horizontal line.

Why, then, is a dark halo required to interpret rotation curves that flatten at large distances? The answer is simple: the surface density of the luminous baryonic matter (stars + gas) in real disks does not follow the $1/r$ law but decreases much faster, exponentially as a rule. Thus, the presence of DM is suggested not by the form of the rotation curve itself but by the inconsistency with the expected form if all gravitating matter in the galaxy were contained only in stars and gas. To estimate the DM contribution to the mass and rotation curve, it is necessary to find the method for 'calculating' the baryonic mass contribution to the rotation curve. This important problem can be solved in different ways and frequently not with the desired accuracy.

### 2.1 Rotation curves of gas beyond the optical radius

Because most of the disk mass is contained in stars, we can assume in the first approximation that the surface density follows the surface brightness, i.e., the ratio of the stellar mass $M$ to the brightness $L$ is approximately constant,

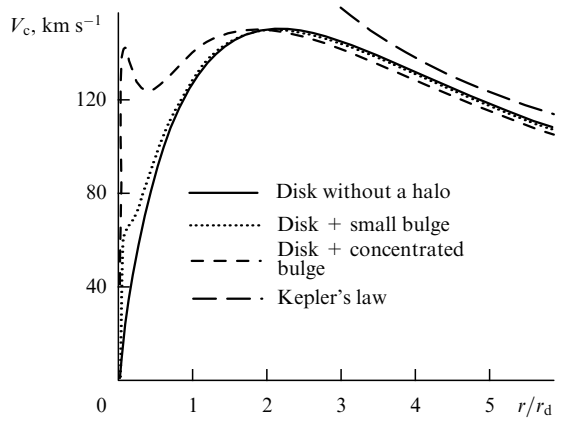


**Figure 2.** Rotation curves in the absence of a halo.

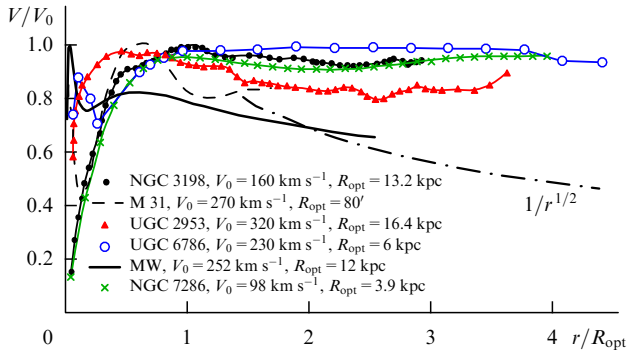


**Figure 3.** (Color online.) Rotation curves of spiral galaxies normalized to the rotation velocity maximum. The distance from the center is in units of the optical radius $R_{opt}$. The long-dashed line shows the Keplerian curve corresponding to the case where all the mass is in the central region. Numerous examples of extended rotation curves can be found in [47–49].

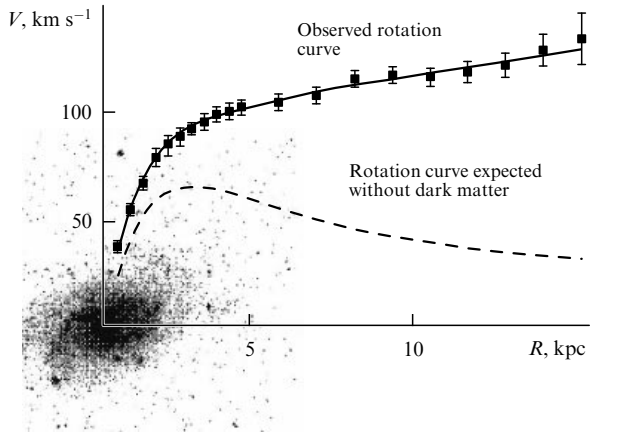


**Figure 4.** Decomposition of the rotation curve of the M33 galaxy suggesting the DM dominance in the region inside the optical radius.

$M/L \approx$ const. This relation holds most precisely for near-infrared (IR) luminosity, because most of the stellar population mass (with very rare exceptions) is contained in old stars that mainly contribute at these wavelengths. Therefore, the surface density of the stellar disk is approximated well by the same law as for the surface brightness: $\Sigma_*(r) = \Sigma_0 \exp(-r/r_d)$ (a discussion of the observed deviations from the exponential law can be found in [44, 45]). With the gas component taken into account, if its mass is significant, this allows using photometry to calculate the rotation curve of the baryonic disk component and, by matching it with observations, to estimate the effect of DM on disk dynamics.

The calculation of the rotation velocity $V_c(r)$, under the assumption that the gravitational potential $\Psi(r)$ is produced by a disk with an exponential density decrease, shows that the circular rotation curve has a specific maximum at the distance $r \simeq 2.2\, r_d$ from the galaxy center and monotonically decreases toward the periphery (Fig. 2). In fact, the rotation velocity at large $r$ in real galaxies does not follow this curve: as a rule, it remains at nearly the same level or continues increasing. The contribution from the bulge to the gravitational potential of the galaxy increases the rotation velocity in the inner part of the disk, but to maintain the high velocity of rotation at large $r$ compared to that expected for an exponential disk, an additional mass is required that is not related to stars or the observed gas. It is this mass that is ascribed to DM.

In the absence of significant noncircular gas motions, the equilibrium condition can be written in the form

$$\frac{V_c^2}{r} = \frac{d\Psi}{dr} + c_s^2 \frac{1}{\gamma \Sigma_g} \frac{d\Sigma_g}{dr}, \qquad (1)$$

where $V_c$ is the circular velocity (which is usually close to the gas rotation velocity $V_g$), $\Sigma_g$ is the gas surface density, $c_s$ is the adiabatic sound velocity, $\gamma$ is the adiabatic exponent, and $\Psi(r)$ is the gravitational potential that is determined from the known mass distribution in the galaxy. The last term in the right-hand side of Eqn (1) describes the deviation of the observed rotation velocity from the circular one, which arises due to the thermal velocity of gas atoms or molecules. In fact, the local gas velocity dispersion is mainly caused not by the thermal motion of particles but by turbulent gas motions or, if we consider the rotation of the stellar rather than the gas disk, by the local stellar velocity dispersion. In these cases, the sound velocity squared $c_s^2/\gamma$ is replaced by the velocity dispersion squared along the radial coordinate $c_r^2$. For a rotating gas, the contribution of this term to (1) is typically small because $c_r^2 \ll V_g^2$ (the characteristic value is $c_r/V_g \simeq 0.05-0.1$), and then the gas rotation velocity $V_g$ is almost equal to $V_c$. Therefore, the difference between these two velocities is often ignored (however, this is not always true for stars [46]).

In Fig. 3, we show examples of rotation curves $V_g(r)$ with a plateau for S galaxies constructed from gas velocity measurements. Without massive dark halos, to explain the rotation curve of a Milky Way (MW)-like galaxy, for which $r_d = 3$ kpc and $V_{max} = 220$ km s$^{-1}$, we should assume very strong deviations from the exponential density distribution in the outer disk zone at $r > 2r_d$, which increase with the distance from the center.

In particular, rotation curves of two nearby spiral galaxies (M31 and M33) behave differently: the rotation curve of M31 (the Andromeda Nebula) does not decrease up to 150 angular minutes from the center [50], with the optical radius of the galaxy being about 80 arc minutes, and remains constant up to 35 kpc [51], whereas the rotation curve of M33 (the Triangle Nebula) keeps slowly increasing even at distances of several $r_d$ (Fig. 4), such that the contribution of a dark halo to the rotation curve of the galaxy already becomes dominant within the observed optical boundary [52].

There are only a few galaxies with rotation curves monotonically decreasing after the maximum (for example,

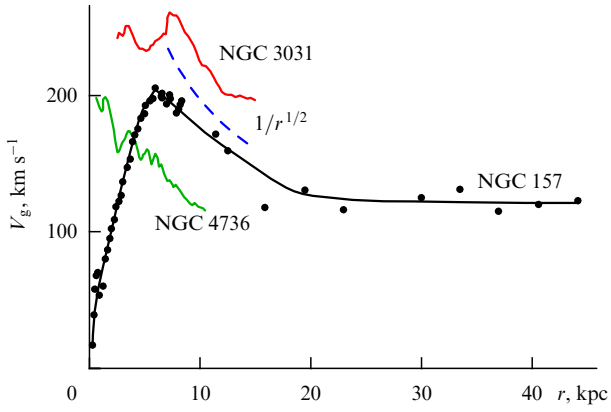


**Figure 5.** Examples of rotation curves of spiral galaxies with a decreasing rotational velocity inside the optical boundaries: NGC 153 [53], NGC 4736, and NGC 3031 [54]. The dashed line is the Keplerian curve $\propto 1/\sqrt{r}$.

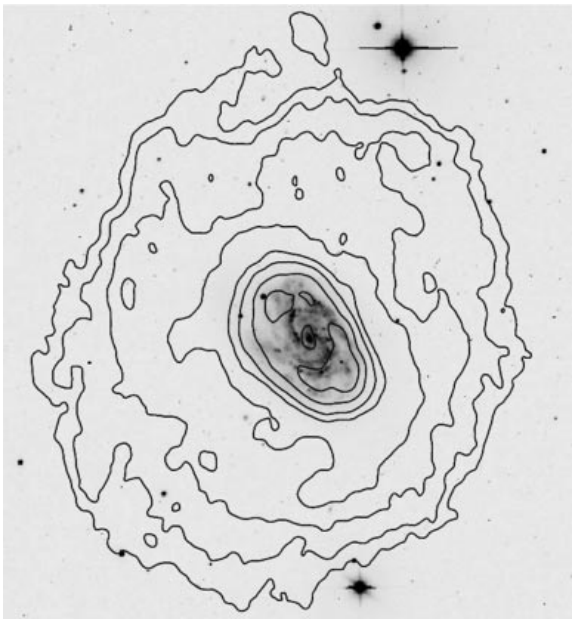

**Figure 6.** Gas disk of the galaxy NGC 157 (shown by the surface isodensities) extends far beyond the stellar disk (the dark central region) and lies in the dark halo gravitational field.

NGC 157, NGC 4736, and NGC 3031) (Fig. 5), and this decrease typically remains flatter than the Keplerian law $V_g(r) \propto r^{-1/2}$, which could be asymptotically expected in the absence of DM (Fig. 6).

### 2.2 Problem of the rotation curve decomposition: the maximum disk model and lower estimates of the halo mass

The decomposition of a rotation curve is understood as a decomposition of the rotation velocity $V(r)$ in accordance with the diverse galactic components. The main components making a contribution to the gravitational potential of a galaxy are the bulge, the stellar disk, and the halo; when necessary, the gas disk and the central core can also be taken into account. The model rotation curve $V_c(r) = (\sum_k (V_c^k)^2)^{1/2}$, where $V_c^k$ is the circular velocity of the $k$th component, is matched to the observed rotation curve. The halo contribution is the most difficult to assess. Because the halo density is a priori unknown, different halo models are assumed, and the results are compared with the observed rotation curves. The following halo models are used most frequently.

The quasi-isothermal halo model characterized by the radial density profile

$$\rho_h(\xi) = \frac{\rho_{h0}}{1 + \xi^2/a^2}\,, \tag{2}$$

where $\xi = |\mathbf{r}| = \sqrt{r^2 + z^2}$ is the radial spherical coordinate and $\rho_{h0}$ is a constant. This model corresponds to a nearly constant velocity dispersion of self-gravitating halo particles.

The Navarro–Frenk–White (NFW) [55] model based on the analysis of cosmological halo formation models:

$$\rho_h^{NWF}(\xi) = \frac{\rho_{h0}}{(\xi/r_s)(1 + \xi/r_s)^2}\,, \tag{3}$$

where $r_s$ is the halo scale; the model has a cusp — a singularity at the center — with $\rho_h^{NWF} \to \infty$.

The Burkert model [56]

$$\rho_h^{B}(\xi) = \frac{\rho_{h0}}{(1 + \xi/b)\left(1 + (\xi/a)^2\right)}\,. \tag{4}$$

An exponential profile of the spatial halo density [57]

$$\rho_h = \frac{M_h}{8\pi e b^3} \exp\left(-\frac{\xi}{b}\right) \tag{5}$$

ensures the convergence of the integral $M_h = \int_0^\infty \rho_h 4\pi\xi^2\,d\xi$, in contrast to distributions (2)–(4). The Einasto profile

$$\rho_h = \rho_0 \exp\left[-\left(\frac{\xi}{r_s}\right)^\alpha\right] \tag{6}$$

is sometimes used, where $\alpha$ is another (third) free parameter of the model. The central density increases with decreasing $\alpha$ ($\alpha \ll 1$), which enables a description of not only models with a smooth central density increase but also models with a cusp. Various halo density profiles are presented in Fig. 7.

Each of the halo models describes the flat rotation curves well with the baryonic component contribution taken into

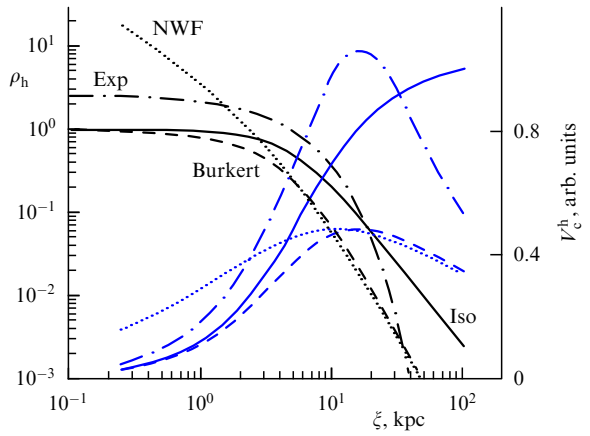


**Figure 7.** (Color online.) Comparison of different profiles of the volume density $\rho_h(r)$ of a spherical halo (the halo scale $a = 5$ kpc). The exponential profile (Exp) corresponds to Eqn (6) with $\alpha = 1$. The Iso curve corresponds to an isothermal halo. The blue curves show the corresponding profiles of the circular velocity $V_c^h$.

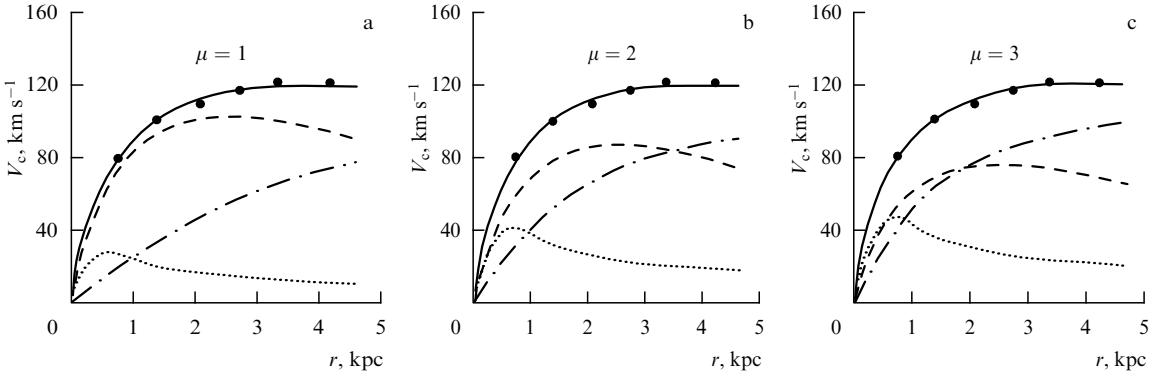


**Figure 8.** Radial model (solid curve) and observed (black dots) rotational velocity for NGC 6503 for various relative halo masses $\mu$: (a) $\mu = 1$, (b) $\mu = 2$, and (c) $\mu = 3$. Contributions of subsystems to the rotation curve are shown by the dotted line (bulge), dashed line (disk), and dashed-dotted line (halo) [59].

account. However, models deviate at small $r$, showing the diverse character of the DM density increase toward the galaxy center. Models with a cusp exhibit a rapid central density increase, while the isothermal halo and Burkert halo models demonstrate a flat profile at the center. The quasi-isothermal halo density decreases most slowly far beyond the optical radius, and therefore the difference between this model and other models is most prominent at large distances, where (with rare exceptions) there are no observational data.

The usually smooth transition from the rotation curve in the inner region, where rotation is determined by the baryonic components, to the outer zone, where rotation is dominated by the halo, remains unexplained. Such disk and halo self-consistency is observed in many cases, and, surprisingly, in galaxies with different disk and halo concentrations. This problem, also known as the 'disk–halo conspiracy', suggests a gravitational coupling between the disk and the halo leading to their parameter correlation. In [60], this feature is discussed in detail and a self-consistent dynamical model is proposed that consists of a thin exponential disk and a nonspherical halo, which reproduces the flat rotation curve in the region between the components. In this model, in the transitional region between the disk and the dark halo, the dark halo should be compressed toward the disk, i.e., should have a significantly nonspherical form.

We note that numerical models of galaxy formation under the modern cosmological assumptions reproduce an extended plateau in the rotation curves of galaxies without assuming a dark halo nonsphericity (see, e.g., [30]), although the smooth transition of the rotation curve in [30] is apparently due to the halo dominance even near the maximum of the disk component.

To interpret rotation curves, we frequently use either the maximum disk solution (MDS) aimed at determining the upper mass limit of the disk component at which its contribution to the circular rotation still does not contradict the observed dependence $V(r)$, or the best-fit method, which minimizes the difference between the model and observed rotation curves. These approaches could provide information on the relative disk and bulge mass; however, the unseen component (dark halo) with an a priori unknown density distribution significantly complicates the problem.

When decomposing the galactic rotation curve, the use of the maximum disk model, as a rule, suggests that the disk can well dominate inside the optical radius of the galaxy (Fig. 8a); however, we cannot ignore DM within the optical boundaries of the galaxy, unless a model of a halo with an empty central part is seriously considered.

As noted above, the disk component contributes maximally at the radius $r = 2.2\,r_d$, where the circular velocity of the exponential disk, $\Sigma_d \propto \exp(-r/r_d)$, reaches a maximum. For the maximum disk model, this velocity is on average $\approx (85 \pm 10)\%$ of the circular rotational velocity at this distance: $V_c^{disk}/V_c = 0.75-0.95$ [60, 61]. The MDS can slightly overestimate the disk mass, and therefore it gives a lower bound on the halo mass. Inside the optical radius of the galaxy, $r \leqslant R_{opt}$, the relative halo mass $\mu = M_h/M_d$ is, according to the MDS, $\mu \simeq 0.4-0.7$. But already inside the radius $r \approx 2R_{opt}$, which is usually reachable by the measured rotation curve (see Fig. 3), $\mu$ can be as high as 2–2.5 in the maximum disk model. Typically, or at least in most cases, we cannot explain the observed rotation curves within the optical radius without invoking a dark mass.

The nonuniqueness of the rotation curve decomposition is a serious problem when estimating galactic component masses from the observed rotation curve $V(r)$, even if the radial dependence of the functional density is known for each component. Generally, the observed rotation curve $V(r)$ can be explained using different relations between the disk and spherical component masses (see Fig. 8), and therefore their masses cannot be determined uniquely. Each galactic component is described as a minimum with respect to two parameters with the dimension of density and length characterizing the conventional size of the component. Three main components (bulge, disk, and halo) require at least six parameters, which must correspond to the observed rotation curve. Other parameters, for example, can include the degree of oblateness of the components or parameters that describe a complex density profile of the star–gas disk. The larger the number of parameters, the more precisely the model rotation curve can fit the observed one, but then the multidimensional parameter space increases.

This problem can be circumvented or at least smoothened in the modeling not only by increasing the precision of determining the curve shape but also by invoking additional a priori information about the galaxy, which is done in practice in almost all cases. This is primarily the relation of the galaxy brightness distribution to the surface (column) density of the stellar disk population. The proportionality coefficient is the ratio $M/L$, which is assumed to be known or is determined from the stellar population model from spectral

or color measurements of the galaxy (after taking the selective light extinction by dust into account). In the best-fit model, when interpreting galactic rotation curves, the $M/L$ ratio is treated as a free parameter (see, e.g., the decomposition of rotation curves from THINGS (The HI Nearby Galaxy Survey) for a fixed and 'free' $M/L$ ratio in [54]).

For gas-rich galaxies, in addition to the brightness distribution, the gas density distribution in the disk obtained from radio observations should be given. To diminish uncertainties, estimates of the stellar velocity dispersion, disk thickness, the gravitational stability condition, and other data are used, which narrows the range of possible solutions.

With the data on the gas density distribution and additional information on the stellar velocity dispersion in the disk, it was confirmed that the disk mass is typically smaller than the MDS model suggests. For example, according to [62], where rotation curves of 30 galaxies, mostly of the Sc and later types, were analyzed taking photometry, velocity dispersion, and the gas layer contribution to the rotation curve into account, the ratio between the 'baryonic' and total rotation curves in the region of the maximum disk contribution to the rotation curve is less than 0.75 (the mean value is 0.6). Assuming that for the MDS this ratio is on average 0.85, the disk masses in this model are overestimated (and the halo masses inside galaxies are underestimated) by a factor of about two.

The rotation curves in most cases are derived from gas velocity estimates. The rotation velocities of the stellar disk are usually measured only in the central part of the galaxy due to the complex procedure of the Doppler shift estimate using absorption lines, which requires a high signal-to-noise ratio, because absorption lines contrast less on the continuum background and are broader than the emission lines. Nevertheless, in the inner disk region, the accuracy of determining the radial velocity curve and hence rotation velocities from stars is sometimes better than from gas, because gas velocities are more frequently distorted by noncircular motions.

Recently, using long-slit spectroscopy on the MMT (Multiple Mirror Telescope), 'stellar' rotational velocities were measured for more than 100 massive galaxies [63]. The obtained statistical material enabled the authors of [63] to conclude that the inner DM density profiles are different, and in DM-dominated galaxies, the rotation curves are well explained by baryonic components and the NWF halo profiles (Fig. 9).

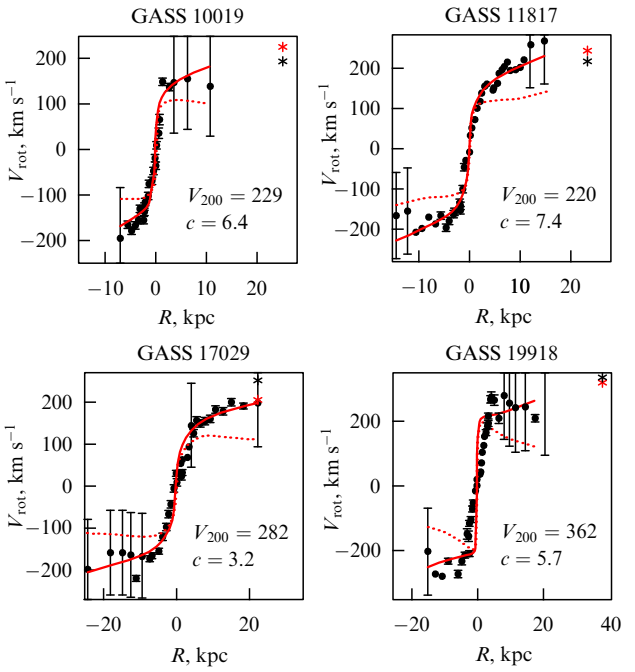


**Figure 9.** (Color online.) Decomposition of rotation curves for several DM-dominated galaxies. The dotted red lines show the baryonic matter contribution to the rotation curve. The black dots show the measured values, the dashed red lines mark the baryonic matter contribution, the solid curve is the model rotation curve with an NFW halo, and $c$ is the model parameter [63].

### 2.3 Dwarf galaxies and low-surface-brightness galaxies

Mass and luminosity are usually expressed in solar units. Without dark mass, the $M/L$ ratio for the galactic stellar population dominated by old stars is up to 10 in the B-band and (according to different estimates) 0.5–1.0 in the IR K-band (2.2 μm). Intensive star formation can decrease the $M/L$ ratio severalfold in the B-band but slightly affects the near IR luminosity, which is preferably used in stellar population mass estimates from photometric data. By comparing the dynamical and photometric integral estimates of the galaxy mass (obtained by multiplying the integral luminosity by the $M/L$ ratio), it is possible, by adding the interstellar mass gas, if present, to the stellar mass, to quantitatively estimate the DM contribution to the galaxy mass without analyzing its rotation curve. If there is gas in a dwarf galaxy, we can estimate its rotation velocity from the integral width of the HI line (with account for the projection effect) and then estimate $M/L$ within the optical boundaries of the galaxy. In the absence of information about rotation curves, the error of such estimates is comparable to the estimated value itself; however, the accuracy can be increased by considering a larger number of galaxies.

Results show that the relative amount of DM in dwarf galaxies varies significantly. Rich statistical data can be found in the Updated Nearby Galaxy Catalog (UNGC) [65], which contains data for several hundred galaxies at distances less than 11 Mpc. In more than half dwarf galaxies containing gas, the $M_{opt}/L_K$ ratio exceeds unity, suggesting a large DM contribution, although the number of galaxies in which the DM mass greatly exceeds the stellar mass is small: just a few objects have $M_{opt}/L_K \geqslant 15$.

A characteristic feature of many dwarf galaxies is an increase of the rotation curve of the gas subsystem, even beyond the optical radius [64, 66, 67] (Fig. 10), which points to the DM domination.

DM mostly contributes to the integral mass in dwarf spheroidal (dSph) galaxies with a size of several hundred parsecs. Dwarf spheroidals belong to the smallest galaxies (except for rare and poorly studied ultrafaint dwarfs). Low-luminosity dSph galaxies have the characteristic dynamical mass $M_{opt} \sim 10^7 M_\odot$, as derived from the stellar velocity dispersion. Large values of $M/L \sim 1/L$, which amount to several tens and sometimes hundreds, definitely suggest the DM domination. These galaxies have no rotating thin disks, and their density distribution is found from dynamically equilibrium models based on velocity dispersion, $c_{obs}$, measurements. Typical values of the central stellar velocity dispersion $c_{obs}$ in such galaxies range from $\simeq 3-10$ km s$^{-1}$ (Segue 1 and 2, Hercules, LGS 3, Carina, Sextans, Sculptor, Leo II, Leo IV, Bootes 1, Coma) to 20–30 km s$^{-1}$ [68, 69].

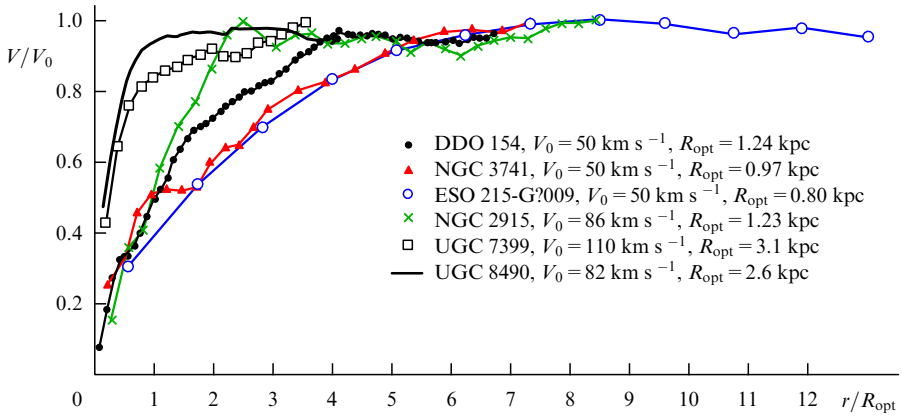


**Figure 10.** (Color online.) Rotation curves of dwarf galaxies according to [64]. Shown are the rotation velocity $V_0$ and the optical radius $R_{opt}$.

More precise and less model dependent is the mass inside the region within the effective radius $R_e$ that constitutes half the integral luminosity: $M(R_e) \propto vR_e c_{obs}^2$, where the proportionality coefficient is $v \approx 580 M_\odot$ [pc$^{-1}$ km$^{-2}$ s$^2$] [70].

The $M/L$ ratio in dSph galaxies is much higher than that expected for galaxies without a dark halo, with the empirical relation $\log(M/L_V) = 2.5 + 10^7/L_V$ [68], where $L_V$ is the luminosity in the V photometric band, and can lie in the range 10–1000 [68, 71]. That the $M/L$ ratio is inversely proportional to $L$ means that the masses of these dwarfs, mostly due to DM, lie within a much more narrow range than their luminosities [70].

Low-surface brightness (LSB) galaxies also have very low mass disks compared to the total mass, assuming that the initial stellar mass function in these galaxies is about the same as in galaxies with normal surface brightness, which is generally not obvious [72, 73]. These galaxies are surrounded by very massive extended dark halos, although part of DM can be in the disks as well [72, 72]. Neutral hydrogen in these galaxies, as a rule, dominates over the stellar component.

LSB galaxies include both dwarfs and giant systems with radii of 100 kpc or more. Despite large difference in sizes, LSB galaxies typically have rotation curves extending far beyond the optical disk boundaries [74]. Of special interest are LSB galaxies with giant mass and size, such as Malin-1 and Malin-2 (Fig. 11). Their formation and origin are challenging for modern galaxy formation theories. The analysis of observations of Malin-2 [75], whose mass exceeds $10^{12} M_\odot$ within the limits of the measured rotation curve, revealed the presence of a very massive halo with an unusually low central density. The authors of [75] also assumed the presence of large masses of so-called dark gas in the disk of this galaxy, which is not observed in radio lines.

## 3. Velocity dispersion of stars in the disk: constraints on dark matter

Extended rotation curves with $V \simeq$ const imply the presence of a hidden mass (assuming that the spatial distribution of the baryonic matter density is known), but do not suggest the location and spatial structure of DM. In principle, DM can be in a spheroidal dark halo, but can also be in the disk, thus maintaining its rapid rotation. Studying dynamical processes in the disk enables imposing additional independent constraints on the gravitating mass distribution. First and foremost, this relates to the analysis of dispersion of old disk stars with an age of several billion years, which constitute most of the stellar population.

Until the mid-1990s, the number of galaxies with the known radial velocity dispersion along the line of sight beyond the bulge was less than a dozen. Over the last 15–20 years, using modern observational methods, stellar velocity dispersion in disks has been measured in many galaxies. These data relate not only to the central parts of the disk where the bulge dominates but also to very remote disk regions, which play the key role in constructing realistic galaxy models with account for DM and its spatial distribution.

Velocity dispersion of old stars is crucial not only for estimates of the disk and halo masses and measurements of the $M/L$ ratio but also for the large-scale structures in the disks (spiral pattern, bars, twists, rings, etc. [76–79]). This is also important for determining the depth of the potential well due to the disk, in which the interstellar gas is located, concentrated toward the galactic plane. In turn, the gravitational potential distribution essentially determines the formation conditions of giant molecular clouds (GMCs) in the gas–

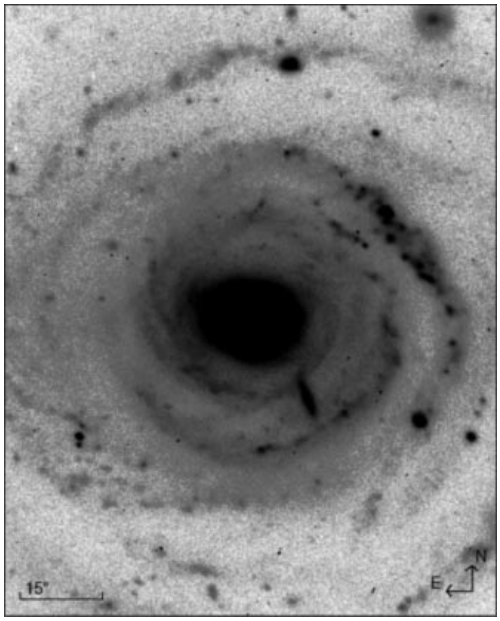


**Figure 11.** One of the largest LSB galaxies Malin-2 (Gemin-North telescope) (see [75]).

dust component [80–83] as well as regions of star formation and its efficiency [84–91].

### 3.1 Disk gravitational stability condition

The star disk dynamics are characterized by both the rotation curve and the velocity dispersion of stars along three directions: $c_r$, $c_\varphi$, and $c_z$. The gas disk, unlike the stellar one, has an almost isotropic local velocity dispersion, because it is a collisional dissipative medium. The gas velocity dispersion usually relates to the velocity of turbulent motions. Because stellar disks are collisionless, they can show various velocity dispersions along different directions. In the epicyclic approximation, in which the velocity dispersion in the disk plane is low compared to the circular velocity, the Lindblad relation $c_r/c_\varphi = 2\Omega/\varkappa$ holds, where $\varkappa$ is the epicyclic frequency (the low-amplitude oscillation frequency relative to the circular orbit) and $\Omega = V/r$ is the disk angular velocity. For disk regions with a flat rotation curve, $\varkappa = \sqrt{2}\Omega$.

Most spiral galaxies have dynamically cold stellar disks, because the radial velocity dispersion, even for old stars constituting most of the stellar disk population, is small compared to the rotation velocity: $c_r/V \simeq 0.1-0.3$ (except for near-central regions), which justifies the epicyclic approximation. In the absence of nondisk components (dark halo, bulge), the disk could be self-gravitating and, as numerical simulations show, the velocity dispersion of stars would significantly exceed the observed one because of the gravitational instability in self-gravitating systems.

The condition of gravitational stability relative to radial perturbations bounds the velocity dispersion $c_r$ in a stellar disk from below [92]:

$$c_r \geqslant c_\mathrm{T} = \frac{3.36\, G\, \Sigma_*}{\varkappa}\,, \tag{7}$$

or, using the Toomre parameter, $Q_\mathrm{T} = c_r/c_\mathrm{T} \geqslant 1$. This relation is valid for thin isothermal disks in the epicyclic approximation. A finite disk thickness makes it more stable. However, the presence of colder components (for example, a gas disk), as well as nonradial perturbations and global modes, facilitate the disk instability. These facts complicate condition (7); as a result, the stable value of $Q_\mathrm{T}$ for real disks can be both close to unity and larger than unity, especially far away from the center. The Toomre criterion should also be used with caution in central parts of galaxies, where the amplitude of epicyclic motions becomes comparable to the mean orbital radius, which violates the epicyclic approximation.

Different criteria of gravitational stability of galactic disks are discussed, e.g., in [46, 77, 93, 94]. These criteria give consistent results and show that at the stability limit, $Q_\mathrm{T}^\mathrm{crit} \sim 1-3$, depending on the local disk parameters [77, 95, 96]. However, there is no simple analytic expression for the critical velocity dispersion that takes all the above facts affecting the stability into account; therefore, in general, numerical modeling is required.

A sufficiently cold disk ($Q_\mathrm{T} < 1$) is always gravitationally unstable, and perturbations increase in it, which at the nonlinear stage leads to stellar disk heating: its velocity dispersion grows. The efficiency of the heating of young stellar disks by short-lived (transient) spirals has been thoroughly studied in numerical experiments of $N$-body simulations [59, 77, 84, 97]. After transient spirals have dissipated, the disk becomes stable ($Q_\mathrm{T} > 1$). Because a more massive disk must be 'hotter' in order to be stable, the maximal disk model (see Section 2.2) requires higher velocity dispersions. Indeed, if most of the galaxy mass inside two to three radial disk scales is contained inside the disk, then the relative velocity dispersion at the double disk radial scale, where the disk mostly contributes to the circular velocity, is $c_r(2r_\mathrm{d})/V_\mathrm{max} \sim 0.5-0.8$, which contradicts the observations, which show that $c_r(2r_\mathrm{d})/V_\mathrm{max} \leqslant 0.5$ for most of disk galaxies.

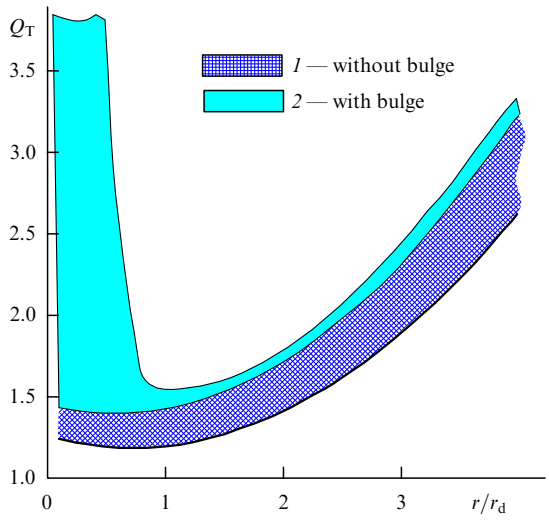


**Figure 12.** (Color online.) Gravitational stability boundaries for a variety of $N$-body models of a marginally stable stellar disk: *1* — models without a bulge, *2* — models with a bulge with a size $r_\mathrm{bulge} < r_\mathrm{d}$.

Under real conditions of an inhomogeneous differentially rotating 3D stellar disk, $Q_\mathrm{T}^\mathrm{crit}$ changes along the radial coordinate (Fig. 12). Numerical models reveal that the development of gravitational instability in the region comprising most of the disk mass stops at $Q_\mathrm{T} \propto 1-1.5$, but if the gravitational field is mainly due to spheroidal components (the bulge in the inner galaxy and the halo in the outer parts), the minimal velocity dispersion for a purely stellar disk continues increasing to $Q_\mathrm{T} \geqslant 3$.

The analysis of velocity dispersions enables narrowing possible galactic models that explain the observed rotation curves. The main idea is using an additional condition in the mass distribution modeling that can be formulated as follows: for a stellar disk that reached a steady state, the observed velocity dispersion at different distances from the center must be greater than or equal to the model values calculated for the threshold (marginal) stability; then the disk is stable.

In a marginally stable disk, i.e., with the parameters $\Sigma_*(r)$, $V(r)$, and $c_r(r)$ corresponding to the gravitational stability limit, the estimate of $\Sigma_*(r)$ found from this condition enables imposing upper bounds on the real disk mass, irrespective of which matter it consists of, and hence constraining the mass of other components. The above method was applied to the galaxy NGC 6503 (Fig. 13). The observed rotation curve $V^\mathrm{obs}(r)$ can be explained by models with different ratios between the spherical and disk subsystems, $\mu = M_\mathrm{s}/M_\mathrm{d} = 0.8-5$. A comparison of the observed radial velocity dispersion of stars $c^\mathrm{obs}(r)$ with a marginally stable galactic model for diverse values of $\mu$ enables setting more stringent constraints on the halo mass (see Fig. 13).

If the critical value $Q_\mathrm{T}$ and the rotational velocity $V$ can be assumed to be approximately constant in the region containing most of the disk mass, the expected ratio of the velocity dispersion to the velocity $V$ turns out to be dependent on the

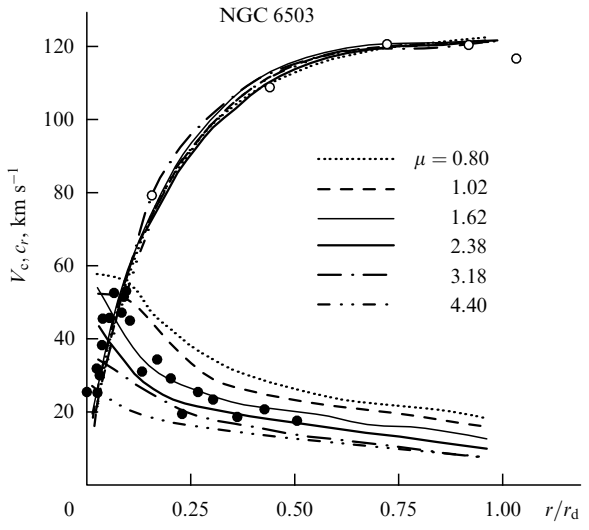


**Figure 13.** Radial profiles of the circular velocity and velocity dispersion along the line of sight for different models of NGC 6503 [59]. The black dots show observations. In models with $\mu < 1.6$, the observed velocity dispersions of stars is less than the calculated ones.

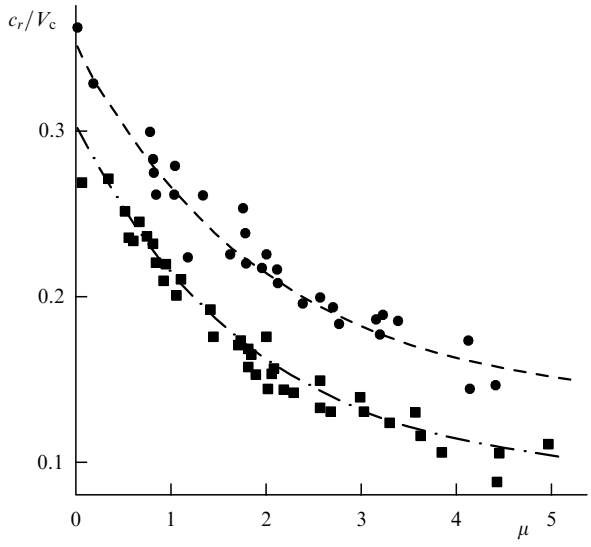


**Figure 14.** The ratio $c_r/V_c$ at the radius $r = 2r_d$ as a function of the relative mass of the spheroidal subsystem $\mu$ from dynamical simulations for marginally stable disks with different parameters. Each symbol (black dot or square) corresponds to one numerical model. The dots correspond to stellar disks with a small initial thickness. All models evolve from an initially unstable state.

relative mass of the spherical component (bulge or halo) $\mu = M_s/M_d$. This follows from the simple considerations given below.

Let the disk region of interest be bounded by a radius $R$ that is $n$ times as large as the radial disk scale, $R = nr_d$. Assuming the balance between the centrifugal and gravitational forces, we obtain the total mass of the galaxy inside $R$ as $M_{tot} = M_s + M_d \approx V^2R/G$. Because the disk mass is $M_d \propto \Sigma_* R^2$, it follows for a marginally stable disk that $c_r \propto \Sigma_*/\varkappa \propto \Sigma_* R/V \propto \propto M_d/RV$ [see Eqn (7)], which yields the dependence $c_r/V \propto M_d/M_{tot} \propto (1+\mu)^{-1}$. This effect is presented in Fig. 14, which is constructed using results of numerical simulations. The figure shows the calculated sequences of points (each point for a separate model) corresponding to the values of $c_r/V$ for galaxies with marginally stable disks of different initial thicknesses. The figure suggests that in the case of a low mass of spheroidal components, the velocity dispersion of stars in the disk must be a substantial fraction of the rotation velocity.

The above relations suggest one interesting constraint on the geometry of marginally stable disks: the vertical size (semithickness) of the stellar disk is determined by its surface density and velocity dispersion along the $z$ coordinate: $z_* \sim c_z^2/\Sigma_d$. The velocity dispersion $c_z$, whose minimum value is related to the bending instability, and the radial velocity dispersion $c_r$ are approximately proportional to each other (observations suggest that $c_z/c_r = 0.5-0.8$). Therefore, by assuming that $c_z$ is proportional to the critical value of $c_r$, we obtain $z_* \sim \Sigma_d R^2/V^2$, whence $z_*/R \sim \Sigma_d R^2/(V^2R) \sim M_d/M_{tot}$. This implies that there is a limit on the relative disk thickness below which the disk is unstable, and the larger the relative dark halo mass is, the lower this limit. Observations indeed suggest a correlation between the relative disk thickness and its relative mass [98].

The relative thickness of disks of late-type galaxies (almost without bulges) seen 'edge-on' were measured in [99] using IR photometry with interstellar light extinction in galaxies taken into account. This analysis confirmed the correlation between $z_*/r_d$ and the deprojected surface brightness of the disks consistent with the marginal disk stability assumption. The relative disk thickness $z_*/r_d$ was found to change little with radius and be $1/6$ on average, which corresponds to the dark-halo-to-disk mass ratio $M_h/M_{opt} \approx 1.3$ inside the optical radius (assumed to be $4r_d$). Without the dark halo assumption, it is impossible to explain the small relative thickness $z_*/r_d$ of such stellar disks.

We must recall the approximate character of these relations, however. For example, the presence of a massive compact bulge, which is frequently found in S0–Sb galaxies, affects the warp instability of the disk and complicates the relation between the velocity dispersions $c_r$ and $c_z$ (see the discussion in [100] and the references therein). We note, however, that the accurate two-dimensional photometry of galaxies seen edge-on has not revealed any dependence between the relative disk thickness $z/r_d$ and the bulge contribution to the galactic integral luminosity [96].

Thus, the existence of a stellar disk with a low velocity dispersion $c_r \simeq (0.1-0.3)V_c$ requires that a significantly large fraction of the total mass be outside the disk. A stellar disk without a halo ($\mu = 0$) is dynamically hot, $c_r/V_c \gtrsim 0.3-0.4$ (see Fig. 14). In addition, if $\mu \ll 1$, the difference between the rotation velocity of the gas–dust disk $V_c(r)$ and that of the stellar disk $V_*(r)$ becomes significant, amounting to $V_*/V_c \simeq 0.5-0.7$ in the outskirts, which occurs very rarely in galaxies.

The approach to the disk and halo mass decomposition taking the stellar velocity dispersion into account has been applied to several galaxy samples [59, 101–103]. It confirmed that the stellar disk gravitational stability condition for Sab–Sd galaxies implies the presence of a more massive dark halo than follows from the maximum disk model.

An important conclusion is that, to make a disk stable with the observed stellar velocity dispersion, most of the DM inside a galaxy must form a spheroidal or at least highly oblate subsystem and cannot be concentrated inside the stellar disk, for example, in the form of dark gas. Otherwise, much of the DM inside the disk would contribute to the disk

self-gravity by increasing the critical stellar velocity dispersion required for its stability.

We emphasize that the condition of the threshold (marginal) gravitational stability generally imposes only an upper bound on the disk density for a given stellar number density (or a lower bound on the velocity dispersion for a given density). In principle, the disk can be dynamically overheated, i.e., can have a large margin of stability [104]. Apparently, disks are frequently marginally stable in a wide range of galactocentric distances but 'overheated' at the periphery; thanks to the low density, the disk can easily be dynamically heated.

To test to what degree the marginal stability conditions can be applicable to real disk galaxies, the surface densities of S and S0 galaxies found from the threshold (marginal) stability condition at the fixed distance $r \approx 2r_\mathrm{d}$ were compared in [102] with the luminosity of the stellar population per unit disk area at the same distance from the center. The resulting $M/L$ ratios were matched to those expected from the model stellar population with a known color index. It turned out that for spiral (S) galaxies, the color–$M/L$ ratio dependence derived from the stability condition is in good agreement with the relation suggested by photometrical stellar population models, and consequently the threshold stability condition can indeed be used to estimate the mass of galactic components. However, for lenticular (S0) galaxies, the situation is more diverse: about half of them have 'overheated' disks [102, 104]. This means that their disks, which have the same density, have higher velocity dispersions and, apparently, a greater thickness than follows from the marginal stability condition.

Clearly, the disk mass and the degree of its dynamical heating are related to the dark halo mass in the optically observed region of the galaxy and therefore to the formation history and evolution of the galaxy (see, e.g., [105]).

### 3.2 Disk density estimates from vertical velocity dispersion measurements

**3.2.1 Local DM density.** The observed thickness of stellar disks is primarily determined by the vertical velocity dispersion $c_z$ and the volume disk density. Therefore, the disk densities can be estimated from measurements of $c_z$ with a known vertical star density profile. For our Galaxy, near the Sun, this approach was applied as early as the first quarter of the 20th century [106, 107], and has been used up to now. A comparison of the total matter density with independent measurements of the baryonic galactic components allows estimating the local DM density in our vicinity (see below).

The vertical velocity of stars characterized by the velocity dispersion $c_z(z)$ is related to the matter density in the disk $\rho(z)$. A vertical balance of forces is derived from the $z$-component of the Jeans equation for collisionless stellar disks (the Poisson equation), which, together with conditions $\rho(z=0)=\rho_0$, $\mathrm{d}\rho(0)/\mathrm{d}z=0$, and $\int_{-\infty}^{\infty}\rho(z;r)\,\mathrm{d}z=\Sigma(r)$ for a given surface density distribution $\Sigma$, determines the vertical disk structure at a given radius $r$. For $c_z=\mathrm{const}$, we have the solution

$$\rho(z)=\frac{\Sigma}{2z_0}\left(\cosh\frac{z}{z_0}\right)^{-2} \tag{8}$$

with the characteristic vertical scale $z_0=\sqrt{c_z^2/2\pi G\rho(0)}=c_z^2/\pi G\Sigma$. Equation (8), along with the exponential density distribution in the disk plane with the vertical scale $h_\mathrm{exp}$,

$$\rho(z)=\rho(0)\exp\left(-\frac{z}{h_\mathrm{exp}}\right), \tag{9}$$

is frequently used to fit the observed brightness profiles of galaxies seen edge-on [109–111].[1]

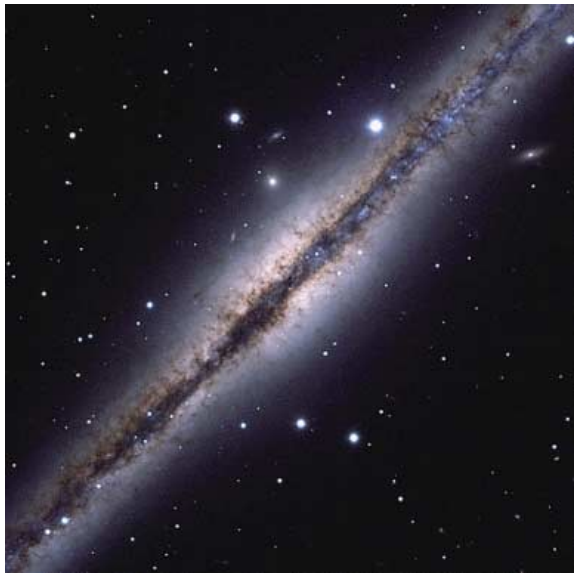

**Figure 15.** The galaxy NGC 891 seen edge-on (Hubble Space Telescope). A thinner gas–dust disk is visible inside the stellar disk.

For our Galaxy, analyzing the observed stellar density along the vertical coordinate perpendicular to the disk plane together with the velocity distribution allows measuring the local disk density near the Sun, which in turn enables a more precise decomposition of the galactic rotation curve and separation of the dark halo contributions. In doing so, data on red dwarf stars are frequently used. The red dwarfs are objects that make the largest contribution to the stellar population mass, although it is also possible to use less numerous red giants or main-sequence stars with better known distances. In any case, the resulting density estimates obtained from the stellar kinematics relate to the total disk density. By comparing the found local density of stars and gas, it is possible to constrain the DM density in the disk.

Because the disk thickness is small compared with its radial size, it is convenient to restrict the analysis to the balance

$$\frac{\mathrm{d}\left(\nu(z)c_z^2\right)}{\mathrm{d}z}=-\nu\,\frac{\mathrm{d}\Psi}{\mathrm{d}z}, \tag{10}$$

where $\nu$ is the relative density of stars in the sample (Fig. 15). However, even for the solar vicinity, the results of various authors give different local DM density estimates. For example, in [112], the surface density inside the disk thickness $\pm 350$ pc is estimated as $\Sigma(|z|<350\ \mathrm{pc})=(42\pm6)\,M_\odot\ \mathrm{pc}^{-2}$. With the baryonic density estimate uncertainty, this value is consistent with the absence of a noticeable amount of DM in the disk. A similar value of the surface density, $(44\pm4)\,M_\odot\ \mathrm{pc}^{-2}$ was found in [113], but for a thicker layer

[1] For some galaxies, the distribution $\rho\propto\cosh^{-1}(z/h_\mathrm{ch})$ (where $h_\mathrm{ch}$ is the vertical disk scale) was also used [108].

of $\pm 1$ kpc. The volume DM density in the solar vicinity is found in [113] to be $\rho_{\rm DM} = (0.0143 \pm 0.0011) M_\odot$ pc$^{-3}$. A close estimate $\rho_{\rm DM} = 0.016\, M_\odot$ pc$^{-3}$ is obtained from the spectral survey of G and K main-sequence stars [114]. In [115], by comparing the baryonic component density with dynamical density estimates, the total density of matter in the solar vicinity was found to be $(0.097 \pm 0.013) M_\odot$ pc$^{-3}$, with the DM density $(0.013 \pm 0.003) M_\odot$ pc$^{-3}$. Therefore, the DM fraction apparently attributable to the halo in the solar neighborhood is slightly more than 10% of the total matter density.

A review of different estimates of the local DM density and the total mass of the dark halo in the Galaxy, as well as of all the difficulties in their determination, can be found in [116].

**3.2.2 Disk mass estimate from vertical velocity dispersion.** In other galaxies, there is no way to estimate the $z$-component of stellar velocities with simultaneous direct measurement of the spatial density of the stellar population. Therefore, to estimate the local disk density, it is necessary to measure both the galaxy thickness and velocity dispersion. Here, two methods are used.

First, observations of galaxies seen edge-on enable direct measurements of the stellar disk thickness, and the velocity dispersion can be taken, for example, to be equal to its marginal gravitational stability value or can be estimated from the empirical relation between the velocity dispersion and the rotation velocity of a galaxy [117]. However, the accuracy of this method is low.

Second, the local disk density can be estimated from direct local velocity dispersion measurements, but the disk thickness should then be given a priori (usually, it is assumed to be constant and corresponding to a certain fraction of the radial scale or the photometrical disk size, although this is a rather crude approximation). This approach is most convenient for galaxies with inclination angles $i = 20^\circ - 30^\circ$ [118]. For these objects, it is possible to obtain the rotation curve with sufficient accuracy (at $i = 0$, the rotation velocity is directed perpendicular to the line of sight and cannot be measured), and the velocity dispersion of stars is close to that perpendicular to the disk plane.

Both these approaches lead to the conclusion that in most galaxies the disks are 'submaximal': the disk contribution to the mass at two radial scales, where it mostly contributes to the rotation curve, is slightly above 50% [118, 119]. The fraction of baryonic matter within these bounds increases from small galaxies to massive and rapidly rotating ones [62].

For edge-on galaxies, it is preferable to consider an equilibrium gas disk instead of a stellar one whenever the angular resolution of the radio telescope allows estimating the gas layer thickness, because the gas velocity dispersion weakly changes both along the radius and from galaxy to galaxy. Here, the gas velocity dispersion is measured either directly [120] or is assumed to be constant (around 10 km s$^{-1}$). Because the gas layer is inside the disk gravitational field, its thickness and velocity dispersion allow measuring the local spatial density of the disk. If the stellar disk thickness is known, we can pass to its surface density at different distances from the center and thus estimate the total disk mass. By separating the disk contribution from the circular velocity curve, it is possible to estimate both the halo mass [121, 122] and oblateness [123] from the observed rotation curve.

### 3.3 Estimates of masses of elliptical galaxies

Elliptical (E) galaxies almost never reveal extended gas disks, and their rotation velocities are much smaller than the stellar velocity dispersion; therefore, the mass estimation methods described in Section 3.2 are inapplicable. Stars move in elongated nonclosed orbits, and hence the notion of circular velocity $V_{\rm c}$, which is frequently applied to these galaxies, has the purely formal meaning of the velocity of conventional test particles in circular orbits. Some E galaxies can significantly deviate from the axially symmetric shape, which complicates the dynamical mass estimate.

The mass of E galaxies can be estimated by the following main methods.

• Based on the measured radial velocity dispersion of stars or globular clusters at various distances from the center, dynamically equilibrium models are constructed. Numerical models depend a priori on the unknown character of stellar motions: nearly circular orbits, orbits with an isotropic velocity distribution, and nearly radial orbits give significantly different results. However, assuming $V_{\rm c}(r)$ to be constant or slowly changing, it is possible to circumvent these uncertainties by jointly analyzing the brightness and radial velocity dispersion distributions. As shown in [124] (see also the references therein), observations allow choosing a radial distance interval (near the effective radius $R_{\rm e}$) in which the estimate $V_{\rm c}$ and hence masses depend on the character of the motion of stars very weakly (see the description of the method and results of its application for several galaxies in [124]).

• When a hot gas observed by X-ray emission is present, equilibrium models for gas coronae in the gravitational field of galaxies are constructed based on the hydrostatic equilibrium equation

$$-\frac{1}{\rho}\frac{{\rm d}P}{{\rm d}r} = \frac{V_{\rm c}^2}{r} = \frac{GM(r)}{r^2}\,,$$

where $P = \rho k_{\rm B} T/(\mu m_{\rm p})$ is the thermal gas pressure and $\mu \approx 0.6$ is the mean atomic weight.

• Methods of weak and strong gravitational lensing (see Section 4) are applied, which are very effective for galaxy mass estimates.

The above methods of mass estimate suggest that the distribution of the gravitational potential in E galaxies, as in disk galaxies, at large $r$ is close to the isothermal one, which means an increase in the DM-to-baryonic mass ratio with the distance from the center. In the central regions of galaxies, the DM mass contribution is small and the $M/L$ ratio is close to that expected for purely stellar models, but at large distances this ratio strongly increases, implying the presence of extended dark halos with the radial density distribution satisfactorily described by NFW profile (3), at least at large $r$ (see, e.g., [125–127]). There are grounds to believe that the DM content in E galaxies within optical boundaries is higher than in spiral galaxies [126]. However, the situation can be different from galaxy to galaxy. In rare cases (for example, in NGC 7507 — an isolated E-galaxy with a two-component stellar halo) dynamical modeling has not revealed signatures of a dark halo at all [128].

## 4. Dark matter from gravitational lensing and X-ray and gamma-ray observations

Progress in observations led to the appearance of new methods of mass distribution studies, including the invisible

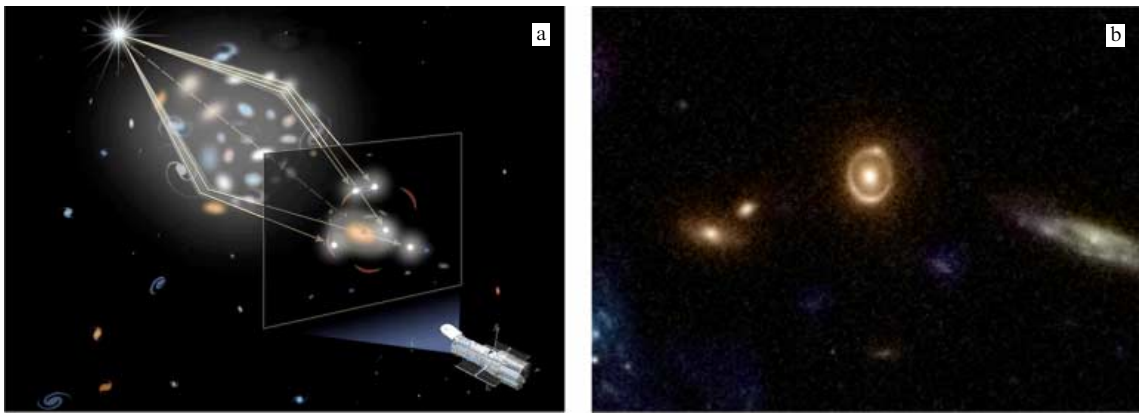


**Figure 16.** (a) Schematics of rays passing through a gravitational lens. (b) Image of an almost ideal Einstein ring on the gravitational lens 0038 + 4133 (Hubble Space Telescope).

component mass. The most impressive results were obtained from gravitational lensing of background sources by masses located between the source and the observer. Here, we discuss the methods for restoring the gravitational field of astronomical objects from gravitational lensing images; the interested reader is referred to papers [129, 130].

### 4.1 Gravitational lensing effects

Gravitational lensing offers the possibility not only of observing remote objects with multiple brightness amplifications but also of studying the lens itself, because its properties are determined by the spatial distribution of gravitating matter, including DM (Fig. 16). A gravitational lens has no focal point at which parallel rays converge; it is more appropriate to consider the focal straight line passing through the lens and the observer, with the rays from the remote object far behind the lens crossing this line at different distances depending on how far the rays pass from the lens center. The space bending caused by the gravitational field of the lens results in the appearance of several images of the source, which are generally very different in brightness. In the ideal case of an axially symmetric lens and an object lying exactly behind it, the source image stretches into a ring (Einstein ring). Such rings were first discovered in both radio and optical observations. The first optical image of the Einstein ring formed by a galaxy was obtained in 1997 by the Hubble Space Telescope [131].

There are several different gravitational lensing effects: the microlensing effect, when lenses are low-mass bodies (their nature is unimportant), and strong and weak lensing. Microlensing offers a unique opportunity to probe the DM halo in our Galaxy. The method includes the search for and statistical analysis of lensing effects from individual stars by objects of an arbitrary nature, which theoretically allows revealing the presence of unseen compact bodies of the planetary mass or much larger. The search for microlensing effects from single brightness enhancement of a star that accidentally lies in line with a gravitating body is a complicated process, which requires separation of physically variable stars and long-term monitoring of several million stellar images in densely populated patches of the sky. This method and its potential are discussed in [132–135]. We only note that the results of several independent groups searching for microlenses suggest that their total mass can amount to only a small fraction of the required mass of the galactic dark halo; apparently, the discovered microlenses are due to ordinary low-mass stars, which confirms the nonbaryonic nature of DM [136]. The only fact unaccounted for could be the presence of unusually heavy bodies, with a mass greater than $100M_{\odot}$ (primordial black holes?), which cannot be found by microlensing due to the long time scale of brightness variations [137]. However, there is no solid observational support for the existence of such exotic components of dark halos.

In strong lensing, the original image of a lensed source (a galaxy, or, less frequently, a quasar) is split into several images in the form of arcs and sometimes more complicated shapes. The strong lensing image allows estimating the lens mass or its density distribution if the distance to the lens and to the remote source is known (from redshift measurements). As a rule, a galaxy cluster serves as a strong lens; therefore, the lensing allows measuring the central mass of the cluster. In some cases, the lens is a galaxy [138] or its central part [139].

We note the interesting possibility of determining the internal structure of gravitating matter by the strong lensing (quadrupole lenses) of quasars with an anomalous flux ratio from observed multiple images, which are not described by a simple mass distribution model but can be explained by the microlensing effect on inhomogeneities (stars?) inside the lens galaxy. This offers the possibility to estimate the mass contribution from stars to the total mass of the lens galaxy. The analysis of 14 X-ray quadrupole images of quasars in [140] suggests a substantial excess of the distributed DM component at the mean projected distance of 6.6 kpc from the center of galaxies. This, however, is inconsistent with other results suggesting that in the inner regions of galaxies with normal brightness, the dark halo contribution to the total mass is significantly smaller than the stellar mass.

In the weak lensing effect for a large number of background galaxies, statistical methods are used to discover systematic distortions of the shape of remote background galaxies due to lensing by a closer galaxy (tangential stretching of images, which is less than 1% in each individual case) (see Fig. 16). Thanks to the weak lensing effect, it is possible to reconstruct the mass distribution around individual galaxies, as well as in clusters, and to estimate the mass of DM, which turns out to be dominant over other forms of matter, as expected [141].

For weak gravitational lensing, large sky surveys, such as CFHTLS (Canada–France–Hawaii Telescope Lensing Sur-

vey) [142], RSCS (Red-Sequence Cluster Survey) [143], SDSS (Sloan Digital Sky Survey) [144], COSMOS (Cosmological Evolution Survey) [145], etc., are important. Unlike dynamical methods (see Sections 2 and 3), weak lensing allows determining properties of lenses (i.e., the spatial distribution of gravitating matter) at larger distances from the center. This relates not only to galaxy clusters but also to individual massive galaxies.

To estimate the characteristic parameters of galactic halos, the effects of weak lensing by one galaxy (with a known redshift) of background dimmer galaxies (galaxy–galaxy lensing) are statistically analyzed by stacking a large number of images [146]. In [146], this approach was applied to the SDSS data and revealed, in particular, that galaxies with optically active nuclei do not differ from ordinary galaxies by halo masses; however, radio-loud active galactic nuclei were found to have about two times more massive halos for the same stellar galactic masses. This conclusion is far from certain if radio-loud quasars represent a short active stage of evolution. Another conclusion obtained by the same method relates the difference between the dark halo masses of 'active' star-forming galaxies (blue group) and 'passive' galaxies (red group), which predominantly include elliptical galaxies and some disk galaxies: with the same stellar mass, the halo mass in passive galaxies is about two times as high [147].

Importantly, even if the original density profile in a forming galaxy corresponds to the NFW profile, the integral density distribution, as well as the dark halo shape, can change during the formation of the 'baryonic' galaxy inside the dark halo. The authors of [147] applied the weak lensing method to elliptical galaxies from the SDSS survey to conclude that density profiles in the halo outskirts are consistent with the NFW profile. Here, the comparison of the NFW model with kinematic estimates of the stellar population in the inner, 'baryonic', part of the galaxies shows disagreement, suggesting that galactic dark halos apparently experienced adiabatic compression due to gravitation of baryonic matter.

Earlier attempts to match the density in the inner parts of elliptical galaxies (from strong lensing) and in outer parts of the same galaxies (from weak lensing) were made in [148]. The authors of [148] concluded that the integral density profile can be described by a two-component model: the de Vaucouleurs profile that describes the inner galaxy well, plus the NFW profile for outer parts of the galaxy. Here, the total profile satisfies the empirical relation $\rho \propto r^{-2}$ typically used for a pseudo-isothermal halo.

In general, the use of different methods, including weak lensing, consistently suggests a significant dominance of the dark halo mass (by an order of magnitude or more) inside the virial radius over the baryonic mass (of stars and gas) [148–150]. In the central parts of galaxies, gravitational lensing points to insignificant traces of dark mass, in agreement with dynamical modeling of the galaxy rotation curves. For example, parameters of the Einstein cross shown in Fig. 17 suggest that the DM fraction inside $r = 2/3R_e$ is less than 20% of the total mass [139]. According to [148], inside the effective radius of E galaxies, dark mass is on average about 1/4 of the total matter mass, and the virial mass of the halo is several dozen times as large as the baryonic mass (although the baryon-to-DM mass ratio should be close to 1/6 in the standard cosmological model).

We note that no lensing-related methods are applicable to low-luminosity galaxies with stellar masses $\sim 10^{10} M_\odot$ or below.

**Figure 17.** Example of the Einstein cross for the quasar QSO 22237 + 0305 (Hubble Space Telescope).

In Fig. 18, taken from [149], the $M_{vir}/M_*$ ratios of the total mass of galaxies inside the virial radius to the baryonic mass (of stars) are compared to the mass $M_*$ derived in various papers for early-type and late-type galaxies. The estimates of $M_{vir}$ are obtained by diverse methods, including the analysis of the kinematics of galactic satellites, weak lensing, parameters of galaxy groups, and comparing the rate of occurrence of galaxies with different stellar masses (the luminosity function of galaxies) with that of halos with different masses (the halo mass function), as followed from cosmological collisionless $N$-body simulations. The last method is referred to as halo abundance matching (HAM). A unique correspondence between the two compared quantities is assumed here. As seen from Fig. 18, there is a significant deviation between estimates obtained by the different methods, but generally the estimates suggest that the ratio of the virial halo mass to the stellar mass is above 30, with this ratio being systematically higher for massive early-type galaxies, in which it can exceed 100. The relative mass of stellar matter is less than 30% of the mean value expected in the standard cosmological model.

The increase in the virial halo mass with the stellar mass in galaxies and in galaxy groups is confirmed in [151] (Fig. 19), although so far there is no good agreement among estimates obtained by different methods.

To analyze the weak gravitational lensing effects around passive (red) and star-forming (blue) galaxies, data from a large sky region from CFHTLS comprising 154 square degrees were used in [152] together with a photometric survey carried out by the same telescope. Importantly, the gravitational effect of the baryonic component on the general distribution of the potential was taken into account. It was confirmed that the correlation between the stellar mass and DM mass is different for blue and red galaxies. As the stellar mass $M_*$ and luminosity of galaxies increases, the virial halo mass $M_{vir}$ increases faster for objects with an old stellar population ($\sim M_*^{1.5}$) than for star-forming galaxies ($\sim M_*^{0.8}$), which apparently is related to their different formation conditions.

### 4.2 Dark matter and hot gas coronae around galaxies

To date, thanks to the operation of the space X-ray observatories XMM-Newton (X-ray Multi-Mirror Mission), Chandra, and ROSAT (from the German Röntgensatellit), the characteristics of hot gas with a temperature of

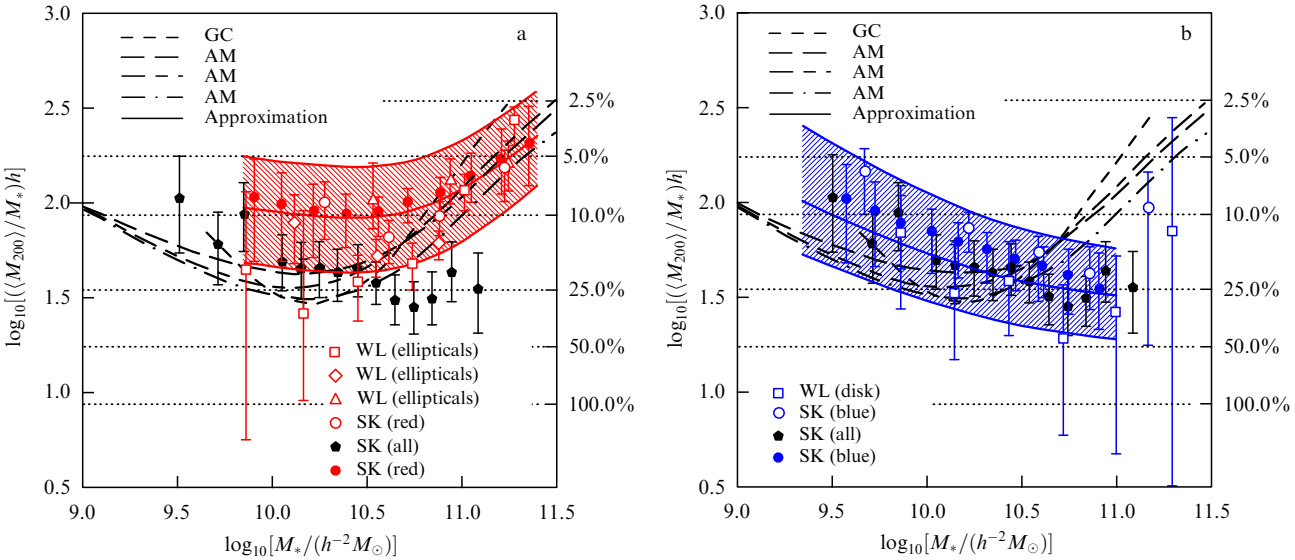


**Figure 18.** Virial-to-stellar population mass ratio $M_{\rm vir}/M_*$ for galaxies with different masses $M_*$ compiled from the literature (from [149]). The red symbols and the strip in panel (a) and the blue symbols and the strip in panel (b) respectively relate to early-type and late-type galaxies. The methods used: SK — galactic satellite kinematics, WL — weak lensing, AM — the HAM method, GC — from parameters of galaxy groups (see [149] for more details). The dark curves and symbols are the same in panels (a) and (b) and show the relations obtained irrespective of the galaxy type. The baryon fraction in stars relative to the expected cosmological value is plotted along the ordinates to the right. The Hubble parameter is assumed to be $H_0 = 100h$ km s$^{-1}$ Mpc$^{-1}$, the mass of stars is in units $h^{-2}M_\odot$, and the dark halo mass is in units $h^{-1}M_\odot$.

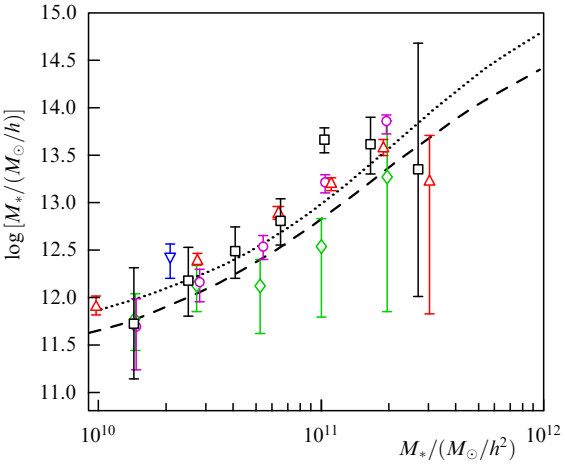


**Figure 19.** (Color online.) Comparison of the virial dark halo masses obtained from weak lensing for galaxies and galaxy groups with their stellar population mass. Various symbols show results of different studies (see [151] for more details).

$\sim 10^6$ K inside and around several giant elliptical galaxies and in several disk galaxies have been measured [153–156].

The X-ray coronae suggest the presence of a significant amount of dark mass, without which a galaxy could not retain the hot gas (see, e.g., [157]). The observed hot gas parameters enable evaluating the mass necessary to retain it, and measuring how the total mass $M(r)$ changes with the distance from the galaxy center. For estimates, the simple formula for hot gas equilibrium in the gravitational field of a galaxy with a massive halo can be used assuming centrally symmetric thermal gas velocities $c_{\rm g} \sim \sqrt{GM/R}$. This yields the temperature $T \sim GMm_{\rm p}/(3k_{\rm B}r)$, where $m_{\rm p}$ is the mass of the proton and $k_{\rm B}$ is the Boltzmann constant. For example, for $M = 10^{12}M_\odot$ and $r = 20$ kpc, the temperature is $T \simeq 10^6$ K.

Simultaneous analysis of the temperature and intensity of X-ray emission from gas coronae around bright elliptical galaxies enables constructing the total gravitational potential, which suggests the presence of a massive extended dark halo. We note that a noticeable increase in $V_{\rm c}(r)$ is observed in some bright elliptical galaxies [158, 159],[2] whereas in disk galaxies the circular velocity $V_{\rm c}(r)$ is usually constant beyond the optical radius. For $r \geqslant 2R_{\rm e}$ (where $R_{\rm e}$ is the effective radius of a galaxy), dark mass dominates over the baryonic mass. A similar conclusion regarding the dark halo parameters was obtained from the kinematics of planetary nebulae [160, 161].

The presence of unresolved X-ray binaries, ultra-compact young stellar objects (YSOs), and X-ray remnants of the evolution of massive stars gives additional uncertainties when inferring DM properties from X-ray observations of gas around galaxies. The hydrostatic equilibrium can be too crude an approximation, especially for galaxies in which gas was influenced by the active galactic nucleus.

Despite these difficulties of DM estimates from X-ray coronae of spiral galaxies, pioneering papers have appeared that study a hot gas beyond the optical disks (galaxies NGC 1961 and NGC 6753, [154, 156]). The relative mass of baryons inside $(0.05-0.15)R_{\rm vir}$, where $R_{\rm vir}$ is the virial radius, turned out to be around 0.1 for these galaxies, which is already close to the values predicted by cosmological models. This means that the halo gas can contain a sizable fraction of all baryonic matter in such galaxies.

### 4.3 Dark halo and gamma-ray emission

Indirect evidence of the existence of weakly interactive massive particles (WIMPs) forming DM can be obtained from searches for theoretically predicted high-energy gamma-radiation or neutrino emission from the annihilation of DM particles and antiparticles in rare collisions. The birth of high-energy photons from particle annihilation can significantly

[2] We recall that the circular velocity is formally defined as the rotation velocity of a test particle in a circular orbit. The galaxy itself cannot rotate.

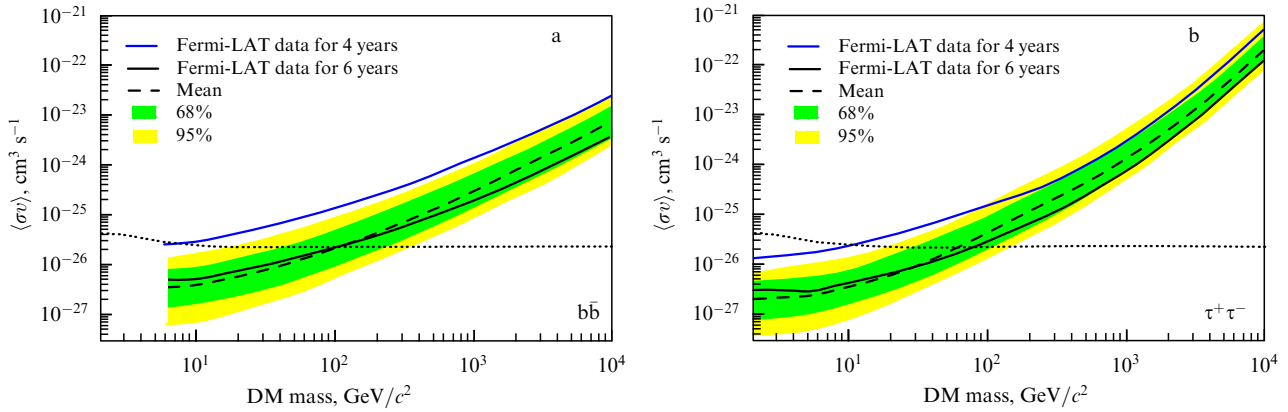


**Figure 20.** (Color online.) Bounds on the DM particle (WIMP) annihilation cross section as a function of its mass for two possible annihilation channels: (a) $b\bar{b}$ and (b) $\tau^+\tau^-$ obtained from the results of searches for excessive gamma emission in the direction of 25 dwarf spheroidal galaxies (Fermi Large Area Telescope (Fermi-LAT) data). The width of color bands corresponds to confidence levels of 68% and 90%. The blue solid line shows the results of previous measurements of 15 galaxies over four years. The dashed, almost horizontal, curve is the cross section calculated for an isotropic annihilation background from relic WIMPs. (From [167].)

contribute to the cosmic gamma-ray background (CGB) in a wide energy range (see review [168]). In theory, the annihilation radiation can be detected from regions with an especially high density of DM particles. In our Galaxy, it is the galactic center region, but there are many gamma sources of another nature, which hampers detection of the annihilation radiation, if it does exist. Dwarf spheroidal galaxies without young stars, where DM strongly exceeds baryonic matter in mass, could be more suitable.

Detection of the annihilation signal from DM particles could shed light on their nature and would provide independent constraints on the dark halo parameters. This is complicated by two facts, however. First, the annihilation quanta can be produced in several branched channels, which causes great uncertainty in the expected gamma-ray flux and its spectrum. Second, the presence of the annihilation excess depends both on the model DM distribution and on background sources unrelated to DM, which are difficult to take into account. Because the rate of annihilation events in DM particle collisions per unit volume is proportional to the relative velocity of particles times their effective annihilation cross section and their squared number density, the annihilation flux (number of photons per cm$^2$ per second) can be expressed as

$$F = \frac{N_\gamma \langle\sigma v\rangle}{2\, m_{\rm DM}^2} \int_V \frac{\rho_{\rm DM}^2(\mathbf{x})}{4\pi\, d^2(\mathbf{x})}\, {\rm d}^3 x\,, \qquad (11)$$

where $N_\gamma$ is the number of photons in one annihilation event, $\langle\sigma v\rangle$ is the averaged product of the relative velocity by the effective annihilation cross section, $\rho_{\rm DM}$ is the DM density, $V$ is the halo volume, $m_{\rm DM}$ is the mass of a DM particle, and $d$ is the distance between the halo and the observer.

Excessive gamma-ray emission was detected from the galactic center region [163], with the signal power being sufficiently high for the spectrum and angular resolution to be measured. However, distinguishing the annihilation signal from gamma-ray emission from other processes in the galactic center remains a difficult and ambiguous task. According to [164], the DM profile in the Galaxy has a cusp with a logarithmic slope $> 1.5$. However, later analysis of the HESS (High Energy Stereoscopic System) data led to the opposite conclusion, that the DM distribution in the galactic center demonstrates no cusp [165]. As a result, the data on the gamma-ray emission from the galactic center have so far not been uniquely interpreted. Despite the possibility of explaining the observations without DM, it is still too early to state with certainty that they contradict model DM distributions due to uncertainties in the foreground and background sources.

Another channel of information on WIMP annihilation is provided by searches for excessive gamma-ray emission from galaxies in which the DM mass significantly dominates over the baryonic mass. These are dSph dwarf galaxies like the satellites in our Galaxy. Because the dwarf galaxies show no intensive star formation, their gamma-ray emission is almost free from the intrinsic gamma-ray background noise, which gives hope to observe DM annihilation signatures more clearly. These galaxies are being studied by both space observatories and ground-based Cherenkov gamma-ray telescopes in a very high energy range. Although the results have been negative so far, they do not rule out the existing DM models due to uncertainty of the expected flux estimates and complications related to the gamma-ray background [166]. Nevertheless, the observational data are already putting certain constraints on the parameters of DM particles [167, 168].

In Fig. 20, taken from [167], we show the upper bounds on the annihilation cross section for different WIMP masses calculated for two possible annihilation channels, obtained from six years of observations of 25 dSph galaxies by the Fermi gamma-ray space observatory (Fermi-LAT telescope). The nearly horizontal dotted line is the calculated annihilation cross section for the background emission from relic WIMPs, assuming that they form all of the DM and were in thermal equilibrium in the early Universe. In spite of the lack of observed annihilation fluxes, it is possible to infer upper bounds on the annihilation cross section and WIMP masses, although with a large uncertainty.

## 5. Shape and structure of dark halos

Cosmological models describing the evolution of collisionless DM demonstrate the formation of triaxial DM halos (Fig. 21). Differences in the density profile scales along different directions correspond to the ellipticity $\varepsilon$ about 0.3

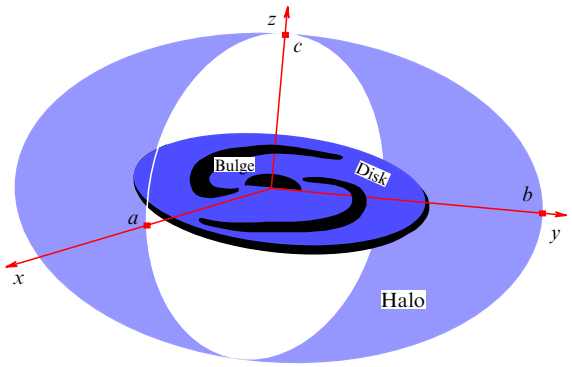


**Figure 21.** (Color online.) Structure of a galaxy in a triaxial halo with semiaxes $a$, $b$, $c$. Shown are the halo cross sections by perpendicular planes.

(for a spherical halo, $\varepsilon = 0$). Interaction with the dissipative component changes the central ellipticity, but at the outskirts the effect of this interaction is insignificant [169].

Measuring the shape and structure of dark halos can be used to test their formation models and hence galaxy formation models. Moreover, any statistically significant proof of the nonsphericity of the DM halo is an argument against the dark halo explanation without DM, as is proposed, for example, in the modified Newtonian dynamics, where the difference from the classical Newtonian gravity field is related to the gravitational acceleration of particles or to the radial coordinate, but does not violate isotropy.

In our Galaxy, the velocity dispersion anisotropy of halo stars can indicate a structure and possible anisotropy of the dark halo in whose gravitational potential the stellar component was formed [170]. A statistical analysis of the shapes of disks in other spiral galaxies indirectly points to an asymmetry of the potential in the disk plane, at least for some galaxies, which may suggest the motion of stars in the field of a triaxial halo. For example, according to [171], in the photometric $K_s$-band, the ellipticity of disks is 0.02 for late-type spirals Sc–Sd (i.e., their disks are almost circular); however, it reaches 0.30 for early-type galaxies. But despite indirect evidence for a triaxial density distribution in halos, their shape and ellipticity for individual galaxies are poorly known so far, and, moreover, the estimates of halo shapes are sometimes contradictory.

In some papers (e.g., [172–178]), different aspects of the effect of a nonaxially symmetric gravitational potential on the dynamics of galactic disks were studied. In particular, it was noted that the triaxial halo shape complicates interpretation of the galaxy rotation curve and velocity field, especially if the dark halo dominates even in the inner galaxy (for example, in LSB galaxies) [177, 179]. Warped galaxies can also be well described by numerical $N$-body models with triaxial dark halos [180, 181]. Triaxial halo perturbation effects of the already existing bar could be significant [176, 182–185]. The angular momentum exchange between the halo particles and the bar can destroy the bar structure [186].

Nevertheless, it should be recognized that the role of halo asymmetry in the dynamic evolution of star–gas disks remains unclear. Because quantitative estimates of the halo oblateness or triaxiality are sparse, the analysis of numerical simulations is important in studies of their shapes and effects on the disk dynamics.

### 5.1 Halo shape from numerical models

Cosmological $N$-body simulations provide a large amount of information on the plausible structure of dark halos, in particular, on the shape, mass distribution, and kinematics of DM. Usually, it is initially assumed that the dark halos generally have a triaxial shape balanced by anisotropic velocity dispersion [178, 187–190], with the azimuthally averaged density profile of a sufficiently universal shape in a wide range of masses and redshifts [the NFW profile in Eqn (3)] (see, e.g., [55, 191–193]).

When studying the halo evolution, it is not possible to ignore the baryonic component, which during the formation of a galaxy is concentrated in the center by forming a star–gas system and affects the general mass distribution, including the DM profile. Models taking the baryonic matter feedback into account, including star formation and the active nucleus role in the energy powering of gas, put constraints on the dark halo parameters, in addition to those from the classical $N$-body method [55, 194].

When stellar components of a galaxy form in the central halo, the angular momentum exchange between the dark and baryonic components must have altered the initial halo shape [195]. The effective radiation cooling provides baryon concentration in the halo center to form a disk balanced by rotation. In this scenario, the dark halo, via gravitational interaction with the disk, becomes more oblate, with the ratio of semiaxis density distribution $s = c/a \approx 0.85$ approximately constant along the radius [196, 197].

Different collisionless cosmological cold dark matter (CDM) models yield different values of the DM halo axis ratio $s$. It depends on the initial conditions and decreases as the halo virial mass increases, and for a given mass this ratio is higher at lower redshifts (Fig. 22) (see [189]). For the present epoch ($z = 0$), a more spherical halo shape is obtained than at the early evolutionary stages. Remarkably, the halo shape transformation occurs already after the hierarchical DM halo formation at redshifts $z < 2$.

Cosmological models predict a certain dependence of the ratios $b/a$ (in the disk plane) and $c/a$ as a function of the distance to the halo center [178, 179, 189]. As a rule, the central halo is more asymmetric than at the periphery, where

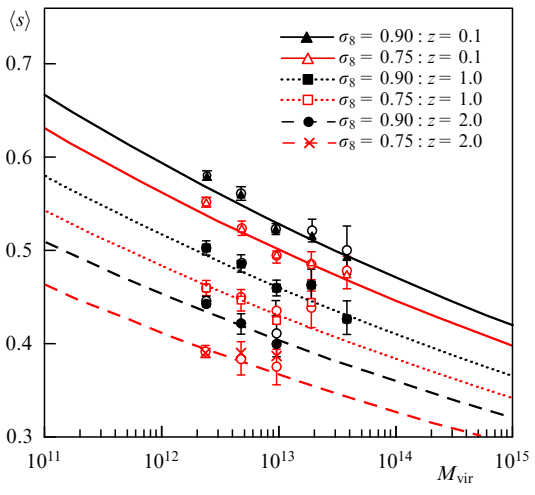


**Figure 22.** The DM halo axis ratio $s = c/a$ as a function of the halo virial mass for three redshifts $z$ and different values of the $\sigma_8$ parameter describing the fluctuation spectrum in the ΛCDM model. (From [189].)

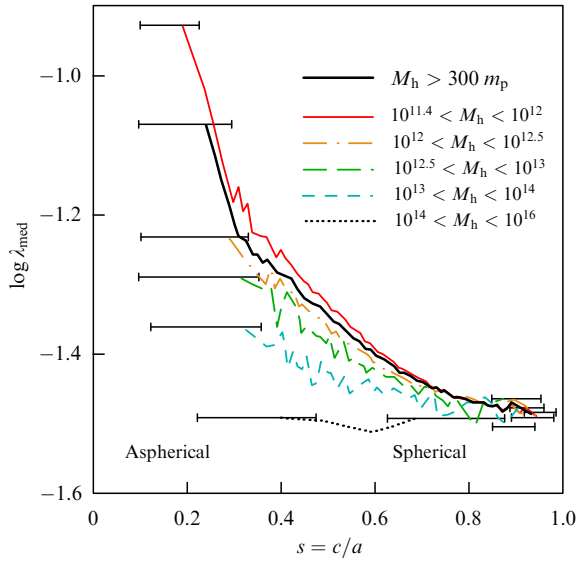


**Figure 23.** (Color online.) Halo shape at $z = 0$ vs. the median spin $\lambda_{med}$ according to $N$-body simulations (from [190]) for halos with different virial masses. The dark curve is the mean value over more than 300 particles. For each plot, the horizontal bars show the range inside which the averaging was done. There is an anticorrelation between the spin and the DM halo axis ratio, which is strongest for aspherical halos.

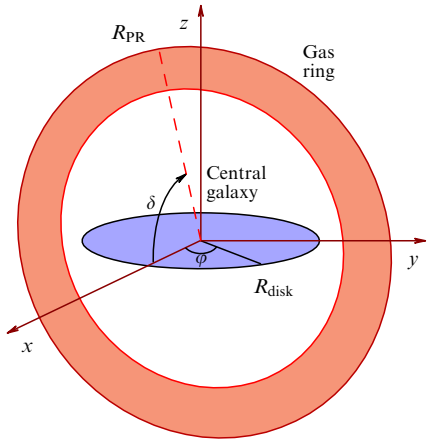


**Figure 24.** (Color online.) Structure of a polar-ring (PR) galaxy. Shown in blue is the central galaxy (most frequently, S0), and in red, the polar ring mostly consisting of gas.

$b/a$ and $c/a$ asymptotically tend to unity. This effect is found in most numerical cosmological models, including those with a large number of particles $N \geqslant 10^8$ (for example, in the Via Lactea project [198]). However, quantitative results in various models can differ widely, depending not only on the numerical model parameters but also on the spectrum of initial perturbations (see Fig. 22).

The possibility of halo rotation has also been studied to date only from numerical cosmological simulations. DM halos, despite being balanced as a whole not by rotation but by velocity dispersion, can have a nonzero integral angular momentum. Analyses of various nondissipative cosmological simulations suggest that more 'spherical' halos rotate significantly more slowly than nonspherical ones (see, e.g., [190, 199]) (Fig. 23). We note that the reliability of model relations suffers from halos being nonfully relaxed systems; in addition, they can experience tidal interactions with nearby galaxies.

### 5.2 Galactic polar rings and tidal streams as dark matter markers

Polar rings are extended looped or nonclosed rings of stars and the gas–dust medium rotating around the galaxy center in the plane tilted by a large angle to the main galactic disk (in disk galaxies) (Fig. 24) [200–204]. There are around 300 known galaxies with polar rings (PRGs) [205]. On rare occasions, the angle $\delta$ between the galaxy and the polar ring can differ greatly from 90°, for example $\delta = 73°$ in the galaxy SPRC-7 [206].

Polar rings around galaxies are thought to form due to the close passing of a neighboring galaxy (satellite) accompanied by a loss of some mass by the latter [207, 208] or by its total tidal disruption [209], or they result from the accretion of cold gas in the galaxy from cosmological filaments [210, 211]. Irrespective of the formation scenario, the existence of two connected galactic substructures rotating in mutually perpendicular planes allows estimating the three-dimensional gravitational potential in the galaxy, including the mass and shape of the DM halo [204, 212]. Initially, the ring–disk inclination could be arbitrary. The dominance of polar rings suggests that ring planes rapidly evolve to an orthogonal orientation. An important argument in favor of a nonaxially symmetric halo in PRGs is the stability of polar orbits just for such gravitational potentials [213].

The first collection to include confirmed PRGs, PRG candidates, and most probable PRGs was published in [207]. The list of known PRGs was significantly extended based on the SDSS data [205]. Polar rings are mainly observed around Sa–S0 galaxies, which have no significant amount of gas at the periphery and therefore there are no complex interactions of supersonic gas streams. Due to the small amount of cold gas and weak emission, the rotation curves of such galaxies are known, as a rule, only for the innermost parts, but spectral observations of a ring many times larger than the exponential scale of the main galaxy disk offers the possibility of measuring the circular velocity at the galactic periphery. To compare rotational velocities of the disk and the ring, it is very important to 'continue' the rotation curve as far as possible from the galactic center using absorption lines in stellar spectra and to match it with the gas kinematics in the polar ring [214–216].

Estimates of the mass and shape of the dark halos for several PRGs were obtained as early as the 1980s [217]. However, even presently the results remain quite contradictory. For example, for the best studied PRG, NGC 4650A, the first measurements of the halo shape based on isolines of the gravitational potential suggested a nearly spherical halo with the semiaxis ratio $c/a \sim 0.86 \pm 0.21$ [217]. A similar result was obtained for another two PRGs (ESO 415-G26 and A0136-0801) by comparing the two maximum rotation velocities in the polar ring and the central galaxy disk. Later, a more careful analysis of the rotation curves based on the decomposition of the circular velocity into two mutually orthogonal directions for NGC 4650A (Fig. 25) suggested a highly oblate halo toward the central galaxy plane: $c/a \sim 0.3–0.4$ [214].

An estimate of deviations of the gravitational potential from the spherical shape was attempted in [215] based on the location of PRGs on a Tully–Fisher diagram relating the galactic rotation velocity to its luminosity. Using the

**Figure 25.** One of the best-studied PRGs, NGC 4650A (Hubble Space Telescope).

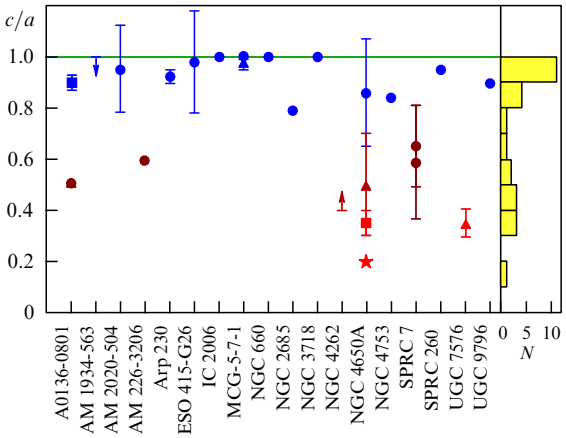


**Figure 26.** (Color online.) Halo oblateness $c/a$ in PRGs compiled from the literature. To the right is the number of galaxies with a given axis ratio. References: A0136-0801 [214, 220], AM 1934-563 [221], AM 2020-504 [222], AM 236-3206 [217], Arp 230 [223], ESO 415-G26 [224], IC 2006 [225], MCG-5-7-1 [223, 226], NGC 660 [227], NGC 2685 [228], NGC 3718 [229], NGC 4262 [206], NGC 4650A [200, 214, 217, 230], NGC 4753 [231], NGC 5122 [226], NGC 5907 [232], SPRC 7 [206], SPRC 260 [233], UGC 4261 [234], UGC 7576 [235], UGC 9796 [236]. (Data on NGC 5122, NGC 5907, and UGC 4261 can be found in the cited references.)

observed Doppler width of the integral HI line profile as an indicator of the rotation velocity, the authors of [215] found that the positions of PRGs on the Tully–Fisher diagram are noticeably different from ordinary galaxies: most of the PRGs are shifted toward larger velocities [215]. A comparison with model disk galaxies with polar rings allowed interpreting this feature by the interaction of the ring with a halo extended along the minor disk semiaxis [218, 219]. For NGC 4650A, the semiaxis ratio $c/a$ is close to 2 [215]. Figure 26 presents the data on the dark halo shapes compiled from the literature.

An effective approach to determining the halo parameters is based on constructing a numerical self-consistent gas-dynamic $N$-body model for the disk and the polar ring taking the dark halo potential into account. From a comparison of the results of numerical simulations with photometric and kinematic parameters of the star–gas disk of the main galaxy, all basic halo characteristics can be obtained. In some cases, a sufficiently complicated dark mass distribution was found [206]. For example, the dark halo shape in NGC 4262 was found to depend on the radius: it is significantly flattened in the immediate vicinity of the galactic disk ($c/a \simeq 0.4$), but stretched along the minor semiaxis far away from the center ($c/a \sim 2$) [206]. A similar complex character of the DM distribution follows from numerical cosmological simulations of PRG formation. A change in the spatial orientation of the halo major semiaxis was found in [208], which in fact means a change in the halo shape with distance. For example, in the central parts of a galaxy, the halo can be flattened toward the central galaxy plane, while far away from the center the halo can be flattened toward the perpendicular plane. With such a complicated halo shape, it is not surprising that contradictory estimates of the halo oblateness in galaxies like NGC 4650A are obtained. Confirming the changeable halo shape for PRGs can significantly modify our understanding of the structure and DM mass both in ordinary disk and in elliptical galaxies.

Other information about the halo shapes can be inferred from stellar tidal streams found in our Galaxy halo and in some other galaxies, which resulted from tidal disruption of dwarf galaxies (see, e.g., review [237] as well as [238–241]). In fact, these are test halo objects, along which a velocity change reflects the matter distribution far from the disk. The dynamics of destroying the satellites depends on the main halo mass profile; therefore, the spatial and kinematic parameters of formations observed far from the disk plane can be very important tracers of the dark halo shape and orientation.

Measurements of the observed shape and radial velocity distribution along tidal streams can significantly constrain the possible shape of equipotential halo surfaces [242]. From observations of the Sagittarius tidal stream, Sagittarius dSph [239], the halo axis ratio was derived to be $c/a \geqslant 0.8$, which means that the halo can be spherical [234], but if this stream is dynamically young, then $c/a \simeq 0.6$ is required [244]. Later, a three-dimensional $N$-body model of the stream motion in a triaxial halo was constructed, which simultaneously explained its location and kinematics for the halo axis ratio $c/a = 0.72$, with the halo minor semiaxis lying in the stellar disk plane (!) [245].

Studies of the dark halo structure from observations of the GD-1 tidal stream [246] seem very promising. The GD-1 stream is a long and very thin formation with well-distinguished density disruptions (about ten) along the length. From the numerical model, it was proposed that one of the possible reasons for the density disruptions could be a fly-by of a subhalo near the stream. This requires that there be about 100 subhalos in the Galaxy with masses $\leqslant 10^6 M_\odot$ inside the radial distance to the stream orbit apocenter (about 30 kpc).

Studies of the stellar tidal stream in the galaxy NGC 5907 yielded $c/a = 0.5$ for the halo [247, 248].

### 5.3 Other sources of information about dark halos

The halo shape affects the distribution and velocity of motion of all its components. For example, the kinematics of globular clusters and dwarf satellites of the Andromeda Nebula suggest a prolate dark halo shape with the major semi-axis perpendicular to the stellar disk plane [249]. We note that the large stellar halo of the Andromeda Nebula extending to several optical radii has a shape ruling out the strong oblateness of the external halo toward the disk plane and rather suggesting prolateness in the perpendicular direction [241].

However, the correspondence between the dark halo and the stellar halo shapes remains unknown. For example, the shape of the latter in our Galaxy was inferred from the distribution of stars near the turning point of the main sequence obtained in the survey by the Canada–France telescope in Hawaii (CFHTLS). The halo axis ratio was

found to be $c/a = 0.70 \pm 0.10$ (within the galactocentric distance 5–35 kpc), which almost coincides with the estimate $c/a = 0.72$ inferred for the dark halo from the kinematics of the Sagittarius tidal stream [245]. However, the directions of the halo minor semiaxis found in these papers do not coincide.

The characteristic halo axis ratio can be found from gravitational lens statistics, although this method is reliable only for axially symmetric halo models. To determine the halo shape, weak gravitational lensing seems to be the most appropriate: initially, an ellipsoidal halo model is assumed and its parameters are determined from the best fit of observational data [250]. The first such measurements of the halo ellipticity were carried out in [251], with the ratio of the halo ellipticity $\varepsilon$ to the brightness distribution ellipticity found to be $0.77^{+0.18}_{-0.21}$; in other words, the halo turned out to be more 'spherical' than the visible matter distribution. Taking the ellipticity of lenses into account allowed finding the DM halo ellipticity equal to 0.3. According to [252], halos around elliptical galaxies seem to be even more oblate.

The weak lensing method was applied in [253] to about 70,000 giant elliptical galaxies (from the SDSS digital sky survey) with virial masses $\geqslant 10^{13} M_\odot$. The best-fit results correspond to a halo with the axis ratio $c/a = 0.78$. The halos turn out to be more spherical than for galaxies with an order-of-magnitude smaller masses ($c/a = 0.62$ according to [254]). However, accounting for the possible difference between the symmetry axis in the dark mass and galaxy brightness distributions, which can be expected from numerical cosmological models, decreases the resulting $c/a$ ratio and brings these estimates for galaxies with different masses into agreement.

Strong gravitational lensing was used to estimate the degree of oblateness of the dark halo of individual galaxies only in some cases. For example, strong lensing data in combination with the results of analyses of star and gas kinematics in the galaxy SDSS J2141 at the redshift $z = 0.14$ suggested that the galaxy has a significant (but not dominant inside the optical disk limits) DM halo mass, which is satisfactorily fitted by the NFW profile and, apparently, is slightly 'compressed' toward the galaxy plane ($c/a = 0.75^{+0.27}_{-0.16}$) [255].

Other information on the halo shape can be obtained from measuring the cold gas thickness in the disk. The equilibrium gas-layer thickness depends on both the stellar disk density and the density of the halo and the gas itself, which increasingly contributes to the total disk gravitational potential as the radial distance increases. Therefore, the dark halo shape within the optical disk of a galaxy and near it can be probed from the analysis of the HI gas layer thickness change with the distance from the center (flaring gas layer), assuming that the gas turbulent velocity dispersion is isotropic. Of course, the most reliable results are obtained for edge-on galaxies, because in them the gas layer thickness can be measured directly [256, 257]. As shown in [258], the radial profile of the HI layer thickness in our Galaxy agrees better with the halo model prolate along the minor axis of the Galaxy than with a spherical halo model: the axis ratio reaches $c/a = 2$ at $r = 24$ kpc. However, for the edge-on galaxy UGC 7321, observations of HI suggest a gravitational potential distribution close to that of the spherical isothermal halo model [256]. The radial dependence of the HI vertical scale in M31 is best fit by an oblate halo model with the axis ratio $c/a = 0.4$ [259].

Thus, contradictory results have been obtained for diverse galaxies. We note that the methods for determining the halo shape from flat components should be applied with caution, because the results are model dependent and not very sensitive to the halo density distribution at large distances from the disk plane. In addition, for periphery regions of the gas disk, the hydrostatic equilibrium assumption can be too crude.

The existing methods for determining the dark halo shape suggest plausible deviations of the halo density from spherical symmetry, and not only near the disk plane but also far beyond its boundaries, although quantitative estimates of the halo shape for individual galaxies are not always in agreement with each other, and the whole picture remains quite controversial. Nevertheless, we have gradually come to the understanding that the halo can have a triaxial spatial shape and, moreover, the orientation of the disk and halo axes can differ significantly (see models in [260]).

We list possible processes capable of affecting the halo shape. Dissipationless cosmological models predict triaxial halos whose shape reflects the anisotropic character of matter compression during their formation. Accounting for hydrodynamic processes in baryonic matter (gas) that forms a dissipative medium inside a collisionless halo must decrease the triaxiality effect by making the halo shape more spherical (see, e.g., [195]). At the same time, the formation of massive disks at halo centers inevitably leads to the halo flattening toward the galaxy plane. The efficiency of these processes is different at various spatial scales, which complicates the picture. In addition, the accretion of matter onto the halo from intergalactic space, as well as the escape of gas from galactic disks, continues after the galaxy formation, which affects the general mass distribution. The most general statement is that the mass distribution in the halo can be anisotropic and different at various distances from the center. It would also be correct to accept that galaxies can have various halo shapes.

### 5.4 Subhalos

We also draw attention to the possible structure of dark halos: in addition to spatially distributed DM, extended galaxy halos can include smaller structures that could form during initial perturbation growth (see [261, 262] and the references therein). High-resolution cosmological models demonstrate systems of substructures, also known in the literature as subhalos, minihalos, and microhalos (which can be called 'halolets'). The typical number of such halolets with $\gtrsim 10^{-6} M_{\rm vir}$ (about $10^6 M_\odot$) in a large halo with the size $R_{\rm vir} = 400$ kpc in the Via Lactea simulations exceeds $10^4$ [262], and in the Via Lactea II, GHALO (Galactic dark matter halo) models, their number can be as high as $10^5$ inside a 200 kpc region. These gravitationally bound formations are in turn triaxial structures with $a \neq b \neq c$ slowly changing over cosmological time. Their relative scales are characterized by the axis ratios $\langle q \rangle = b/a = 0.8-0.9$ and $\langle s \rangle = 0.6-0.9$, and they have a complicated spectrum of masses, sizes, spin, and internal kinematics [198]. There are traces of the internal structure of the halolets themselves; therefore, it is possible to believe that a complex hierarchical system of scales — from several hundred kiloparsec to fractions of a kiloparsec — is formed in a dark halo.

The halo mass functions inferred from numerical structure formation models are in agreement with the spectrum of masses (internal velocities) of galaxies and their systems;

however, the observed number of dwarf galaxy satellites of the Milky Way and other large galaxies turns out to be too small compared with the number of more massive galaxies [263, 264]. Therefore, the problem of low-mass subhalo detection remains relevant, providing additional verification of cosmological models. Being a mixture of dark and baryonic matter, subhalos can both contain stars and be fully starless. In the first case, they must be observed as dwarf satellites of DM-dominated galaxies, while in the second case they can be difficult to discover. A large number of fully dark dwarf galaxies almost free from baryonic matter may exist: the gas can be lost in the course of evolution due to ionization or sweeping-out when moving in a medium, such that stars had no capability to form. If this is confirmed, the very term *galaxy* will need to be clarified.

The dynamic-to-baryonic mass ratio in very low-mass dwarf galaxies amounts to several hundred solar units, which is likely related to the lack of conditions for active star formation in these objects at all stages of their evolution due to the low density or a small amount of gas. When cold gas is present, subhalos can be observed as compact HI regions with a very low and even undetectable optical luminosity, but they can be difficult to separate from tidally formed clouds observed near interacting galaxies without analyzing their internal motions [265]. Amazingly, recently in one of the HI clouds near the dwarf galaxy Leo T, traces of regular gas rotation were discovered, allowing the determination of its dynamic mass ($\sim 10^8 M_\odot$), which is several dozen times higher than the observed gas mass. There are no signatures of stars in the cloud [266], i.e., the mass–luminosity ratio is extremely high: stars in this structure, apparently, had not formed at all.

The inconsistency between the observed number of dwarf satellites and the ΛCDM model predictions for subhalos is an open and actively discussed issue (see, e.g., [267–269] and the references therein). The problem is partially solved by accounting for the effect of baryonic matter and star formation on the DM density profile and distribution inside a subhalo [269]. One of the proposed solutions is to use a cosmological model with 'warm' DM, in which low-mass subhalos have a low central density, which changes the relation between the observed and predicted number of dwarf satellites with a given velocity of internal motions [270]. Nor can it be ruled out that the number of subhalos is indeed very high, but in the vast majority of cases they do not contain a sufficient number of baryons to be detectable by radiation.

## 6. Dark halos and structure details of the disk

### 6.1 Dark halos and galactic bars

A significant portion of S galaxies belongs to the SB type, in the centers of which an oval-like stellar structure called a bar is observed. The size of a typical stellar bar varies in a wide range $r_{\rm bar} \simeq (0.1-0.5)R_{\rm opt}$; therefore, sufficiently long bars go well outside the region where the bulge gravitation dominates, and hence the bars are controlled by the disk and halo gravitational fields. Stellar bars form due to gravitational instability of the so-called bar mode. Most progress in its studies is obtained from *N*-body numerical simulations, pioneered in [271], where the disk stability condition relative to the global bar mode was formulated: $T_{\rm rot} < 0.28T$, where $T$ is the total kinetic energy of stars and $T_{\rm rot}$ is the kinetic energy of rotation. The gravitational field of the halo decreases the effect of disk self-gravitation by hampering bar formation owing to the gravitational instability suppression.

As regards a collisionless gravitating system with $T_{\rm rot}/T \sim V^2/(V^2 + 2\,c_r^2)$, up to an order of magnitude we have $c_r \sim V$; hence, without the spheroidal component of a galaxy, the disk must be very hot to stabilize the bar mode. The bar-mode stabilization conditions depend on many factors (the spatial distribution of the matter density, kinematical parameters, the bulge and its properties) [46]; however, under otherwise equal conditions, a more massive halo stabilizes the bar mode at smaller stellar velocity dispersion in the disk.

Well-distinguished bars are observed in almost one third of disk galaxies, and if the weaker bars best seen in IR images are taken into account, the fraction of barred galaxies exceeds 50%. This evidences a long life of galactic bars. Nevertheless, a bar, by rigidly rotating inside a galaxy, can evolve and be destroyed by gravitational interaction with slowly rotating components (the halo and/or the bulge). This interaction is similar to the dynamic friction of a massive body moving relative to the surrounding stars. Due to the loss of angular momentum, the bar length $r_{\rm bar}$ should increase with time, and its angular velocity $\Omega_{\rm bar}$ should decrease, and with time the bar should 'dissolve' by dynamically heating the ambient inner disk (see, e.g., [272, 273]). The bar, however, is not long-lived at a high matter density in the galactic center (the result of scattering of stellar orbits), which could initially exist or appear, for example, due to the motion of part of the gas toward the disk center.

If we account for not only the effect of a halo on the disk and its structure but also the back reaction of the bar on the halo, i.e., pass from a 'rigid' to a 'live' halo model, then the picture becomes not so simple: although at the initial stage of the bar growth its formation occurs more rapidly in the self-gravitating disk, at the nonlinear stage, due to resonance interaction effects with the halo, the bar attains a large amplitude if the halo mass is comparable to or even somewhat exceeds the disk mass [184]. In other words, the increase in the bar amplitude inside a 'live' axially symmetric halo occurs even when the disk is not self-gravitating: this is related to the angular momentum transfer from the bar to a slowly rotating or nonrotating halo. The triaxiality of the 'live' dark halo further complicates the picture of its interaction with the bar and can destroy bars that have an angular velocity different from that of the halo [176].

To conclude, the bar effect on the formation and the time of existence of the bar in a galactic disk seems to be obvious and is supported by numerical simulations, but the bar interaction process turns out to be quite complicated, such that no unique correspondence between halo parameters and the presence of a bar in galaxies is observed.

### 6.2 Dark halo triaxiality and the spiral structure of the disk

The lack of central symmetry in the DM distribution, prolateness, or triaxiality of the halo discussed in Section 5, raises a question regarding the influence of such features on the galactic disk dynamics [174, 274, 275]. Different aspects of how the nonaxial symmetry of the gravitational potential affects the disk dynamics were considered in [172, 173, 177, 178, 276]. The halo triaxiality was invoked to explain the gas velocity field in galaxies, in particular, in LSB galaxies [177, 178]. Central bar generation and features of its dynamics in

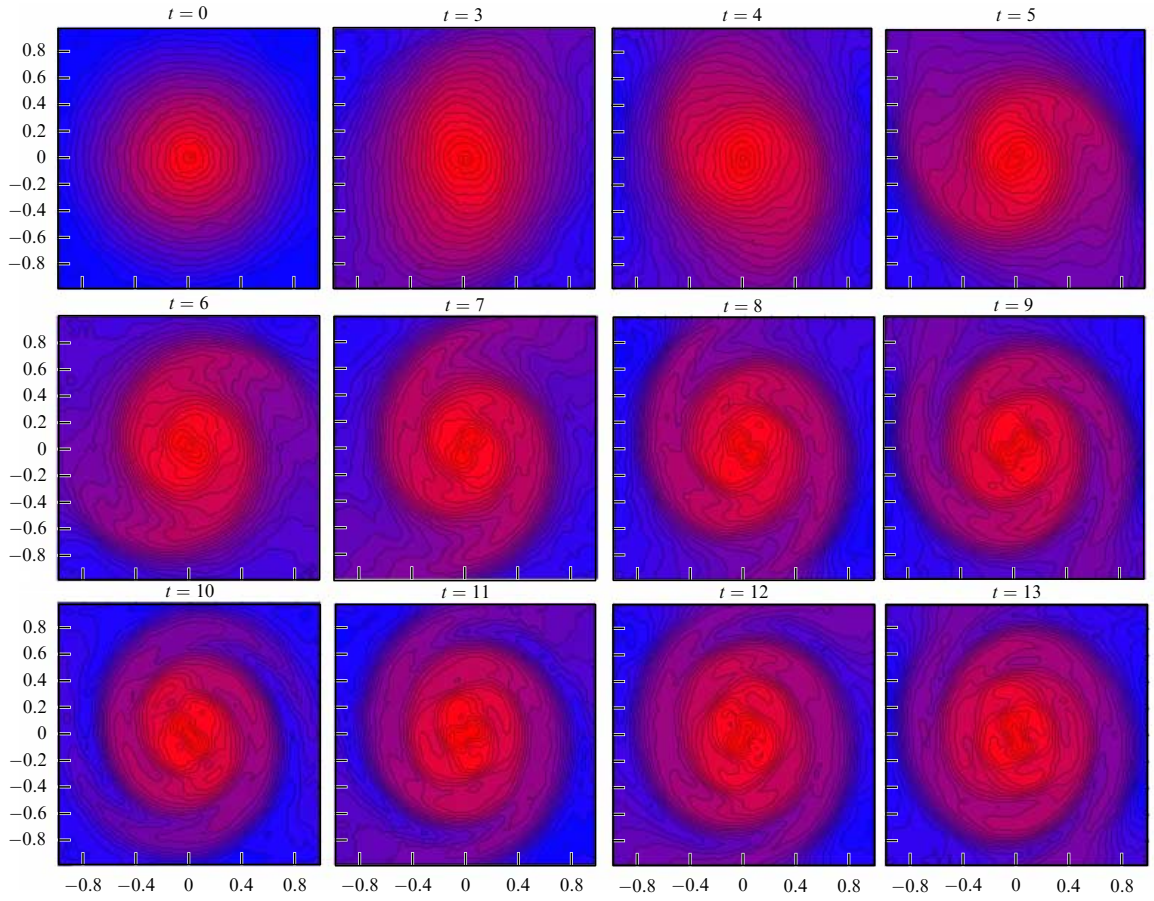


**Figure 27.** (Color online.) Isolines of the logarithm of the stellar disk surface density in the *N*-body model immersed in the gravitational field of a nonaxially symmetric dark halo at different times $t$ for $\varepsilon = 1 - b/a = 0.2$.

the presence of a nonaxially symmetric halo have been studied in detail (see, e.g., [182, 277, 278]). Disk modeling in triaxial halos also provides an explanation for the nature of observed warps at the galactic disk periphery [180, 181].

Of special interest is the possibility of explaining the appearance and support of a regular spiral structure of galaxies due to the interplay of the disk and a nonaxially symmetric halo. Numerical simulations clearly showed how the nonaxially symmetric gravitational potential of a massive halo in the disk plane leads to the formation of a two-arm spiral pattern in the gaseous [172] and stellar [173] disks. Figure 27 illustrates this process for a stellar disk model. Images shown in this figure correspond to different times from the beginning of the experiment (in the adopted units, the period of rotation of the outer parts of the disk is equal to three). The stellar disk of the model galaxy is assumed to be sufficiently hot to rule out the development of gravitational instability both in the disk plane and in the perpendicular direction. Under the same initial conditions but without the halo asymmetry, the disk remains axially symmetric over several dozen rotation periods (about 10 billion years).

In spite of a noticeable halo asymmetry (the ellipticity is 0.2) and the related perturbation in the form of a two-arm spiral, the disk as a whole preserves its symmetric shape at late evolutionary stages. In the process of spiral structure formation and later, during many rotation periods of the disk, the azimuthally averaged disk parameters (the surface density, three components of the local stellar velocity dispersion $(c_r, c_\varphi, c_z)$, the rotation velocity $V$, and the disk thickness $h_z$) do not exhibit any significant changes: neither disk heating nor radial density redistribution occur. Thus, the original source of spiral structure generation is preserved by sustaining a long-lived spiral pattern. The lack of disk heating is an important difference from the spiral wave dynamics caused by gravitational instability, which is accompanied by increasing velocity dispersions $c_r$, $c_\varphi$, $c_z$ [173].

A nonaxially symmetric halo significantly affects the dynamics of both the stellar and gas subsystems. In numerical models, a long-lived quasi-steady spiral structure forms [172]. The two-arm wave encompasses almost the entire gas disk except the very center, in which more complex structures are observed (Fig. 28). For the typical disk and halo parameters, the wave amplitude increases to the nonlinear level by forming a system of global shocks. A massive asymmetric halo can generate nonlinear waves in the gas component even for a small ellipticity $\varepsilon \simeq 0.01$, but the time of growth of the wave amplitude in this case increases, reaching eight periods of rotation of the disk periphery parts. The spiral pattern geometry depends on the rotation curve $V(r)$, the DM halo density distribution, the radial surface density profiles $\Sigma_g(r)$, and the speed of sound $c_s(r)$.

A triaxial halo can also be responsible for another phenomenon typical in some galaxies (NGC 1512, NGC 2841, NGC 2915, NGC 3198, NGC 3359, NGC 5055, NGC 5236, NGC 6744, NGC 6946, and NGC 7793), in which an extended sufficiently regular global spiral structure is observed in the gas component far beyond the stellar disk boundaries (Fig. 29). Such an external spiral pattern is

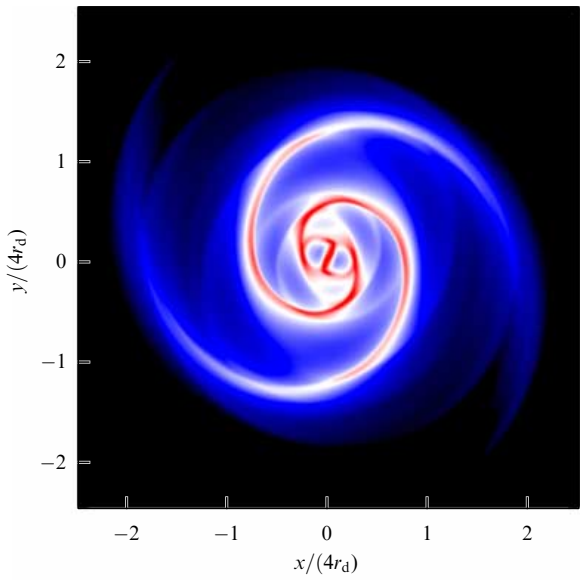


**Figure 28.** Surface gas density from modeling the gas disk dynamics in a nonaxially symmetric halo potential.

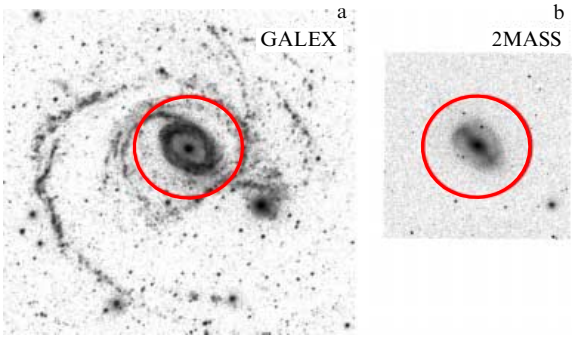


**Figure 29.** (Color online.) Galaxy NGC 1512 [279]. Images (a) in the ultraviolet range taken by the GALEX (Galaxy Evolution Explorer) telescope and (b) in the near-IR range from 2MASS (Two Micron All Sky Survey), which characterize the stellar component distribution. The red circle corresponds to $R_{opt}$.

revealed by HI, UV, and even $H_\alpha$ observations [280, 281]. The gas density beyond the radius $R_{opt}$ is likely to be insufficient to form a spiral wave due to gravitational instability. In this case, a massive nonaxially symmetric halo can be an efficient generator of the density wave in the external gas subsystem of the galaxy, as suggested by numerical gas-dynamic simulations [279].

### 6.3 Central cusp problem

The widely known central cusp problem stems from comparing the results of numerous cosmological galaxy formation models with observations. The problem is that in numerical models, the spatial density $\rho$ in the halo center diverges by forming the so-called central cusp, whereas observations, as a rule, do not demonstrate a dramatic central density increase. The density profile in a dark halo at small $r$ is usually approximated as $\rho \propto r^\alpha$ with $-1.5 < \alpha < -1$. We recall that for the most frequently used NFW profile [191],

$$\rho \propto \frac{\rho_0}{(r/r_s)\left(1+(r/r_s)\right)^2}\,, \qquad (12)$$

where $r$ is the distance from the center and $\rho_0$ and $r_s$ are model parameters describing the radial halo profile. Clearly, in this case, $\alpha = -1$. If the radial density profile reliably gives $\alpha > -1$, it is referred to as a 'core'-type distribution. To infer the DM profile from observations, rotation curves (or velocity dispersion) in the central parts of galaxies are typically used. Here, dwarf galaxies or LSB galaxies are preferable, in which DM can significantly contribute to the rotation velocity both at the periphery and in the center, and therefore the DM contribution can be easier to separate from stellar–gas components.

In the vast majority of cases, the rotation curves and stellar population models for inner disks disagree with $\alpha = -1$; the $V(r)$ curves typically admit a better fit with a pseudo-isothermal model with a 'core'-type profile (see, e.g., [54, 67, 74, 282–284] and the references therein). A sufficiently comprehensive review of the problem can be found in [285].

Several scenarios of the formation and evolution of galaxies have been proposed that eliminate contradictions with the cosmological galaxy formation scheme. Two possibilities are considered in the literature: either the cusp emerges but is rapidly smoothed due to baryonic matter redistribution, or for some reason it does not appear at all.

It is assumed in the first approach that the cusp forms, but rapidly disappears due to gravitational interaction between DM and the gas, because during intensive star formation in the galaxy center, the energy supplied by massive stars to the gas (by supernova explosions, stellar winds, and radiation pressure) leads to the gas outflow from the center. This scenario is supported by numerical hydrodynamic calculations taking the feedback between baryonic and dark matter into account [196, 286–288]. For flattening the central density gradient, the star formation rate at the time after the cusp formation and the total mass and degree of the central concentration of matter are crucial. For galaxies with stellar masses of the order of $10^9 M_\odot$, the deep central potential well hampers the gas outflow and smears out the cusp, and in low-mass dwarf galaxies with stellar masses $10^6 M_\odot$ and below, the cusp can be preserved because of an insufficiently high star formation rate. The most effective cusp destruction occurs in galaxies with intermediate stellar masses of several hundred million solar masses [268]. Bulge formation makes the central density profile somewhat steeper; however, even for massive galaxies with bulges, the modulus of the logarithmic slope $\alpha$ in the center remains less than unity [289].

In the second approach, the solution of the problem is sought in certain nontrivial DM properties and initial conditions for the growth of density perturbations. For example, a transition from cold DM to warm DM is assumed [290], or a DM model based on the existence of hypothetical ultralight axions in which quantum mechanical pressure prevents cusp formation is used [291]. All these hypotheses meet with certain theoretical difficulties and, most importantly, are difficult to test. Another solution was proposed in [292]. In the framework of the standard cosmological model, the authors of [292] showed analytically that random motions of matter in collapsing protohalos 'heat up' the DM at the collapse stage by suppressing the cusp formation. In [293], to solve the cusp problem, a modified version of DM was proposed, in which DM can be inhomogeneous and include particles with very different masses (for example, sterile neutrinos in addition to massive particles). Such a mixture of cold and warm DM changes the spectrum of growing perturbations by suppressing low-scale fluctuations

and, theoretically, can solve both the cusp problem and the issue of an insufficient number of low-mass halos (dwarf galaxies) compared to what is expected in the ΛCDM model (see Section 5.5).

## 7. Statistical relations between the dark halo mass and other parameters of galaxies

The search for and analysis of statistical relations between the dark halo mass and other observable characteristics of galaxies play the key role in disclosing the nature of DM. These characteristics include the luminosity, the mass of the stellar population, and the surface brightness or color index of a galaxy (the difference between stellar magnitudes in different photometrical filters). We consider the most important of these characteristics.

### 7.1 Baryonic Tully–Fisher relation

The close relation between the dark halo mass within optical boundaries and the stellar mass of a galaxy is clearly manifested in the relation between the galaxy rotation velocity and luminosity, which was first discovered in [294] and later named after Tully and Fisher [295], who envisaged its use it for galaxy distance estimates. This relation connects the circular velocity at large distances from the galaxy centers, which is primarily determined by the mass and degree of concentration of the dark halo, with the integral luminosity of the galaxy, which directly depends on the mass of the stellar population.

Since its discovery, the Tully–Fisher (TF) relation has been reproduced many times in papers by various authors for luminosities in different spectral bands and for rotation velocities estimated both from the HI line width and more precisely from rotation curves (see, e.g., [296]). Formally, this dependence can be applied to galaxies without disks (ellipticals) by taking the rotation velocity estimates for them from dynamic models. The TF relations constructed separately for galaxies of diverse morphological types show that early-type galaxies (for example, S0) have a lower luminosity for the same circular velocities as spirals (see, e.g., [297, 298]), which is quite expected, at least qualitatively, because the aging of a stellar system leads to its luminosity decrease. Indeed, for a baryonic TF (BTF) relation, in which the baryonic mass (the total mass of stars and gas) is used instead of luminosity, the difference between the locations of early- and late-type galaxies in the TF diagram disappears (see [297]). This correlation is tighter than for the classical TF relation (see, e.g., [299]) and admits a deeper physical interpretation, because it is independent of the stellar population properties. Here, we should bear in mind the difficulty of estimating the baryonic mass in massive galaxies because it is mostly concentrated in stars and the integral stellar mass depends on the mass–luminosity ratio used. This estimate is affected not only by the adopted model of evolution of stars with different masses but also by the form of the initial stellar mass function, which is especially poorly known for low-mass stars that mostly contribute to the stellar mass in galaxies.

The BTF relation can in principle be used to test the MoND predictions (see [300] and the references therein). The slope of the BTF dependence (in logarithmic scales) is, according to different estimates, between 3.5 and 4; MoND predicts the coefficient 4. In [301], the BTF relation slope derived from the reliable optical and near-IR multicolor photometry and rotation velocities on flat parts of galaxy rotation curves does not contradict the MoND prediction, and the conclusion is confirmed that low-mass and dwarf galaxies lie along one linear BTF dependence. However, a smaller slope close to 3.5 was obtained in [209] for galaxies from a statistically large sample (903 galaxies); in that paper, a BTF relation was obtained with a quite small dispersion of points (0.18 dex on the logarithmic scale). The location of dwarf galaxies on the diagram, however, is crucial in estimating the slope of this dependence. In many dwarf galaxies, the gas mass dominates over stars; therefore, the baryonic mass weakly depends on the stellar mass estimates, and the location of gas-rich dwarfs on the BTF diagram is used for its calibration (assuming a linear logarithmic dependence). This supports the possibility of quite accurately determining the baryonic mass in galaxies, and hence the dark halo mass, from the rotation velocity.

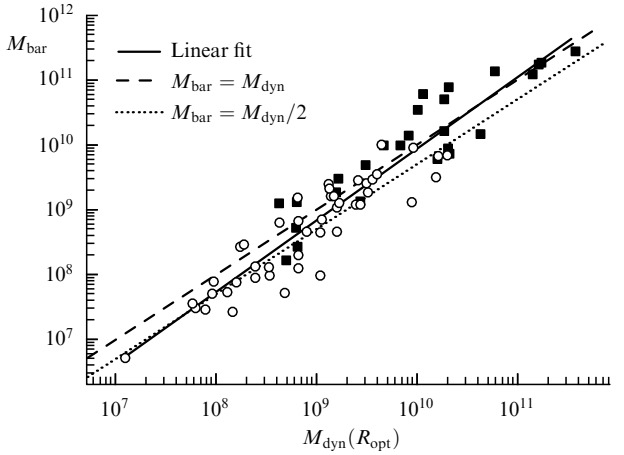


**Figure 30.** Matching of the baryonic and total mass (in units of $M_\odot$) inside the optical radius (from data in [301]). The solid curve is the least-mean-square fit. The dotted and dashed lines respectively show the expected dependences for equally massive dark and baryonic components and the lack of DM. The black and white symbols relate to galaxies in which the baryonic mass is respectively dominated by stars and gas.

The BTF diagram can easily be rearranged by deriving a relation between the baryonic mass and the dynamic mass within the optical radius, $M_{\rm dyn} = V^2 R_{\rm opt}/G$, which includes both baryonic and nonbaryonic components of a galaxy (see Fig. 30 constructed using the BTF relation [301]). The galaxy sample used in [301] included both massive galaxies (black symbols) and gas-dominated dwarfs (white symbols). The dashed and dotted lines in Fig. 30 show the respective dependences expected in the absence of DM and in the case of equal dark and baryonic masses. The mass estimates are accurate up to a factor of 2–3; therefore, in fact, the correlation between the compared quantities must be very high. Galaxies located above the dashed line are due to random errors, because the dynamical mass cannot be smaller than the baryonic one. The figure suggests that dwarf and massive galaxies follow close relations, and the mass ratio weakly changes from dwarfs to massive systems: $\log M_{\rm bar} = (-1.02 \pm 0.43) + (1.09 \pm 0.04) \log (M_{\rm dyn}(R_{\rm opt}))$, with the correlation coefficient 0.94. Thus, $M_{\rm dyn}$ and $M_{\rm bar}$ can be assumed to be almost linearly related. Because $M_{\rm dyn} = M_{\rm bar} + M_{\rm DM}$, the dark-to-baryonic mass ratio within the optical radius, $\eta = M_{\rm dyn}/M_{\rm bar}$, is 1.5–2 on average for low-mass galaxies and $\sim 1$ for massive systems, which suggests a

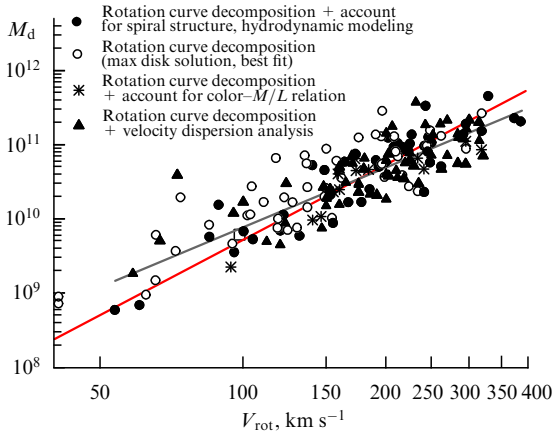


**Figure 31.** (Color online.) Baryonic TF relation obtained by dynamic methods of the disk mass estimates. The grey line is the least-mean-square fit. The red line is the dependence obtained in [305], where disk masses were derived from photometry. Different symbols show the results obtained by various methods.

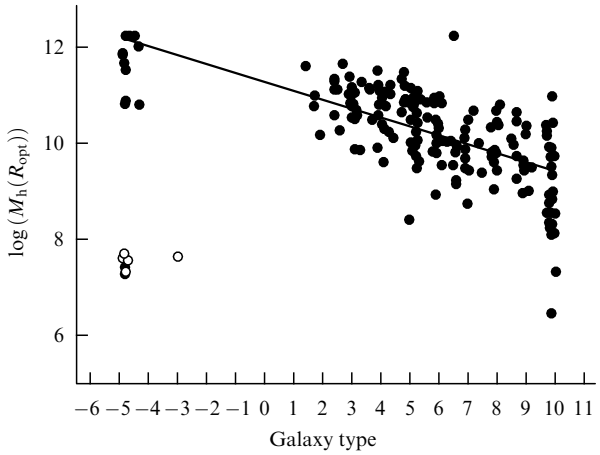


**Figure 32.** Matching of the dark halo mass inside the optical radius and the galaxy morphological type $t_{dV}$. White dots show dwarf spheroidal galaxies.

decrease in the DM contribution to the total mass as the galaxy mass increases. However, the large dispersion of points on the diagram does not allow precise estimates of $\eta$.

Physical reasons for tight (small-dispersion) TF and BTF relations have been actively debated up to now. In theory, the dependence can follow from the virial theorem relating the integral mass and rotation velocity; however, here, putting aside the MoND theory, it requires a certain tuning between the masses and radial scales of the disk and dark halo (see, e.g., [302, 303] and the references therein). It is very important that a BTF relation close to the observable one can be inferred from cosmological numerical models of galaxy formation and evolution using Newtonian gravity [304], although the results remain model dependent.

Because the stellar baryonic component mass estimated via the $M/L$ ratio depends on the adopted stellar population model and has some uncertainties (first and foremost, in the initial stellar mass function), it is important to check the existence of the BTF relation constructed without using a stellar population model. Figure 31 presents such a dependence inferred from disk mass estimates obtained by different dynamical methods. The grey line shows a least-mean-square (LMS) fit: $\log M_d = (4.5\pm 0.3)+(2.67\pm 0.15)\log V$, with the correlation coefficient $R = 0.85$ (estimates obtained by the maximum disk method were ignored). Most of the dispersion is due to uncertainties in the disk mass estimates. Although the dependence demonstrates a larger dispersion than in the case of the disk mass estimates from photometrical data, the results obtained by both methods are in agreement. However, we note a tendency to higher dynamic disk estimates in galaxies obtained by the maximum disk method (see the discussion in Section 3).

### 7.2 Dark matter and morphological type of galaxies

Of separate interest is the relation between dark halo masses within optical radii and the morphological type of galaxies. Their correlation can suggest that the morphological types depend, in particular, on the joint evolution of the dark halo and baryonic matter in galaxies.

As shown in [306], the column density of dark halos (the central spatial density times the halo core radius) is higher for brighter galaxies and for earlier morphological types (Sa – Sbc), for which the bulge contribution to the luminosity is typically more significant. Bulge formation can therefore be directly or indirectly related to the halo mass and central density. This problem is unsolved and requires more studies. Interestingly, a similar increase in the column density was found with an increase in the total (virial) halo mass [307]. The column density of a dark halo is weakly sensitive to the effect of baryonic matter on the halo spatial density distribution, which is difficult to take into account, and therefore it is convenient to compare it with numerical simulations [307].

In Fig. 32, following [306], the dark halo mass within the optical boundaries is matched with the galaxy morphological type. The morphological type $t_{dV}$ is given in the numerical coding by de Vaucouleurs (S0, Sa, Sb, Sc, Sd, and Irr correspond to $t_{dV} = -1, 1, 3, 5, 7$, and $> 7$). The white symbols show dwarf spheroidal galaxies (dSph). In the figure, they form a separate group, which reflects their lower luminosity than that of spiral galaxies. The figure suggests that except for dwarf spheroidals, the dark halo mass tends to increase for earlier morphological types: $\log(M_h(R_{opt})) = (11.3\pm 0.1) - (0.18\pm 0.01)t_{dV}$, with the correlation coefficient 0.68. This relation is largely due to the statistical dependence between the morphological type and luminosity of galaxies, because the baryonic-to-dark mass ratio remains virtually constant (up to a factor of $\sim 2$) along the morphological sequence. A dependence between the halo mass and color index of a galaxy was also noted in [306]: redder systems with a mostly evolved stellar population and low gas content (which predominantly belong to earlier morphological types) have on average a higher DM mass within $R_{opt}$.

As noted above, the highest dark-to-baryonic mass ratio occurs in dwarf galaxies, especially in dSph (see Section 2.3). But in the gas-rich dwarf dIrr, which unlike dSph have rotating gas disks, the dark halo can constitute most of the mass: for many dIrr dwarfs, the rotation curve continues increasing even at significant distances from the center, beyond the optical disk boundaries (see, e.g., [85, 308, 309]).

Generally, dwarf galaxies form an inhomogeneous class of objects, and the DM contribution to their total mass varies

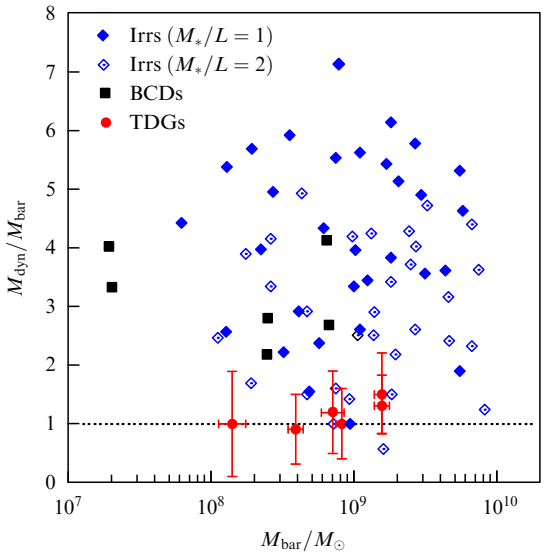


**Figure 33.** (Color online.) Matching the baryonic mass (horizontal axis) with the dynamic-to-baryonic mass ratio inside three radial scales for various types of dwarf galaxies.

in a wide range (see Section 2). Figure 33 taken from [310] compares the $M_{\rm dyn}/M_{\rm bar}$ ratio with the baryonic mass inside three radial disk scales for red irregular galaxies (Irrs), blue compact galaxies (BCGs), and tidal dwarf galaxies (TDGs). The last are of special interest because they were formed from matter that earlier belonged to disks of interacting galaxies. Therefore, it can be expected that TDGs are almost DM free.

The last conclusion is apparently supported by observations, although they need further testing. The results of optical and HI observations of six galaxies with gas disks were used in [310] to reliably conclude that the dynamical and baryonic masses of these dwarfs coincide: from the location on the BTF diagram, they rotate two times more slowly than ordinary dwarf galaxies, suggesting a low DM content. However, it is unclear how well the measured gas velocities correspond to those of equilibrium circular rotation in these nonstationary systems.

For massive elliptical galaxies, dark halo estimates require a more sophisticated analysis than for disk galaxies, because these galaxies, with very rare exceptions, have almost no cold gas, and the stars move in different planes, which complicates their kinematic mass estimates. The initial data to determine the mass or stellar density as a function of the galactocentric distance $r$ can include: (a) the dispersion of the radial velocities of stars and its change along $r$; (b) the radial distribution of brightness and temperature of X-ray emission from the hot gas filling a galaxy; (c) the effects of weak, and in some cases, strong gravitational lensing (see Sections 3.3. and 4).

The analysis of weak and strong lensing suggests that the total density profiles of elliptical galaxies are well fit by a combination of the stellar spatial density profile corresponding to de Vaucouleurs surface brightness distribution, $\ln I(r) = -(r/R_{\rm e})^{1/4} + \text{const}$, and the NFW dark halo profile suggested by cosmological simulations (see [148]). The DM mass fraction found in [148] is $27 \pm 4\%$ within one effective radius $R_{\rm e}$ that (by definition) contains half the integral luminosity of a galaxy. Although there are different opinions about this ratio, all present estimates suggest a significant stellar mass domination over DM inside $R_{\rm e}$. Observations of X-ray emission from hot gas in elliptical galaxies, as well as lensing data, suggest an NFW dark halo density profile beyond $R_{\rm e}$. Here, the ratio of the total mass to luminosity decreases by an order of magnitude as $r$ increases from $R_{\rm e}$ to $10R_{\rm e}$ (according to the Chandra observatory data), which evidences a large DM mass fraction in galaxies [311].

The richest sample (up to 98,000 objects) from the SDSS survey was used in [312] to estimate the dynamical and stellar (i.e., baryonic) masses within the effective radius $R_{\rm e}$. The stellar population mass was found from the luminosity and color index for different stellar mass functions, and the dynamical mass was estimated from the velocity dispersion at the effective radius using the virial relation. It was found in [312] that the DM mass fraction inside $R_{\rm e}$ does not exceed several percent. This is lower than the estimates found by other methods, but the resulting mass estimate depends on the adopted mass function and assumptions about its universality (see the discussion in that paper).

We recall that in the foregoing, we mainly discussed inner galaxy parts. Inside large radial distances, the DM content can be preferably derived from lensing observations and X-ray data, which suggest an $M/L$ ratio increase up to several tens of solar units at a distance of several $R_{\rm e}$ from the center, such that the ratio of the total (virial) halo mass of galaxies to their integral luminosity in the V-band amounts to 100 [148]. The radial density profile of E galaxies (including DM) in a wide range of distances $r$ is almost isothermal ($\rho \sim r^{-2}$), although far away from the center it can be satisfactorily fit by the NFW profile [148].

A comparison of the DM content in disk and elliptical galaxies is difficult because in both cases the result is highly dependent on the radial distance from the galaxy center and on the galaxy luminosity: the relative DM mass in both types of galaxies increases with the distance from the center and is higher in dwarf systems. However, a comparison of the relative DM content in spiral and elliptical galaxies inside the effective radius reveals that it is likely to be lower for elliptical galaxies. Indeed, estimates show that the role of DM for elliptical galaxies at $r \leqslant R_{\rm e}$ is comparatively small (see above). This not so for spiral galaxies: their radius $R_{\rm e}$ is only slightly smaller (by $\sim 22\%$) than the radius at which the exponential disk contribution to the rotation curve is maximal, with its contribution to the rotation velocity being 0.6–0.7 of the observed rotation velocity (see Section 3), which suggests a noticeable contribution of a nondisk dark component to the total mass. However, the situation can significantly differ from galaxy to galaxy, which demonstrate diverse rotation curves within 2 to 3 radial scales.

### 7.3 Correlation between dark matter and neutral hydrogen densities

An interesting feature noted as early as the beginning of the 1980s [313] and confirmed later (see [314] and the references therein) is that the DM density projection on the galaxy disk plane is in many cases proportional to the gas density distribution, mainly comprised by neutral hydrogen. Based on this finding, a hypothesis was proposed that DM is a gas that is difficult to observe because it is distributed in the form of small, dense, and very cold molecular clouds not related to star formation regions, with its total mass exceeding that of the observed gas by many times (see, e.g., [34]). The 'dark' gas that radiates neither in radio nor in optical emission actually exists in our Galaxy, thus forming the baryonic part of DM in galaxies (see, e.g.,

[315, 316]). Indirectly, such a gas is manifested in weak gamma-ray emission generated by collisions of cosmic-ray protons with gas atoms or in excessive thermal dust radiation in this medium. The 'invisibility' of the gas can be due to both the destruction of CO molecules, whose radio emission is typically used to estimate the molecular gas content, and the very low temperature of the medium. Part of the gas can be unobservable due to the large optical depth of the clouds, which is confirmed by observations [317].

Generally, dark gas can constitute a sizable fraction of the total mass of the cold gas in our and nearby galaxies (see the discussion in [75, 317]), but it is definitely insufficient to explain the DM effects. In addition, if DM is indeed concentrated in a planar layer, its thickness must be very large for such a self-gravitating disk to be gravitationally stable. However, as shown in [36], the correlation between the DM and neutral hydrogen column densities can be explained without invoking exotic DM forms. This correlation can arise because gas disks in most galaxies are in a nearly marginally stable state, which dictates a certain radial gas density profile, which turns out to have a shape similar to the expected column density distribution (projected onto the disk plane) for a pseudo-isothermal spherical halo.

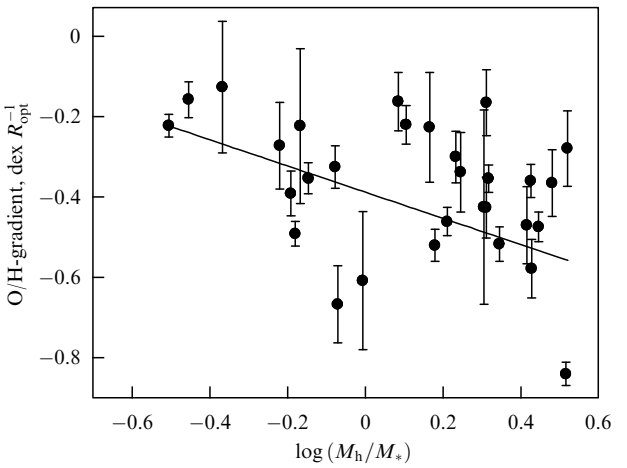


**Figure 34.** Matching of the radial gradient of oxygen abundance with the dark halo to stellar mass ratio inside the optical radius. (From [318].)

### 7.4 Dark matter and gas metallicity relation

The dark halo effect on the chemical evolution of galaxies is primarily manifested as a dependence between the star and gas metallicity and the mass of a galaxy or of its stellar population (the mass–metallicity or luminosity–metallicity dependence). Low-mass galaxies have a poorer metal content than massive galaxies. Clearly, this correlation results primarily from different star formation rates, which control metal ejection into the interstellar medium, but the result is also related to the galaxy gas exchange with the surrounding medium, which depends on the dark halo properties. Accretion of gas on the disk, the possibility of gas ejections from the galaxy due to stellar activity, and the efficiency of gas mixing in the disk also depend on the halo mass. A massive halo, on the one hand, serves as a hot gas reservoir, which, by cooling, supplies low-metallicity gas to the galaxy, and on the other hand, produces a potential well preventing gas ejection from the galaxy, such that the gas enriched with heavy elements returns to the disk, although maybe at a different distance from the center. Therefore, the galaxy mass–metallicity relation can be regarded as a manifestation of the relation between the halo mass and chemical evolution of a galaxy.

Because the halo-to-stellar (or baryonic) mass ratio varies in a sufficiently wide range, it is interesting to clarify the role of the relative halo mass (within the optical limits) $M_{\rm h}/M_*$. No tight correlation between parameters describing the chemical abundance of the gas and $M_{\rm h}/M_*$ has been discovered; however, it was found that galaxies with a low relative halo mass, as a rule, also demonstrate small (by modulus) radial gradients of the oxygen abundance (O/H) (Fig. 34) [318]. A possible explanation of such a relation, if confirmed by larger statistical data, is a more efficient radial gas mixing in galaxies with the lowest dark halo mass fraction, i.e., in disks residing in shallower DM potential wells.

The most intensive gas mixing occurs in closely interacting systems. The interaction can affect the halo masses: numerical simulations [319] show that halos can be partially destroyed. Efficient gas mixing, which results in flat radial profiles of oxygen abundance, can also be related to turbulent viscosity or accretion of gas with a low angular momentum (see [320]), although the efficiency of these processes in galaxies with low-mass halos remains unclear.

### 7.5 Relation between the virial halo mass–baryonic (stellar) mass and the baryon deficit problem

In Sections 7.1–7.4, unless stipulated otherwise, the halo mass was considered within the optical boundaries of a galaxy, $R_{\rm opt}$. This boundary is taken sufficiently arbitrarily, because galaxies extend beyond this limit, and the relative halo mass continues to gradually increase with the radial distance $r$ above $R_{\rm opt}$. The total, or virial, halo mass $M_{\rm vir}$ within the virial radius $R_{\rm vir}$ is about one order of magnitude higher than $M_{\rm h}$ (see Section 4). We recall that the virial radius is defined as the distance inside which the mean density of the total (baryonic + dark) matter is several times as high as the present-day critical density of the Universe. The ratio of these densities is usually taken to be 200. If the halo is not highly oblate, the virial mass is $M_{\rm vir} = V_{\rm vir}^2 R_{\rm vir}/G$, where $R_{\rm vir}$ is the virial radius and $V_{\rm vir}$ is the circular velocity at $R_{\rm vir}$. The virial mass so defined is uniquely related to $R_{\rm vir} \gg R_{\rm opt}$ and $V_{\rm vir}$, which enables the estimation of $M_{\rm vir}$ from kinematic measurements.

As noted in Section 3, the flat part (plateau) on the rotation curve is explained by assuming a pseudo-isothermal halo for which $V_{\rm c} = \text{const}$ at large $r$. Unlike the circular velocity in this model, the circular velocity $V_{\rm c}^{\rm h}(r)$ in an NFW halo, which is usually invoked in calculations, passes through a smooth maximum at a large distance $r$ from the center and then starts decreasing. Therefore, although the velocity $V_{\rm vir}$ is frequently assumed to be equal to the observed rotation velocity of disks in the plateau region, in the general case $V_{\rm vir}$ can noticeably, by 20–30%, deviate from the observed velocity. The relation between the observed galaxy rotation velocity at the plateau and the velocity at the virial radius imposes certain constraints on the halo structure and its density change during the galaxy formation process [321].

The problem of the $M_{\rm vir}/M_*$ ratio or of the virial-to-baryonic mass ratio $M_{\rm vir}/(M_* + M_{\rm gas})$ is considered in many papers (see Section 4). Estimating the relative baryonic mass is interesting, primarily because the dark-to-baryonic mass ratio is assumed to be known on cosmological scales, where it can be derived from cosmological data with high accuracy: the respective mass fractions of dark and baryonic matter

should be around 30% and 5% of the critical density, and their ratio should be about 6:1. Comparing this value with the one actually measured inside the virial radius brings information on the different character of the evolution of collisional (baryonic) and collisionless (dark) matter, on the star formation rate during galaxy formation, and on what fraction of baryonic matter, initially mixed with DM, remains undiscovered.

The method of comparison of mass functions (or circular velocities) of galaxies and model halos (HAM) suggests that the deficit of baryons is especially significant for low-mass galaxies and is minimal for systems like our Galaxy with the halo mass $M_{\rm vir} \approx 10^{12} M_\odot$; however, the $M_{\rm vir}/M_*$ ratio for any masses does not exceed 25–30% of the cosmological value [322]. We recall that inside an optically observed galaxy, the situation is opposite: there, the baryonic and dark masses are comparable, whereas on cosmological scales the DM density must be on average about six times as high as the baryonic mass density. The nature of this baryonic 'deficit' is apparently different in massive and low-mass galaxies. In dwarf systems, the baryonic deficit is most likely due to the loss of gas from the galaxy at the early epoch when it dominated the baryonic galaxy mass. In massive galaxies, it is due to a significant amount of gas having a high temperature and residing outside the disk, filling the dark halo volume up to the virial radius (see below).

The virial mass and hence the $M_{\rm vir}/M_*$ ratio in galaxies can be estimated not only by the weak lensing method or HAM, both of which have their own difficulties, but using alternative approaches, which is important. For example, in galaxies with rotation curves measured far away from the center, it is possible to extrapolate the rotation curves using the NFW profile of the DM halo [323]. The masses $M_{\rm vir} = M_{200}$ for our Galaxy and the Andromeda Nebula found by this method in that paper turned out to be $(81 \pm 7) \times 10^{10} M_\odot$ and $(193 \pm 15) \times 10^{10} M_\odot$, respectively. The mean mass ratio of baryonic components (disk and bulge) to the halo virial mass is here $6.2 \pm 1.8$.

In disk galaxies, most of the baryonic matter (stars and interstellar medium) resides, as a rule, in the disk, whose mass can be estimated by several methods mentioned above. To compare different approaches, in Fig. 35 we compare virial masses $M_{\rm vir}$ and disk masses $M_{\rm d}$ calculated by the photometric and kinematic methods listed below:

- the photometric method, in which, to decompose the rotation curve, constraints on the disk and bulge surface density are taken from the observed color index and the $M/L$–color relation derived by population synthesis [324];
- the method based on the disk marginal stability condition using stellar velocity dispersion estimates [59, 117];
- modeling the rotation curve using the best-fit model or the maximum disk model [325, 326, 327, 328, 53, 329];
- methods based on hydrodynamic modeling of gas motion in spiral arms [330] and on the spiral density wave condition [76].

To proceed from the mass inside the optical galaxy to the virial mass, the rotation velocity at the galaxy disk periphery was assumed to be proportional to the virial rotation velocity ($V_{\rm vir}/V \approx 0.79$, according to [331]), and the mass $M_{\rm vir}$ was assumed to directly follow from $V_{\rm vir}$ (see, e.g., [332]).

Most of the galaxies shown in Fig. 35 are related to galaxies with comparatively high mass and active star formation. The solid line in the figure is the least-mean-square approximation: $\log M_{\rm vir} = (3.2 \pm 0.4) + (0.85 \pm 0.04) \log M_{\rm d}$ (the correlation coefficient is 0.85). Despite a significant dispersion, the results obtained by different methods are consistent with the general dependence, which is somewhat different from the linear law ($M_{\rm vir} \sim M_{\rm d}^{0.85}$) in a wide range of the baryonic (disk) mass of galaxies, from $10^9 M_\odot$ to $\sim 3 \times 10^{11} M_\odot$. The main uncertainty is due to galaxies with low-mass halos.

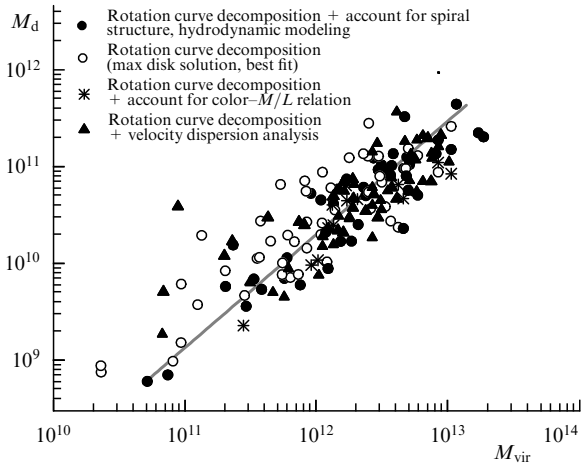


**Figure 35.** Comparison of the virial halo mass with the total disk mass. The solid line is the least-mean-square best fit. Different symbols show the disk mass estimates by various methods based on kinematical and photometrical data.

Thus, the virial (predominantly dark) mass differs from the baryonic mass in the disk by 1.5–2 orders of magnitude, which is much larger than the cosmological dark-to-baryonic mass ratio. The baryon deficit problem on the virial radius scale can be substantially relaxed or completely fixed by allowing for difficult-to-observe gas in the galaxy halo far beyond its optical boundaries. The mass of the hot gas with a temperature of about $10^6$ K observed in the inner halo of some massive galaxies is manifestly too small to explain the baryon deficit. However, large gas masses far beyond the optical galaxy are 'detected' indirectly from ultraviolet absorption lines in spectra of remote quasars observed at small angular separations from comparatively nearby galaxies. The redshift of an absorption line being close to that of a galaxy may suggest that the absorption is directly related to the gas in an extended galactic halo. In this way, using the spectrograph of the Hubble Space Telescope, absorption lines of OVI [333] and Ly$\alpha$ [334] were measured for several dozen low-redshift galaxies. The absorption lines were observed at distances up to 150–250 kpc from the galaxies (of the order of their virial radius!). The absorbing gas has the temperature $10^5$ K and is gravitationally bound to the galaxies. Analysis showed that the mean gas density decreases monotonically with $r$, and the total mass is likely to exceed the mass of the interstellar gas in the galaxies themselves by many times. For our Galaxy, for example, calculations in [335] show that the missing baryonic mass of the order of $10^{11} M_\odot$ could be located in the hot gas of an extended corona, which shows up in observations of oxygen ion absorption lines. It should also be borne in mind that a large fraction of galaxies belong to groups and clusters that also have dark halos and gas with the virial temperature; the mass of this gas in giant clusters can exceed the total stellar mass of the cluster galaxies.

The mass of a sufficiently massive group or cluster of galaxies can also be estimated using an original method that

gives the total system mass beyond the virial radius, if present. The method is based on the examination of galactic radial velocities (Hubble flows) near groups and clusters and on the analysis of the difference between this velocity field and that expected for the classical Hubble expansion law, according to which the relative velocities of galaxies are proportional to the distances between them. In other words, how the gravitational interaction of the galaxy system with surrounding galaxies slows down the Hubble expansion (the Hubble flow) near a given system is examined. To do it, however, many galaxies with distances known independently of the Hubble law (for example, from stars with known luminosities) must be present in the direction toward the chosen galaxy group or cluster.

The galactic velocity field near a group or cluster allows finding the conventional radius of the 'zero' velocity sphere $R_0$ inside which the gravitational field of a given galaxy system had time since the beginning of the expansion of the Universe to fully stop the cosmological expansion. Outside this sphere, galaxies continue receding from the system and, with distance, their recession velocities asymptotically tend to the Hubble law. Estimating $R_0$ allows determining the integral mass of a galactic system. This method was first used to estimate the mass of the Local Group of galaxies by Lynden-Bell [336] and Sandage [337]. The increase in the number of galaxies with distance not determined from the redshift made it possible to use this method for many systems (see [41, 338] and the references therein).

It is important that the estimates of masses and density distributions inside large spatial volumes require taking the cosmological repulsion force (dark energy) into account, which decreases the gravitational interaction of sufficiently remote bodies (see [338–340] for more details). Without this effect, the mass inside $R_0$ would be significantly underestimated. The mass of several galactic systems for which the zero-velocity radius $R_0$ was measured taking the repulsion force into account turned out to be close to their virial mass $M_{\rm vir}$ in spite of the virial radius $R_{\rm vir}$ being much smaller than $R_0$ (see [338] and the references therein). For example, for the massive Virgo cluster closest to us, the zero-velocity radius was found to be around 7 Mpc, which is several times larger than the virial radius of the cluster, and the mass within $R_0$ is $(8.0 \pm 2.3) \times 10^{14} M_\odot$, in good agreement with the virial mass estimate [338]. This suggests that beyond $R_{\rm vir}$, and hence in the space between galactic systems, there is little dark matter.

The last conclusion agrees with the galactic mass measurements by the weak lensing method. This most certainly follows from [341], where the DM distribution was analyzed based on weak lensing data by averaging (stacking) more than 100,000 galaxy systems (from small groups to clusters) with redshifts $0.1 < z < 0.3$. It was found that at all scales, from several hundred kpc to several dozen Mpc, the stellar mass fraction is approximately constant (about 1% of the total mass), and this value does not depend on the radius of the volume being considered. The mass–luminosity $M/L$ ratio beyond several hundred kpc from the system center stops changing significantly. The authors of [341] conclude that the integral masses of groups and clusters of galaxies, mainly dominated by DM, are equal to the sum of the mass of individual galaxies, including their dark halo masses. Little DM is present where there are no galaxies.

The effect of gravitational fields of galaxy systems on the Hubble flow in the local Universe around our Galaxy is clearly demonstrated in [342, 343], where the location of about 11,000 comparatively nearby galaxies on the velocity–distance Hubble diagram inside a 50 Mpc sphere around the Local Group of galaxies was investigated. This volume contains numerous galactic systems with diverse scales (mainly groups). The authors of [342, 343] estimated the mean density of matter related to the galaxy systems of different multiplicities (the matter must be mostly dark) within the 50 Mpc distance and found it to be about a third of the expected 28% of the mean density of matter in the Universe. What fraction of DM resides beyond the galactic systems is an open question, because it is not ruled out that the Local Group lies inside a giant low-density volume (void) several Mpc in diameter.

### 7.6 Dark halos and supermassive black holes

At the centers of most high-luminosity galaxies there are massive compact objects — nuclear stellar clusters and supermassive black holes (SMBHs). The latter can be responsible for the activity of galactic nuclei, if powerful accretion onto the black hole occurs. SMBH formation, their role in the parent galaxy evolution, and the relation to the integral galactic parameters and kinematic features are actively being discussed [344, 345]. The existence of powerful quasars at high redshifs suggests that SMBHs in these quasars must have been formed and have increased to several hundred million solar masses very rapidly, over the first billion years of cosmological expansion, when the process of galaxy formation had not completed.

The dynamics and mass concentration in galaxies or nondisk galactic components (bulge and halo) play a fundamental role in the formation and growth of SMBHs. This clearly follows from the well-known tight correlation between the SMBH mass and stellar velocity dispersion in the bulge, and the disk angular velocity in the central 1–2 kpc region (see the discussion in [344, 346]). Because the central velocity dispersion correlates, although not very strongly, with the circular velocity at large $r$, it is natural to expect that there is a correlation between the SMBH mass and the rotation velocity of the galaxy, which in turn characterizes the virial halo mass $M_{\rm vir}$.

The dark halo of galaxies could indeed play a major role in the SMBH mass growth, because the halo gravitational field determines the depth of the potential well in which galactic gas concentrates and where the stellar bulge and the black hole are formed. The possible relation between $M_{\rm vir}$ and the central SMBH mass $M_{\rm BH}$ has been discussed in many papers (see, e.g., [347–350]). But tests of the dependence of $M_{\rm BH}$ on the maximal galactic rotation velocity $V_{\rm c}$ gave no compelling results, although on the statistical level the dependence certainly exists, because the most massive black holes are not found in low-luminosity galaxies with comparatively small halos. The tight correlation between $M_{\rm BH}$ and the rotation velocity obtained in some papers is likely to be the result of using indirect estimates of mass and velocities based on their empirical dependence on the velocity dispersion. This relates first and foremost to the empirical correlation between $M_{\rm BH}$ and the central velocity dispersion [344], which is especially strong for elliptical galaxies. Direct measurements of $V_{\rm c}$ and $M_{\rm BH}$, however, showed that the relation between these quantities is rather loose (see, e.g., [346, 351] and the references therein). According to [352], the mass $M_{\rm BH}$ in disk galaxies closely correlates only with the bulge parameters, and the correlation with the velocity $V_{\rm max}$ arises only as a

result of the relation between the circular rotation velocities of the bulge and the disk (the bulge–disk conspiracy). In addition, as noted in [350], if the central black hole mass were closely related to the dark halo mass, very massive black holes should be found in the central galaxies of clusters, because the clusters have halos with masses several orders of magnitude heavier than individual galaxies.

When matching the central black hole masses with the DM mass, it should be borne in mind that the virial mass estimate from the galaxy rotation velocity is not fully correct: the directly measured disk rotation velocities could differ from the circular velocity at the virial radius, and therefore they do not yield a definitive assessment of the halo mass $M_{\rm vir}$. The authors of [353], by using the galactic masses derived from strong gravitational lensing for 43 galaxies (mainly the early type), found the relation between $M_{\rm BH}$ and the virial halo mass $M_{\rm vir}$ in the form $\log M_{\rm BH} = (8.18 \pm 0.11) + (1.55 \pm 0.31)(\log M_{\rm vir} - 13.0)$, but indirect estimates inferred from the empirical $M_{\rm BH}$–central velocity dispersion were used there. Later, a similar relation was obtained in [354],

$$M_{\rm BH} \sim M_{\rm vir}^{1.8^{+0.7}_{-0.8}},$$

for more than three thousand elliptical galaxies, but the authors also used empirical relations and not direct estimates: $M_{\rm BH}$ was derived from the stellar velocity dispersion and $M_{\rm vir}$ from the dependence of this mass on the galactic X-ray luminosity $L_{\rm X} \sim M_{\rm vir}^{2.4}$ found in [355].

In any case, SMBH formation is a complex process, and whatever role is played by DM there, the resulting SMBH mass must significantly depend on the evolution of baryonic components of galaxies, which is different for high-mass and low-mass galaxies (see review [350]).

The physical connection between dark halo and SMBH masses also emerges in numerical or theoretical models of the SMBH mass growth (see, e.g., [356, 357]). As follows from theoretical model calculations, the SMBH mass is determined not only by the dark halo mass but also, and to a significant degree, by its central density [356].

In general, the problem of the dark halo effect on the black hole mass growth in galactic nuclei is far from being solved. The relation between the halo and SMBH masses, which is apparently weak at present, could be much stronger at the epoch of galactic youth, when the central black holes were forming [358].

## 8. Conclusion. Dark matter and processes in galaxies

The main purpose of this review has been to show that the conclusion on the presence of dark, directly unobservable, matter is based on many facts and is therefore sufficiently reliable, in spite of the nature of DM being unclear. The role of dark halos in the evolution of galactic disks is one of the hot topics in the physics of galaxies.

To conclude, we stress that the most important (but not unique) parameter of a dark halo is its mass. All DM mass estimates reduce to determining the total mass (density) — local or inside a certain radius — and to subtracting the observable matter (stars and gas) from the obtained mass (density). We recall the main methods of DM mass estimates in galaxies (without estimates from empirical relations) discussed above:

- The construction of dynamical galactic models based on measurements of rotation curves and the stellar velocity dispersion with photometrical data taken into account for assessing the stellar mass fraction in the integral mass and radio data in HI and CO lines in order to estimate the gas mass.
- The use of data on radial velocities and velocity dispersion of halo objects (halo stars and globular clusters, dwarf satellites, tidal stellar streams), as well as measurements of the hot halo gas temperature. Here, the virial relation between the kinetic and gravitational energy of the component is assumed.
- The use of the condition of the gravitational stability of the disk with respect to perturbations in the disk plane and of the disk stability to warp perturbations.
- The construction of galactic polar ring models and of models of the tidal interaction of galaxies based on measurements of the velocity and structure of tidal formations.
- The application of methods of strong and weak gravitational lensing to estimating the mass of lensing galaxies.
- The construction of equilibrium models of stellar disks and cold gas layers in the disk plane with account for data on the rotation velocity and velocity dispersion of stars and gas.
- The use of the density wave propagation condition and of gas-dynamic calculations of gas crossing a spiral arm, to estimate the disk density [76, 330].

The DM dominance over ordinary matter (consisting of atoms) on large spatial scales follows from analyses of the dynamics of gas and stars in both galaxies and galaxy systems. It is supported by gravitational lensing methods and is consistent with the cosmological concept of large-scale structure formation that started more than 13 bln years ago. The total density of stars and gas confined in galaxies being much lower than the baryonic matter density required by the standard cosmological Big Bang model implies that a certain portion of DM must be contained in the missing baryons (apparently, in hot gas); however, most DM must be of a nonbaryonic origin (see Section 1).

The natural question arises as to how the existence of DM affects processes inside galaxies. Some aspects of this issue were discussed above. Here, to conclude, we briefly consider the possible channels of DM influence (more precisely, of its gravity) on processes inside massive halos.

In the inner parts of most galaxies with normal brightness, both disks and ellipticals, the baryonic matter dominates, and only a small fraction of matter can be related to DM. Therefore, DM in the inner parts has no effect on both stellar and gas motions, star formation and stellar evolution processes, and the activity of galactic nuclei.[3] Nevertheless, the DM mass and distribution can affect a number of processes determining the observable properties of galaxies and their evolution. The most obvious features are as follows.

(1) A massive dark halo creates a deep potential well in which a galaxy resides. In the case of elliptical galaxies, this leads to a larger velocity dispersion of stars and to the

[3] We note, however, that one possible DM candidate particle is the so-called asymmetric weakly interacting particle (the asymmetry is in unequal numbers of particles and antiparticles), which, like WIMPs, has a very small interaction cross section with baryons. A tiny fraction of these particles, by being scattered when flying through stars, can lose their kinetic energy and be stored for a long time in the center of stars, thus affecting the process of energy generation and transport (see [359] and the references therein).

possibility of retaining the observed hot gas inside the galaxy. For disk galaxies this, first of all, means higher linear and angular rotation velocities of stars and gas, which make the disk more stable to gravitational perturbations. If the stellar disk is close to marginal stability, the rapid rotation corresponds to the lowest velocity dispersion of stars, which results in the smallest vertical scale of the stellar disk (see Section 2). This, in turn, renders the gas layer in the disk plane more compressed and denser. With the same surface density, the mean volume density of the gas turns out to be higher than in the absence of a halo, which affects the local star formation rate (see the discussion of the relation between the star formation rate and the gas volume density in [87]).

(2) At the galaxy formation stage, the DM concentration in the center of the system could facilitate rapid SMBH growth. Accretion onto the SMBH is responsible for the phenomenon of an active galactic nucleus (a quasar). A powerful energy release from the active nucleus can affect the total gas content and subsequent evolution of the galaxy. The degree of dark halo concentration also influences the disk formation from baryonic matter, which initially, before the energy dissipation, was mixed with DM. An anomalously low central density and a very large radial scale of the dark halo could result in the formation of very rarefied disks. Such a scenario was proposed, for example, for the giant galaxy Malin-2 in [75].

(3) The halo can play an important role by determining the formation of and maintaining large-scale structures in the disk (the bar and spiral arms). A nonaxially symmetric outer halo is apparently responsible for the generation of long-lived density waves in the disk, which explains the regular spiral structure even in galaxies where the disk has a large margin of gravitational stability (see Section 3). This is not the only mechanism of maintaining long-lived spiral arms, but it could be quite widespread. If the mass of a disk is much smaller than that of the halo in whose gravitational field it resides (for example, in LSB galaxies), the halo not only stabilizes the growth of local gravitational perturbations due to rapid rotation but also prevents the formation of a small-scale wave structure by suppressing the swing amplification mechanism of wave growth [360]. The massive halo played an important role during the formation of massive (globular) clusters in young forming galaxies. This is suggested by the correlation between the number or the total mass of globular clusters in a galaxy and its dark halo mass (see [361] and the references therein).

(4) The presence of massive halos increases the relative velocity of galaxies in systems (pairs, groups, and clusters), which reduces the effects of tidal interactions between them that distort the form of the galaxies and the velocity field of gas and stars. Taking the halo mass into account can dramatically change estimates of trajectories of galaxies that are close to each other, of their orbital periods, and of the collision rate. A clear example is the nearby system of apparently gravitationally bound galaxies: Large and Small Magellanic Clouds. In these galaxies, proper motions of stars have been measured, and therefore we know not only radial (along the line of sight), as usually, but also three-dimensional velocity vectors. This offered the unique possibility of estimating possible masses of their extended halos, which were found to significantly exceed the total mass of stars and gas, and also to refine the parameters of their orbits and evolution [362]. Dark matter filling a galaxy cluster over long time intervals can 'pull over' galaxies in the inner parts of the cluster by dynamical friction, giving them a higher central concentration and leading to the formation of central cD galaxies [363], although the efficiency of this process remains an open question.

(5) A massive halo facilitates the merging or destruction of satellites flying into the halo due to dynamical friction and tidal interactions. The dynamical friction shortens the large semiaxis of orbits of the most massive dwarfs, and tidal forces partially or fully destroy them, thus favoring additional DM and baryonic (including gas) mass inflow into the inner regions of the 'host' galaxy. Extended tidal stellar streams associated with destroyed dwarf systems are definitely observed in our and other galaxies, and the velocity of stars in these streams reflects the mass and density of the halo in which they are found. Dwarf systems merged with the galaxy supply low-metallicity gas, thus effecting the chemical evolution of the galaxy and its gas content.

(6) Like dwarf galaxies, similarly important can be numerous subhalos (minihalos), i.e., low-mass, including starless objects partially or fully consisting of nonbaryonic DM and therefore unobservable or difficult to discover in the optical range. Their number remains an unresolved issue. The observed dwarf satellites of galaxies are frequently considered to be low-mass subhalos, in which some number of stars could form. However, the number of subhalos predicted by model calculations by many times exceeds the directly observed number of dwarf satellites with similar values of directly measured circular velocities (see Section 5).

Dark subhalos, if present in a sufficient amount, can differently manifest themselves in the 'host' galaxy. Dark subhalos, for example, can significantly increase the velocity dispersion of stars $c_z$, especially at the disk periphery, excite long-lived vertical oscillations in the disk, or even stimulate the formation of large-scale structures in the disk (see the discussion in [364]). By crossing the disk gas layer, the subhalos, if they contain the gas mass of at least a few percent, can be responsible for the appearance of low-density 'holes' in the gas distribution and enhanced star formation at their edges, which is confirmed by hydrodynamic simulations [365]. The authors of [365] note that such details are indeed observed in galaxies, but their number is too high for the subhalos to be the only reason for their formation. Unfortunately, the role of subhalos is difficult to assess with certainty, because their number and spatial density remain unknown.

(7) The dark halo mass and its central density determine the character of gas exchange between the galaxy and its surroundings. Apparently, this is the most important effect of halos in galaxy evolution. A deep potential well caused by a halo hampers gas ejection (or the galactic wind) from the disk into the ambient medium, which results from the activity of young stars or nuclear activity of the galaxy. By leaving the galaxy, the gas can remain within the halo virial radius and after cooling can partially return to the galaxy to continue participating in the star formation process. On the other hand, the massive halo favors accretion of the intergalactic gas, although the gaseous medium filling the halo hinders the accreting gas falling into the central halo part, i.e., into the optically observed galaxy. The directly observed gas accretion rate onto our and other galaxies is lower than required to sustain star formation; however, the accretion rate is difficult to estimate: most of the infalling gas is rarefied and ionized, which makes its discovery at large distances from the disk a

difficult task. Nevertheless, there are many arguments suggesting that gas accretion onto our Galaxy and other massive galaxies indeed occurs, and the accretion rate can be comparable to the star formation rate, especially several billion years ago, and largely determines the evolution of galaxies and their gas components (see, e.g., [366–368]).

Galactic halos accrete gas (or accreted gas in the past) from the intergalactic space. The accretion flows must contain both gas and DM. However, while DM is collisionless and mixes with the dark halo DM, the fate of the gas is not so clear. The infalling gas streams can directly impinge on the galactic disk as gas clouds or individual flows, but the situation is also possible when the infalling gas enters the galaxy with a time lag of one billion years or more, depending on the depth of the halo potential well.

Theoretical calculations and numerical models of galaxy formation imply that accretion onto a disk must occur differently in galaxies with low-mass and high-mass halos (see, e.g., model calculations in [369] or review [368] and the reference therein). In massive halos, the accreting gas heats to temperatures close to virial values (of the order of $10^6$ K). The accreting gas flows in the halo pass through the shock front and dissolve in the hot gas. In star-forming galaxies, gas falls from the inner halo regions after cooling. This is the so-called hot accretion mode. Most of the hot gas has a characteristic cooling time exceeding the Hubble age of the Universe, i.e., cannot fall into the galaxy disk at all.

In low-mass galaxies, the gas temperature in the halo is lower and the cooling time is shorter than in massive galaxies. Therefore, by entering the halo, flows of a relatively cold and low-metallicity intergalactic gas do not heat to the virial temperatures. They fragment and fall through the rarefied halo gas, reaching its central parts. Gas accretion rates onto the galaxy in this case are determined not by its cooling rate but by the accretion from the intergalactic space. This regime is called the cold accretion mode. Both accretion modes can be present in galaxies, and their roles can interchange with time. The cold mode is more efficient, and presently dominates in galaxies only if their halo mass is not too high (not much greater than the halo mass in our Galaxy), although this accretion apparently dominated in the mass growth of galaxies at large redshifts. In principle, both accretion modes can coexist.

The cold accretion regime can explain the presence of the gas and star-forming regions sometimes observed in lenticular galaxies. Unlike other disk galaxies, such galaxies usually have an insignificant amount of cold gas; therefore, the gas in some of them is likely to be of external origin. However, concurrently with accretion mechanisms, there is the galaxy merging or supply of chemically processed gas from nearby galaxies. Measurements of the kinematic features and metallicity of the gas acquired by the galaxy allows distinguishing the most probable gas supply mechanism (see the discussion in [370]). From the analysis of isolated lenticular (S0) galaxies, the authors of [371] concluded that the morphological type and observed gas content of disk galaxies that have no comparable-mass neighbors can be fully determined by a significant cold gas accretion or by the merging of small gas-rich satellites. Clearly, in the case of accretion, as well as during merging, the gas supply into the galaxy and its passing through the halo to the disk is fully controlled by the dark halo gravitational field.

Close interaction between nearby galaxies, as well as the blowing of galaxies by intergalactic gas flows, strongly complicates the gas exchange between the galaxy and the surroundings. These processes affect the mass and physical state of the gas filling a halo, and thus influence the gas supply and evolution in galactic disks. If accretion onto a galaxy stops for some reason, the lack of 'fresh' gas inflow quenches star formation in several billion years.

Thus, galaxy evolution is determined not only by the mass and structure of galaxies but also by the degree of concentration and shape of their dark halos. It is very important to quantitatively explain (although this is not a task not for the near future) how dark matter affected processes in galaxies at different redshifts and in different surroundings (from isolated galaxies to galaxies in close groups and rich clusters) and what the role of DM was in the formation of galaxies of diverse morphological types.

In this review, we used the results of numerical simulations carried out on the Lomonosov and Chebyshev supercomputers of the Research Computing Center of Lomonosov Moscow State University. The work was supported by the Russian Foundation for Basic Research (grants 14-22-03006, 15-02-06204, NNIO_a 15-52-12387, 15-52-15050, 16-02-00649, and 16-32-60043) and by grants from the President of the Russian Federation (MK-4536.2015.2), the Russian Science Foundation (15-12-10017) (Section 6.2 of the review), and the State Task of the Ministry of Education and Science of the RF (2.7860.2017/BCh, 2.852.2017/PCh).

## References

1. Morselli A *Acta Polytech.* **53** 545 (2013)
2. Oort J H *Science* **170** 1363 (1970)
3. Einasto J *Braz. J. Phys.* **43** 369 (2013)
4. Trimble V "History of dark matter in galaxies", in *Planets, Stars and Stellar Systems* Vol. 5 *Galactic Structure and Stellar Populations* (Eds T D Oswald, G Gilmore) (Dordrecht: Springer, 2013) p. 1091
5. Roos M *J. Mod. Phys.* **3** 1152 (2012)
6. Zwicky F *Astrophys. J.* **86** 217 (1937)
7. Zwicky F *Phys. Today* **6** (4) 7 (1953)
8. Oort J H *Bull. Astron. Inst. Netherlands* **6** 249 (1932)
9. Karachentsev I D *Sov. Phys. Usp.* **16** 279 (1973); *Usp. Fiz. Nauk* **109** 761 (1973)
10. Karachentsev I D *Phys. Usp.* **44** 818 (2001); *Usp. Fiz. Nauk* **171** 860 (2001)
11. Einasto J, Kaasik A, Saar E *Nature* **250** 309 (1974)
12. Peterson C J et al. *Astrophys. J.* **208** 662 (1976)
13. Rubin V C, Thonnard N, Ford W K (Jr.) *Astrophys. J. Lett.* **225** L107 (1978)
14. Rubin V C et al. *Astrophys. J.* **289** 81 (1985)
15. Zeldovich Ya B, Einasto J, Shandarin S F *Nature* **300** 407 (1982)
16. Dolgov A D *Phys. Usp.* **57** 199 (2014); *Usp. Fiz. Nauk* **184** 211 (2014)
17. Gurbatov S N, Saichev A I, Shandarin S F *Phys. Usp.* **55** 223 (2012); *Usp. Fiz. Nauk* **182** 233 (2012)
18. Schumann M "Dark matter 2014" *EPJ Web. Conf.* **96** 1027 (2015)
19. Bernabei R et al. *Int. J. Mod. Phys. A* **28** 1330022 (2013)
20. Blinnikov S I *Phys. Usp.* **57** 183 (2014); *Usp. Fiz. Nauk* **184** 194 (2014)
21. Ryabov V A, Tsarev V A, Tskhovrebov A M *Phys. Usp.* **51** 1091 (2008); *Usp. Fiz. Nauk* **178** 1129 (2008)
22. Berezinsky V S, Dokuchaev V I, Eroshenko Yu N *Phys. Usp.* **57** 1 (2014); *Usp. Fiz. Nauk* **184** 3 (2014)
23. Milgrom M *Mon. Not. R. Astron. Soc.* **437** 2531 (2014)
24. Milgrom M *Scholarpedia* **9** 31410 (2014)
25. Chan M H *Phys. Rev. D* **88** 103501 (2013)
26. Mannheim P D, O'Brien J G *Phys. Rev. D* **85** 124020 (2012)
27. Cardone V F et al. *Mon. Not. R. Astron. Soc.* **423** 141 (2012)
28. Dodelson S *Int. J. Mod. Phys. D* **20** 2749 (2011)
29. Carignan C et al. *Astron. J.* **146** 48 (2013)
30. Santos-Santos I M et al. *Mon. Not. R. Astron. Soc.* **455** 476 (2016)

31. Okun' L B *Phys. Usp.* **50** 380 (2007); *Usp. Fiz. Nauk* **177** 397 (2007)
32. Blinnikov S I, Dolgov A D, Postnov K A *Phys. Rev. D* **92** 023516 (2015)
33. Capela F, Pshirkov M, Tinyakov P *Phys. Rev. D* **87** 123524 (2013)
34. Pfenniger D, Combes F, Martinet L *Astron. Astrophys.* **285** 79 (1994)
35. Hoekstra H, van Albada T S, Sancisi R *Mon. Not. R. Astron. Soc.* **323** 453 (2001)
36. Zasov A V, Terekhova N A *Astron. Lett.* **39** 291 (2013); *Pis'ma Astron. Zh.* **39** 323 (2013)
37. Karachentsev I D, Makarov D I *Astrophys. Bull.* **63** 299 (2008); *Astrofiz. Byull.* **63** 320 (2008)
38. Makarov D, Karachentsev I, in *Dark Galaxies and Lost Baryons, Proc. of the 244th IAU Symp., Cardiff, Wales, United Kingdom, June 25 – 29, 2007* (IAU Symposium Proc., Vol. 244, Eds J I Davies, M J Disney) (Cambridge: Cambridge Univ. Press, 2008) p. 370
39. Diaz J D et al. *Mon. Not. R. Astron. Soc.* **443** 1688 (2014)
40. Karachentsev I D, Kudrya Y N *Astron. J.* **148** 50 (2014)
41. Karachentsev I D et al. *Mon. Not. R. Astron. Soc.* **393** 1265 (2009)
42. Ilyina M A, Sil'chenko O K *Astron. Astrophys. Trans.* **27** 313 (2012)
43. Afanasiev V L, Moiseev A V *Baltic Astron.* **20** 363 (2011)
44. Pohlen M, Trujillo I *Astron. Astrophys.* **454** 759 (2006)
45. Barbosa C E et al. *Mon. Not. R. Astron. Soc.* **453** 2965 (2015)
46. Fridman A M, Khoperskov A V *Fizika Galakticheskikh Diskov* (Physics of Galactic Disks) (Moscow: Fizmatlit, 2011)
47. Sofue Y *Publ. Astron. Soc. Jpn.* **67** 75 (2015)
48. Rubin V C, in *Internal Kinematics and Dynamics of Galaxies. Proc. of the Symp., Besancon, France, August 9 – 13, 1982* (IAU Symp., Vol. 100, Ed. E Athanassoula) (Dordrecht: D. Reidel Publ. Co., 1983) p. 3
49. Del Popolo A *Int. J. Mod. Phys. D* **23** 1430005 (2014)
50. Rubin V *Phys. Today* **59** (12) 8 (2006)
51. Tamm A, Tempel E, Tenjes P, in *The Galaxy Disk in Cosmological Context, Proc. of the 254th IAU Symp., Copenhagen, Denmark, June 9 – 13, 2008* (IAU Symp. Proc., Vol. 254, Eds J Andersen, J Bland-Hawthorn, B Nordström) (Cambridge: Cambridge Univ. Press, 2009) p. 73
52. Saburova A S, Zasov A V *Astron. Lett.* **38** 139 (2012); *Pis'ma Astron. Zh.* **38** 163 (2012)
53. Ryder S D et al. *Mon. Not. R. Astron. Soc.* **293** 411 (1998)
54. de Blok W J G et al. *Astron. J.* **136** 2648 (2008)
55. Navarro J F, Frenk C S, White S D M *Astrophys. J.* **490** 493 (1997)
56. Burkert A *Astrophys. J. Lett.* **447** L25 (1995)
57. Fux R *Astron. Astrophys.* **327** 983 (1997)
58. Amorisco N C, Bertin G *Astron. Astrophys.* **519** A47 (2010)
59. Khoperskov A V, Zasov A V, Tyurina N V *Astron. Rep.* **45** 180 (2001); *Astron. Zh.* **78** 213 (2001)
60. Kent S M *Astron. J.* **93** 816 (1987)
61. Sackett P D *Astrophys. J.* **483** 103 (1997)
62. Martinsson T P K et al. *Astron. Astrophys.* **557** A131 (2013)
63. Kauffmann G et al. *Mon. Not. R. Astron. Soc.* **451** 878 (2015)
64. Meurer G R, Zheng Z, de Blok W J G *Mon. Not. R. Astron. Soc.* **429** 2537 (2013)
65. Karachentsev I D, Makarov D I, Kaisina E I *Astron. J.* **145** 101 (2013)
66. Moiseev A V *Astrophys. Bull.* **69** 1 (2014); *Astrofiz. Byull.* **69** 1 (2014)
67. Salucci P et al. *Mon. Not. R. Astron. Soc.* **420** 2034 (2012)
68. Mateo M L *Annu. Rev. Astron. Astrophys.* **36** 435 (1998)
69. Walker M G, Mateo M, Olszewski E W *Astron. J.* **137** 3100 (2009)
70. Walker M G et al. *Astrophys. J.* **704** 1274 (2009)
71. Muñoz R R et al. *Astrophys. J. Lett.* **650** L51 (2006)
72. Saburova A S *Astron. Rep.* **55** 409 (2011); *Astron. Zh.* **88** 446 (2011)
73. Fuchs B *Asrophys. Space Sci.* **284** 719 (2003)
74. de Blok W J G, McGaugh S S, Rubin V C *Astron. J.* **122** 2396 (2001)
75. Kasparova A V et al. *Mon. Not. R. Astron. Soc.* **437** 3072 (2014)
76. Athanassoula E, Bosma A, Papaioannou S *Astron. Astrophys.* **179** 23 (1987)
77. Khoperskov A V, Zasov A V, Tyurina N V *Astron. Rep.* **47** 357 (2003); *Astron. Zh.* **80** 387 (2003)
78. Khoperskov S A et al. *Mon. Not. R. Astron. Soc.* **427** 1983 (2012)
79. Griv E *Mon. Not. R. Astron. Soc.* **415** 1259 (2011)
80. Miura R E et al. *Astrophys. J.* **761** 37 (2012)
81. Khoperskov S A et al. *Mon. Not. R. Astron. Soc.* **428** 2311 (2013)
82. Dobbs C L *Mon. Not. R. Astron. Soc.* **447** 3390 (2015)
83. Khoperskov S A et al. *Mon. Not. R. Astron. Soc.* **455** 1782 (2016)
84. Sellwood J A, Carlberg R G *Astrophys. J.* **282** 61 (1984)
85. Begum A et al. *Mon. Not. R. Astron. Soc.* **383** 809 (2008)
86. Murray N *Astrophys. J.* **729** 133 (2011)
87. Abramova O V, Zasov A V *Astron. Lett.* **38** 755 (2012); *Pis'ma Astron. Zh.* **38** 843 (2012)
88. Scoville N Z "Evolution of star formation and gas", in *Secular Evolution of Galaxies* (Eds J Falcón-Barroso, J H Knapen) (Cambridge: Cambridge Univ. Press, 2013) p. 491
89. Dobbs C L, Pringle J E, Naylor T *Mon. Not. R. Astron. Soc.* **437** L31 (2014)
90. Romeo A B, Agertz O *Mon. Not. R. Astron. Soc.* **442** 1230 (2014)
91. Braun H et al. *Mon. Not. R. Astron. Soc.* **442** 3407 (2014)
92. Toomre A *Astrophys. J.* **139** 1217 (1964)
93. Morozov A G, Khoperskov A V *Astrophysics* **24** 266 (1986); *Astrofizika* **24** 467 (1986)
94. Romeo A B, Falstad N *Mon. Not. R. Astron. Soc.* **433** 1389 (2013)
95. Rafikov R R *Mon. Not. R. Astron. Soc.* **323** 445 (2001)
96. Jog C J *Astron. J.* **147** 132 (2014)
97. Khoperskov A V, Tyurina N V *Astron. Rep.* **47** 443 (2003); *Astron. Zh.* **80** 483 (2003)
98. Zasov A V et al. *Astron. Lett.* **28** 527 (2002); *Pis'ma Astron. Zh.* **28** 599 (2002)
99. Bizyaev D, Mitronova S *Astrophys. J.* **702** 1567 (2009)
100. Mosenkov A V et al. *Mon. Not. R. Astron. Soc.* **451** 2376 (2015)
101. Zasov A V, Khoperskov A V, Tyurina N V *Astron. Lett.* **30** 593 (2004); *Pis'ma Astron. Zh.* **30** 653 (2004)
102. Zasov A V, Khoperskov A V, Saburova A S *Astron. Lett.* **37** 374 (2011); *Pis'ma Astron. Zh.* **37** 410 (2011)
103. Saburova A S, Zasov A V *Astron. Nachr.* **334** 785 (2013)
104. Zasov A V et al. *Astrophys. Bull.* **67** 362 (2012); *Astrofiz. Byull.* **67** 376 (2012)
105. Zasov A V, Sil'chenko O K *Phys. Usp.* **53** 415 (2010); *Usp. Fiz. Nauk* **180** 434 (2010)
106. Öpik E *Bull. Soc. Astr. Russie* **21** 150 (1915)
107. Kapteyn J C *Astrophys. J.* **55** 302 (1922)
108. de Grijs R, van der Kruit P C *Astron. Astrophys. Suppl.* **117** 19 (1996)
109. van der Kruit P C, Searle L *Astron. Astrophys.* **95** 105 (1981)
110. van der Kruit P C, Searle L *Astron. Astrophys.* **95** 116 (1981)
111. de Grijs R, PhD Thesis (Groningen, The Netherlands: Kapteyn Astronomical Inst., Univ. of Groningen, 1997)
112. Korchagin V I et al. *Astron. J.* **126** 2896 (2003)
113. Bienaymé O et al. *Astron. Astrophys.* **571** A92 (2014)
114. Xia Q et al. *Mon. Not. R. Astron. Soc.* **458** 3839 (2016); arXiv:1510.06810
115. McKee C F, Parravano A, Hollenbach D J *Astrophys. J.* **814** 13 (2015)
116. Famaey B, arXiv:1501.01788
117. Bottema R *Astron. Astrophys.* **275** 16 (1993)
118. Bershady M A et al. *Astrophys. J. Lett.* **739** L47 (2011)
119. Kregel M, van der Kruit P C, Freeman K C *Mon. Not. R. Astron. Soc.* **358** 503 (2005)
120. Olling R P *Astron. J.* **112** 457 (1996)
121. Sotnikova N Ya, Rodionov S A *Astron. Lett.* **32** 649 (2006); *Pis'ma Astron. Zh.* **32** 723 (2006)
122. Khoperskov A et al. *Astron. Nachr.* **331** 731 (2010)
123. O'Brien J C, Freeman K C, van der Kruit P C *Astron. Astrophys.* **515** A62 (2010)
124. Lyskova N et al. *Mon. Not. R. Astron. Soc.* **441** 2013 (2014)
125. Fukazawa Y et al. *Astrophys. J.* **636** 698 (2006)
126. Kalinova V et al. *AIP Conf. Proc* **1551** 84 (2013)
127. Gavazzi R et al. *Astrophys. J.* **667** 176 (2007)
128. Lane R R, Salinas R, Richtler T *Astron. Astrophys.* **574** A93 (2015)
129. Brainerd T G, Blandford R D, Smail I *Astrophys. J.* **466** 623 (1996)
130. Treu T, Marshall P J, Clowe D *Am. J. Phys.* **80** 753 (2012)
131. King L J et al. *Mon. Not. R. Astron. Soc.* **295** L41 (1998)
132. Gurevich A V, Zybin K P, Sirota V A *Phys. Usp.* **40** 869 (1997); *Usp. Fiz. Nauk* **167** 913 (1997)

133. Zakharov A F, Sazhin M V *Phys. Usp.* **41** 945 (1998); *Usp. Fiz. Nauk* **168** 1041 (1998)
134. Bogdanov M B, Cherepashchuk A M *Asrophys. Space Sci.* **317** 181 (2008)
135. Tuntsov A V, Lewis G F *Mon. Not. R. Astron. Soc.* **371** 1259 (2006)
136. Mao S *Res. Astron. Astrophys.* **12** 947 (2012)
137. Frampton P H *Mod. Phys. Lett. A* **31** 1650064 (2016); arXiv:1511.08801
138. Treu T, Koopmans L V E *Astrophys. J.* **611** 739 (2004)
139. van de Ven G et al. *Astrophys. J.* **719** 1481 (2010)
140. Pooley D et al. *Astrophys. J.* **744** 111 (2012)
141. Schneider P "Weak gravitational lensing", in Schneider P, Kochanek C S, Wambsganss J *Gravitational Lensing. Strong, Weak and Micro* (Saas-Fee Advanced Courses, Vol. 33, Eds G Meylan, P Jetzer) (Berlin: Springer, 2006) p. 269; astro-ph/0509252
142. Heymans C et al. *Mon. Not. R. Astron. Soc.* **427** 146 (2012)
143. Gladders M D, Yee H K C *Astrophys. J. Sup.* **157** 1 (2005)
144. York D G et al. *Astron. J.* **120** 1579 (2000)
145. Koekemoer A M et al. *Astrophys. J. Sup.* **172** 196 (2007)
146. Mandelbaum R et al. *Mon. Not. R. Astron. Soc.* **393** 377 (2009)
147. Mandelbaum R et al. *Mon. Not. R. Astron. Soc.* **457** 3200 (2016); arXiv:1509.06762
148. Gavazzi R et al. *Astrophys. J.* **667** 176 (2007)
149. Dutton A A et al. *Mon. Not. R. Astron. Soc.* **407** 2 (2010)
150. Schulz A E, Mandelbaum R, Padmanabhan N *Mon. Not. R. Astron. Soc.* **408** 1463 (2010)
151. Han J et al. *Mon. Not. R. Astron. Soc.* **446** 1356 (2015)
152. Velander M et al. *Mon. Not. R. Astron. Soc.* **437** 2111 (2014)
153. Dai X et al. *Astrophys. J.* **755** 107 (2012)
154. Bogdán Á et al. *Astrophys. J.* **772** 98 (2013)
155. Anderson M E, Bregman J N *Astrophys. J.* **737** 22 (2011)
156. Bogdán Á et al. *Astrophys. J.* **772** 97 (2013)
157. Samurovic S *Publ. Astron. Observ. Belgrade* (81) 1 (2007)
158. Das M et al. *Astrophys. J.* **693** 1300 (2009)
159. Doherty M et al. *Astron. Astrophys.* **502** 771 (2009)
160. de Lorenzi F et al. *Mon. Not. R. Astron. Soc.* **385** 1729 (2008)
161. Napolitano N R et al. *Mon. Not. R. Astron. Soc.* **411** 2035 (2011)
162. Bringmann T, Weniger C *Phys. Dark Universe* **1** 194 (2012)
163. Murgia S, in *Fifth Fermi Symp., Nagoya, Japan, 20–24 October 2014*
164. Ascasibar Y et al. *Mon. Not. R. Astron. Soc.* **368** 1695 (2006)
165. Abramowski A et al. (H.E.S.S. Collab.) *Phys. Rev. Lett.* **114** 081301 (2015)
166. Calore F et al. *Phys. Rev. D* **91** 063003 (2015)
167. Ackermann M et al. (The Fermi-LAT Collab.) *Phys. Rev. Lett.* **115** 231301 (2015)
168. Abramowski A et al. (H.E.S.S. Collab.) *Phys. Rev. D* **90** 112012 (2014)
169. Kazantzidis S et al. *Astrophys. J. Lett.* **611** L73 (2004)
170. Morrison H L et al. *Astrophys. J.* **694** 130 (2009)
171. Ryden B S *Astrophys. J.* **641** 773 (2006)
172. Khoperskov A V et al. *Astron. Rep.* **56** 16 (2012); *Astron. Zh.* **89** 19 (2012)
173. Khoperskov A V et al. *Mon. Not. R. Astron. Soc.* **431** 1230 (2013)
174. El-Zant A A, Haßler B *New Astron.* **3** 493 (1998)
175. Ideta M, Hozumi S *Astrophys. J. Lett.* **535** L91 (2000)
176. Berentzen I, Shlosman I, Jogee S *Astrophys. J.* **637** 582 (2006)
177. Hayashi E, Navarro J F *Mon. Not. R. Astron. Soc.* **373** 1117 (2006)
178. Hayashi E, Navarro J F, Springel V *Mon. Not. R. Astron. Soc.* **377** 50 (2007)
179. Widrow L M *Astrophys. J.* **679** 1232 (2008)
180. Dubinski J, Chakrabarty D *Astrophys. J.* **703** 2068 (2009)
181. Roškar R et al. *Mon. Not. R. Astron. Soc.* **408** 783 (2010)
182. Machado R E G, Athanassoula E *Mon. Not. R. Astron. Soc.* **406** 2386 (2010)
183. Kazantzidis S, Abadi M G, Navarro J F *Astrophys. J. Lett.* **720** L62 (2010)
184. Athanassoula E *Astrophys. J. Lett.* **569** L83 (2002)
185. Dubinski J, Berentzen I, Shlosman I *Astrophys. J.* **697** 293 (2009)
186. Berentzen I, Shlosman I *Astrophys. J.* **648** 807 (2006)
187. Frenk C S et al. *Astrophys. J.* **327** 507 (1988)
188. Jing Y P, Suto Y *Astrophys. J.* **574** 538 (2002)
189. Allgood B et al. *Mon. Not. R. Astron. Soc.* **367** 1781 (2006)
190. Bett P et al. *Mon. Not. R. Astron. Soc.* **376** 215 (2007)
191. Navarro J F, Frenk C S, White S D M *Astrophys. J.* **462** 563 (1996)
192. Navarro J F et al. *Mon. Not. R. Astron. Soc.* **349** 1039 (2004)
193. Navarro J F et al. *Mon. Not. R. Astron. Soc.* **402** 21 (2010)
194. Tenneti A et al. *Mon. Not. R. Astron. Soc.* **453** 469 (2015)
195. Abadi M G et al. *Mon. Not. R. Astron. Soc.* **407** 435 (2010)
196. Khoperskov S A, Shustov B M, Khoperskov A V *Astron. Rep.* **56** 664 (2012); *Astron. Zh.* **89** 736 (2012)
197. Gustafsson M, Fairbairn M, Sommer-Larsen J *Phys. Rev. D* **74** 123522 (2006)
198. Diemand J, Moore B *Adv. Sci. Lett.* **4** 297 (2011)
199. Macciò A V et al. *Mon. Not. R. Astron. Soc.* **378** 55 (2007)
200. Combes F, Arnaboldi M *Astron. Astrophys.* **305** 763 (1996)
201. Reshetnikov V P, Combes F *Astron. Astrophys.* **291** 57 (1994)
202. Reshetnikov V P *Astron. Astrophys.* **416** 889 (2004)
203. Brosch N et al. *Mon. Not. R. Astron. Soc.* **401** 2067 (2010)
204. Moiseev A et al. *Baltic Astron.* **24** 76 (2015)
205. Moiseev A V et al. *Mon. Not. R. Astron. Soc.* **418** 244 (2011)
206. Khoperskov S A et al. *Mon. Not. R. Astron. Soc.* **441** 2650 (2014)
207. Whitmore B C et al. *Astron. J.* **100** 1489 (1990)
208. Snaith O N et al. *Mon. Not. R. Astron. Soc.* **425** 1967 (2012)
209. Reshetnikov V, Sotnikova N *Astron. Astrophys.* **325** 933 (1997)
210. Stanonik K et al. *Astrophys. J. Lett.* **696** L6 (2009)
211. Spavone M et al. *Astrophys. J.* **714** 1081 (2010)
212. Combes F, Moiseev A, Reshetnikov V *Astron. Astrophys.* **554** A11 (2013)
213. Steiman-Cameron T Y, Durisen R H *Astrophys. J. Lett.* **263** L51 (1982)
214. Sackett P D et al. *Astrophys. J.* **436** 629 (1994)
215. Iodice E et al. *Astrophys. J.* **585** 730 (2003)
216. Khoperskov S et al., in *Multi-Spin Galaxies. Proc. of a Conf. 30 September–3 October 2013, Napoli, Italy* (ASP Conf. Ser., Vol. 486, Eds E Iodice, E M Corsini) (San Francisco: Astron. Soc. of the Pacific, 2014) p. 221
217. Whitmore B C, McElroy D B, Schweizer F *Astrophys. J.* **314** 439 (1987)
218. Iodice E *AIP Conf. Proc.* **1240** 379 (2010)
219. Iodice E et al., in *Formation and Evolution of Galaxy Disks. Proc. of the Conf., 1–5 October, 2007, Rome, Italy* (ASP Conf. Ser., Vol. 396, Eds J G Funes, E M Corsini) (San Francisco: Astron. Soc. of the Pacific, 2008) p. 483
220. Sackett P D, Pogge R W *AIP Conf. Proc.* **336** 141 (1995)
221. Brosch N et al. *Mon. Not. R. Astron. Soc.* **382** 1809 (2007)
222. Arnaboldi M et al. *Ann. New York Acad. Sci.* **675** 207 (1992)
223. Schiminovich D, van Gorkom J H, van der Hulst J M *Astron. J.* **145** 34 (2013)
224. Whitmore B C, McElroy D B, Schweizer F *Astrophys. J.* **314** 439 (1987)
225. Franx M, van Gorkom J H, de Zeeuw T *Astrophys. J.* **436** 642 (1994)
226. Cox A L, Sparke L S, in *The Minnesota Lectures on Extragalactic Neutral Hydrogen. Proc. of a Series of Lectures Presented at the University of Minnesota, Minneapolis, Minnesota from 27 March 1994 to 2 June 1994* (ASP Conf. Ser., Vol. 106, Ed. E D Skillman) (San Francisco: Astronomical Society of the Pacific, 1996) p. 168
227. van Driel W et al. *Astron. J.* **109** 942 (1995)
228. Peletier R F, Christodoulou D M *Astron. J.* **105** 1378 (1993)
229. Sparke L S et al. *Astron. J.* **137** 3976 (2009)
230. Sackett P D, Sparke L S *Astrophys. J.* **361** 408 (1990)
231. Steiman-Cameron T Y, Kormendy J, Durisen R H *Astron. J.* **104** 1339 (1992)
232. Reshetnikov V P, Sotnikova N Ya *Astron. Lett.* **26** 277 (2000); *Pis'ma Astron. Zh.* **26** 333 (2000)
233. Khoperskov S, Moiseev A, Khoperskov A *Memorie Soc. Astron. Italiana Suppl.* **25** 51 (2013)
234. Reshetnikov V P, Hagen-Thorn V A, Yakovleva V A *Astron. Rep.* **42** 439 (1998); *Astron. Zh.* **75** (4) (1998)
235. Sparke L S, in *The Shapes of Galaxies and their Dark Halos. Proc. of the Yale Cosmology Workshop, 28–30 May 2001, New Haven,*

*Connecticut, USA* (Ed. P Natarajan) (Singapore: World Scientific Publ., 2002) p. 178
236. Cox A L, Sparke L S, van Moorsel G *Astron. J.* **131** 828 (2006)
237. Belokurov V *New Astron. Rev.* **57** 100 (2013)
238. Newberg H J et al. *Astrophys. J.* **668** 221 (2007)
239. Belokurov V et al. *Astrophys. J. Lett.* **657** L89 (2007)
240. Sackett P D et al. *Astrophys. J.* **436** 629 (1994)
241. Ibata R et al. *Astrophys. J.* **671** 1591 (2007)
242. Price-Whelan A M et al. *Astrophys. J.* **794** 4 (2014)
243. Johnston K V, Law D R, Majewski S R *Astrophys. J.* **619** 800 (2005)
244. Helmi A *Mon. Not. R. Astron. Soc.* **351** 643 (2004)
245. Law D R, Majewski S R *Astrophys. J.* **714** 229 (2010)
246. Carlberg R G, Grillmair C J *Astrophys. J.* **768** 171 (2013)
247. Chin Y-N, Huang Y-L *Nature* **371** 398 (1994)
248. Martínez-Delgado D et al. *Astrophys. J.* **689** 184 (2008)
249. Hayashi K, Chiba M *Astrophys. J.* **789** 62 (2014)
250. van Uitert E et al. *Astron. Astrophys.* **545** A71 (2012)
251. Hoekstra H, Yee H K C, Gladders M D *Astrophys. J.* **606** 67 (2004)
252. Parker L C et al. *Astrophys. J.* **669** 21 (2007)
253. Clampitt J, Jain B *Mon. Not. R. Astron. Soc.* **457** 4135 (2016); arXiv:1506.03536
254. Adhikari S, Chue C Y R, Dalal N *JCAP* (01) 009 (2015)
255. Barnabe M et al. *Mon. Not. R. Astron. Soc.* **423** 1073 (2012)
256. O'Brien J C, Freeman K C, van der Kruit P C *Astron. Astrophys.* **515** A63 (2010)
257. Peters S P C et al., arXiv:1303.2463
258. Banerjee A, Jog C J *Astrophys. J. Lett.* **732** L8 (2011)
259. Banerjee A, Jog C J *Astrophys. J.* **685** 254 (2008)
260. Debattista V P et al. *Mon. Not. R. Astron. Soc.* **434** 2971 (2013)
261. Kuhlen M, Diemand J, Madau P *Astrophys. J.* **671** 1135 (2007)
262. Diemand J, Kuhlen M, Madau P *Astrophys. J.* **649** 1 (2006)
263. Boylan-Kolchin M, Bullock J S, Kaplinghat M *Mon. Not. R. Astron. Soc.* **415** L40 (2011)
264. Garrison-Kimmel S et al. *Mon. Not. R. Astron. Soc.* **444** 222 (2014)
265. Cannon J M et al. *Astron. J.* **149** 72 (2015)
266. Adams E A K et al. *Astron. Astrophys.* **573** L3 (2015)
267. Vera-Ciro C A et al. *Mon. Not. R. Astron. Soc.* **428** 1696 (2013)
268. Brook C B, Di Cintio A *Mon. Not. R. Astron. Soc.* **453** 2133 (2015)
269. Papastergis E, Shankar F *Astron. Astrophys.* **591** A58 (2016); arXiv:1511.08741
270. Lovell M R et al. *Mon. Not. R. Astron. Soc.* **420** 2318 (2012)
271. Ostriker J P, Peebles P J E *Astrophys. J.* **186** 467 (1973)
272. Debattista V P, Sellwood J A *Astrophys. J.* **543** 704 (2000)
273. Combes F *Memorie Soc. Astron. Italiana Suppl.* **25** 45 (2013)
274. Bekki K, Freeman K C *Astrophys. J. Lett.* **574** L21 (2002)
275. Masset F S, Bureau M *Astrophys. J.* **586** 152 (2003)
276. Tutukov A V, Fedorova A V *Astron. Rep.* **50** 785 (2006); *Astron. Zh.* **83** 880 (2006)
277. Heller C H, Shlosman I, Athanassoula E *Astrophys. J.* **671** 226 (2007)
278. Romano-Díaz E et al. *Astrophys. J. Lett.* **687** L13 (2008)
279. Butenko M, Khoperskov A, Khoperskov S *Baltic Astron.* **24** 119 (2015)
280. Koribalski B S, López-Sánchez Á R *Mon. Not. R. Astron. Soc.* **400** 1749 (2009)
281. Radburn-Smith D J et al. *Astrophys. J.* **753** 138 (2012)
282. Walker M G, Peñarrubia J *Astrophys. J.* **742** 20 (2011)
283. Oñorbe J et al. *Mon. Not. R. Astron. Soc.* **454** 2092 (2015)
284. Burkert A *Astrophys. J.* **808** 158 (2015)
285. Wyse R F G, Gilmore G, in *Dark Galaxies and Lost Baryons, Proc. of the 244th IAU Symp., Cardiff, Wales, United Kingdom, June 25 – 29, 2007* (IAU Symp. Proc., Vol. 244, Eds J I Davies, M J Disney) (Cambridge: Cambridge Univ. Press, 2008) p. 44
286. Brook C B et al. *Mon. Not. R. Astron. Soc.* **415** 1051 (2011)
287. Di Cintio A et al. *Mon. Not. R. Astron. Soc.* **437** 415 (2014)
288. Governato F et al. *Mon. Not. R. Astron. Soc.* **422** 1231 (2012)
289. Del Popolo A, Hiotelis N *JCAP* (01) 047 (2014)
290. Bode P, Ostriker J P, Turok N *Astrophys. J.* **556** 93 (2001)
291. Marsh D J E, Pop A-R *Mon. Not. R. Astron. Soc.* **451** 2479 (2015)
292. Doroshkevich A G, Lukash V N, Mikheeva E V *Phys. Usp.* **55** 3 (2012); *Usp. Fiz. Nauk* **182** 3 (2012)
293. Semenov V et al., arXiv:1306.3210
294. Roberts M S *Astron. J.* **74** 859 (1969)
295. Tully R B, Fisher J R *Astron. Astrophys.* **54** 661 (1977)
296. Verheijen M A W *Astrophys. J.* **563** 694 (2001)
297. De Rijcke S et al. *Astrophys. J.* **659** 1172 (2007)
298. Cortesi A et al. *Mon. Not. R. Astron. Soc.* **432** 1010 (2013)
299. Zaritsky D et al. *Astron. J.* **147** 134 (2014)
300. McGaugh S S *Astron. J.* **143** 40 (2012)
301. McGaugh S S, Schombert J M *Astrophys. J.* **802** 18 (2015)
302. Giovanelli R, in *Advancing the Physics of Cosmic Distances, Proc. of the IAU Symp., Beijing, China, August 27 – 31, 2012* (IAU Symp. Proc., Vol. 289, Ed. R de Grijs) (Cambridge: Cambridge Univ. Press, 2013) p. 296
303. Zaritsky D *ISRN Astron. Astrophys.* **2012** 189625 (2012)
304. Aumer M et al. *Mon. Not. R. Astron. Soc.* **434** 3142 (2013)
305. McGaugh S S *Astrophys. J.* **632** 859 (2005)
306. Saburova A, Del Popolo A *Mon. Not. R. Astron. Soc.* **445** 3512 (2014)
307. Boyarsky A et al., arXiv:0911.1774
308. Elson E C, de Blok W J G, Kraan-Korteweg R C *Mon. Not. R. Astron. Soc.* **404** 2061 (2010)
309. Oh S-H et al. *Astron. J.* **149** 180 (2015)
310. Lelli F et al. *Astron. Astrophys.* **584** A113 (2015)
311. Humphrey P J et al. *Astrophys. J.* **646** 899 (2006)
312. Nigoche-Netro A et al. *Mon. Not. R. Astron. Soc.* **446** 85 (2015)
313. Bosma A *Astron. J.* **86** 1791 (1981)
314. Swaters R A et al. *Mon. Not. R. Astron. Soc.* **425** 2299 (2012)
315. Grenier I A, Black J H, Strong A W *Annu. Rev. Astron. Astrophys.* **53** 199 (2015)
316. Ade P A R et al. (Planck Collab.) *Astron. Astrophys.* **536** A19 (2011)
317. Fukui Y et al. *Astrophys. J.* **796** 59 (2014)
318. Zasov A, Saburova A, Abramova O *Astron. J.* **150** 192 (2015); arXiv:1510.08924
319. Libeskind N I et al. *Mon. Not. R. Astron. Soc.* **418** 336 (2011)
320. Elmegreen B G, Struck C, Hunter D A *Astrophys. J.* **796** 110 (2014)
321. Dutton A A et al. *Astrophys. J.* **654** 27 (2007)
322. Papastergis E et al. *Astrophys. J.* **759** 138 (2012)
323. Sofue Y *Publ. Astron. Soc. Jpn.* **67** 759 (2015)
324. Kassin S A, de Jong R S, Weiner B J *Astrophys. J.* **643** 804 (2006)
325. Yoshino A, Ichikawa T *Publ. Astron. Soc. Jpn.* **60** 493 (2008)
326. Saburova A S, Shaldenkova E S, Zasov A V *Astron. Rep.* **53** 801 (2009); *Astron. Zh.* **86** 861 (2009)
327. Moriondo G, Giovanardi C, Hunt L K *Astron. Astrophys. Suppl.* **130** 81 (1998)
328. Dicaire I et al. *Astron. J.* **135** 2038 (2008)
329. Barnes E I, Sellwood J A, Kosowsky A *Astron. J.* **128** 2724 (2004)
330. Kranz T, Slyz A, Rix H-W *Astrophys. J.* **586** 143 (2003)
331. Reyes R et al. *Mon. Not. R. Astron. Soc.* **425** 2610 (2012)
332. Alam S M K, Bullock J S, Weinberg D H *Astrophys. J.* **572** 34 (2002)
333. Tumlinson J et al. *Science* **334** 948 (2011)
334. Borthakur S et al. *Astrophys. J.* **813** 46 (2015)
335. Faerman Y, Sternberg A, McKee C F *Astrophys. J.* **835** 52 (2017); arXiv:1602.00689
336. Lynden-Bell D *Observatory* **101** 111 (1981)
337. Sandage A *Astrophys. J.* **307** 1 (1986)
338. Karachentsev I D et al. *Astrophys. J.* **782** 4 (2014)
339. Chernin A D, Emelyanov N V, Karachentsev I D *Mon. Not. R. Astron. Soc.* **449** 2069 (2015)
340. Chernin A D et al. *Astron. Astrophys.* **553** A101 (2013)
341. Bahcall N A, Kulier A *Mon. Not. R. Astron. Soc.* **439** 2505 (2014)
342. Makarov D, Karachentsev I *Mon. Not. R. Astron. Soc.* **412** 2498 (2011)
343. Karachentsev I D *Astrophys. Bull.* **67** 123 (2012); *Astrofiz. Byull.* **67** 129 (2012)
344. Ferrarese L *Astrophys. J.* **578** 90 (2002)
345. Cherepashchuk A M et al. *Astron. Rep.* **54** 578 (2010); *Astron. Zh.* **87** 634 (2010)
346. Zasov A V, Cherepashchuk A M *Astron. Rep.* **57** 797 (2013); *Astron. Zh.* **90** 871 (2013)
347. Ilyin A S, Zybin K P, Gurevich A V *JETP* **98** 1 (2004); *Zh. Eksp. Teor. Fiz.* **125** 5 (2004)

348. Volonteri M, Haardt F, Madau P *Astrophys. J.* **582** 559 (2003)
349. Barausse E *Mon. Not. R. Astron. Soc.* **423** 2533 (2012)
350. Kormendy J, Ho L C *Annu. Rev. Astron. Astrophys.* **51** 511 (2013)
351. Sabra B M et al. *Astrophys. J.* **803** 5 (2015)
352. Kormendy J, Bender R *Nature* **469** 377 (2011)
353. Bandara K, Crampton D, Simard L *Astrophys. J.* **704** 1135 (2009)
354. Bogdán Á, Goulding A D *Astrophys. J.* **800** 124 (2015)
355. Mathews W G et al. *Astrophys. J. Lett.* **652** L17 (2006)
356. Booth C M, Schaye J *Mon. Not. R. Astron. Soc.* **405** L1 (2010)
357. Di Matteo T et al. *Astrophys. J.* **593** 56 (2003)
358. Volonteri M, Natarajan P, Gültekin K *Astrophys. J.* **737** 50 (2011)
359. Casanellas J, Lopes I *Mod. Phys. Lett. A* **29** 40001 (2014)
360. Ghosh S, Jog C J *Mon. Not. R. Astron. Soc.* **439** 929 (2014)
361. Harris W E, Harris G L, Hudson M J *Astrophys. J.* **806** 36 (2015)
362. Besla G, arXiv:1511.03346
363. Dremova G N, Tutukov A V, Dremov V V *Astron. Rep.* **54** 704 (2010); *Astron. Zh.* **87** 768 (2010)
364. Widrow L M, Bonner G *Mon. Not. R. Astron. Soc.* **450** 266 (2015)
365. Kannan R et al. *Astrophys. J.* **746** 10 (2012)
366. Combes F "Gas accretion in disk galaxies", in *Structure and Dynamics of Disk Galaxies. Proc. of the Conf., 12–16 August, 2013, Petit Jean Mountain, Arkansas, USA* (ASP Conf. Ser., Vol. 480, Eds M S Seigar, P Treuthardt) (San Francisco: Astron. Soc. of the Pacific, 2014) p. 211
367. Dekel A et al. *Mon. Not. R. Astron. Soc.* **435** 999 (2013)
368. Sánchez Almeida J et al. *Astron. Astrophys. Rev.* **22** 71 (2014)
369. van de Voort F et al. *Mon. Not. R. Astron. Soc.* **414** 2458 (2011)
370. Ilyina M A, Sil'chenko O K, Afanasiev V L *Mon. Not. R. Astron. Soc.* **439** 334 (2014)
371. Katkov I Yu, Kniazev A Yu, Sil'chenko O K *Astron. J.* **150** 24 (2015)